Egil Bergstøl Birkeland
Preben Hannevig Huseth
Vegard Kristiansen

CFD calculations on offshore HVDC converter platform

Evaluating temperature and air distribution

Bachelor's project

NTNU
Norwegian University of
Science and Technology

aibel®

Egil Bergstøl Birkeland
Preben Hannevig Huseth
Vegard Kristiansen

CFD calculations on offshore HVDC converter platform

Evaluating temperature and air distribution

NTNU

Norwegian University of
Science and Technology

NTNU

Norwegian University of Science and Technology
Faculty of Engineering
Department of Energy and Process Engineering
Renewable energy, engineer, bachelor

Bachelor thesis

Protject title:	**Given date:**
CFD calculations on offshore HVDC converter platform	11/01/2021
	Date to deliver:
	20/05/2021
Prosjekttittel:	**Number of pages/ appendices:**
CFD kalkulasjoner på offshore HVDC omformerplattform	58/4
Project participants:	**Supervisor:**
Egil Bergstøl Birkeland Preben Hannevig Huseth Vegard Kristiansen	Dag Rune Stensaas dag.r.stensaas@ntnu.no +47 992 12 762
Study program:	**Subject code:**
Renewable energy, engineer, bachelor	TFNE3001
Company:	**Company contact:**
Aibel AS	Simon Nilsen Lingaas Ronny Mæland

Freely available   **X**

Available after agreement with employer

Report released after

Preface

Offshore wind power is set to become one of the most exciting energy technologies in the coming years. The Dogger Bank project, which is going to be the worlds largest offshore wind farm, is a great example of this. In that regard, converter platforms are being developed as a cooperation between Aibel and ABB to efficiently transfer the generated electricity to the United Kingdom. Evaluation of the heat emission on board the converter platforms is a necessary procedure to assure a safe environment for equipment and maintenance staff. An efficient method to assure this is through CFD calculations.

This bachelor thesis is written by the three students; Egil Bergstøl Birkeland, Preben Hannevig Huseth and Vegard Kristiansen. It was conducted at the Department of Energy and Process Engineering at Norwegian University of Science and Technology in the spring semester 2021 and concluded 20/05/2021. The project description was provided by Aibel. The bachelor thesis is the final part of the three year study program *Bachelor in Engineering, Renewable Energy*.

Throughout the process of this thesis, supervising and guidance have been provided from various people. Hence, we would like to express gratitude to our supervisor at NTNU, Dag Rune Stensaas, for weekly guidance, providing essential information and support throughout the thesis. We also want to show appreciation to our external supervisors from Aibel, Simon Nilsen Lingaas and Ronny Mæland, for providing information, guidance and suggestions from start to finish. Furthermore, we want to thank Knut Emil Ringstad and Vidar Ahlberger for their helpful guidance on the application of ANSYS.

<div align="center">

Trondheim, 20/05/2021

Egil Bergstøl Birkeland   Preben Hannevig Huseth   Vegard Kristiansen

Egil Bergstøl Birkeland   **Preben Hannevig Huseth**   **Vegard Kristiansen**

</div>

Abstract

Offshore wind power has become one of the most interesting technologies within the energy sector. Furthermore, there is a continuous increase in efficiency of power transmission, by utilising direct current instead of alternating current. In order to transfer this great amount of power, offshore converter platforms are built. Inside these platforms, there will be areas that must be within a temperature limit in order to function optimally.

The purpose of this thesis is to utilise CFD calculations to verify that selected areas on board the converter platform do not exceed the temperature requirements. The simulations are based on a fundamental literature study, which evaluates methods and models, as well as general knowledge required to conduct CFD calculations. Furthermore, it was necessary to procure knowledge about the structure, and functioning of the ventilation system on board the platform to achieve accurate CFD calculations.

An appropriate indoor climate will ensure a satisfactory environment for both equipment and personnel. One method to regulate the indoor climate is by implementing HVA/C systems. The purpose of HVA/C systems is to regulate temperature, air supply, humidity and air pollution. Before constructing a HVA/C system, an evaluation of the system is of interest to ensure adequate dimensions. An effective way to evaluate the system is by utilising CFD calculations. These calculations implement advanced mathematics, thermodynamics and fluid dynamics to achieve an accurate depiction of how the system will operate. A sufficient mesh is essential to achieve realistic results from CFD calculations.

During this thesis it was necessary to implement various software for different phases of the CFD calculations. The geometry used in the simulations is simplified by neglecting components that have a small impact on the simulation results. Subsequently, a mesh was constructed in order to conduct the CFD calculations. The mesh was reviewed in form of element quality and the number of elements that provided the most computational cost efficient and accurate simulation. The parameters and boundary conditions used in the simulation setup were implemented to recreate the properties of the system in real life.

The CFD calculations resulted in average temperatures of $35,0$°C for the auxiliary transformer room and $40,1$°C for the valve hall. The highest temperatures around the equipment were measured to $36,2$°C in the auxiliary transformer room, and $48,3$°C in the valve hall. By evaluating the air jets within the systems, the air distribution was confirmed as satisfactory. Despite the fact that the temperature exceeded the design temperature above the smoothing reactor, and beneath the ceiling inside the auxiliary transformer room, it was concluded that the ventilation system worked satisfactorily for the two systems.

Sammendrag

Offshore vindkraft har etablert seg til å bli en av de mest spennende teknologiene innenfor energisektoren. Teknologien for å effektivisere energioverføringen ved å konvertere strøm fra vekselstrøm til likestrøm, er under kontinuerlig utvikling. For å overføre store mengder elektrisitet blir det bygget offshore omformerplattformer. Ombord på plattformene vil det være kritiske områder som må holdes innenfor gitte temperaturkrav for å fungere optimalt.

Hensikten med avhandlingen er å anvende CFD kalkulasjoner for å verifisere at utvalgte områder ombord på omformer plattformen ikke overskrider temperaturkravene. Simuleringene er basert på et fundementalt litteraturstudium, som evaluerer forskjellige metoder og modeller, samt viktig bakgrunnskunnskap for utførelsen av CFD kalkulasjoner. Videre var det nødvendig å bli kjent med strukturen og ventilasjonssystemet på plattformen for å oppnå en presis numerisk strømninganalyse.

Et ventilert inneklima sørger for gode arbeidsforhold for både personell og industrielt utstyr. En måte å regulere innendørs klima er ved å anvende HVA/C-systemer, som regulerer temperatur, luftfuktighet, lufttilførsel og forurensning i luften. Det er av interesse å evaluere HVA/C systemer før de er konstruert, for å forsikre tilstrekkelig dimensjonering. En effektiv måte å evaluere systemene er ved bruk av CFD kalkulasjoner. Denne type kalkulasjoner anvender avansert matematikk, termodynamikk og fluiddynamikk for å simulere hvordan systemet opererer når det er ferdigstilt. Det er essensielt for resultatene at brukeren utfører en tilstrekkelig utvikling av rutenettet til underdomenene for å oppnå realistiske resultat.

For utførelsen av avhandlingen var det nødvendig med diverse programvarer for ulike faser av CFD kalkulasjonene. Geometrien som brukes i simuleringene er forenklet ved å neglisjere komponenter som har liten påvirkning på resultatene. Deretter ble geometrien bygd opp av elementer som muliggjorde CFD kalkulasjoner. Nettverket av elementer ble vurdert i form av kvalitet, og hvilket antall av elementer som ga en raskest og mest mulig presis simulering. Parametrene og grensebetingelsene som ble brukt i simuleringen ble implementert for å gjenskape egenskapene til systemet i virkeligheten.

CFD kalkulasjonene resulterte i gjennomsnitts temperaturer på $35,0°$C i hjelpetransformator rommet og $40,1°$C i ventilhallen. De høyeste temperaturene rundt utstyret ble målt til $36,2°$C i hjelpetransformator rommet, og $48,3°$C i ventilhallen. Ved å evaluere strømningslinjene i systemene ble det bekreftet at luftfordelingen var tilfredsstillende. Til tross for at temperaturen oversteg design temperaturen over utjevningsreaktoren, og under taket i hjelpetransformator rommet, ble det konkludert med at ventilasjonen fungerte tilfredsstillende for de to systemene.

Contents

Symbol List

Latin letters

Symbol	Definition	Unit
$\vec{dr}$	Arc length	$[m]$
E_t	Energy	$[J]$
$\vec{g}$	Body accelerations acting on the continuum	$[m/s^2]$
M_w	Molecular weight	$[kg/mol]$
p	Static pressure	$[Pa]$
p_{op}	Operating pressure	$[Pa]$
Q	Heat	$[J]$
R	Gas constant	$[J/(K \cdot mol)]$
T	Temperature	$[K]$
u	Decompressed directional velocity vector in x direction	$[m/s]$
u^+	Dimensionless velocity	$[-]$
u_τ	Friction velocity	$[m/s]$
U	Mean velocity components in x direction	$[m/s]$
v	Decompressed directional velocity vector in y direction	$[m/s]$
$\vec{v}$	Mass velocity	$[m/s]$
$\vec{V}$	Velocity vector	$[m/s]$
w	Decompressed directional velocity vector in z direction	$[m/s]$
W	Work	$[J]$
y	Variation with distance from the surface	$[m]$
y^+	Dimensionless, sublayer-scaled, distance	$[-]$

Greek letters

Symbol	Definition	Unit
∇	Gradient operator	$[-]$
ϵ	Dissipation per unit mass	$[W/kg]$
κ	Specific turbulence kinetic energy	$[J/kg]$
μ	Viscosity coefficient	$[(N \cdot s)/m^2]$
ν	Kinematic viscosity	$[m^2/s]$
ρ	Density	$[kg/m^3]$
$\bar{\bar{\tau}}$	Viscous stress tensor	$[-]$
τ_w	Surface shear stress	$[Pa]$
ω	Specific dissipation rate	$[s^{-1}]$

Abbreviations

Term	Definition
CAD	Computer-aided design
CFD	Computational fluid dynamics
DO	Discrete ordinates
HVAC	High-voltage alternating current
HVA/C	Heating, ventilation and air conditioning
HVDC	High-voltage direct current
PV	Photovoltaics
RANS	Reynolds average Navier-Stokes
RMS	Root-mean-square
RNG	Re-normalisation group
SST	Shear stress transport
S2S	Surface to surface

Term List

Term	Definition
Auxiliary transformer	Component used to supply low voltage for alternating current power systems inside substation such as lighting.
Blending functions	Functions designed to make closure coefficients assume a set of values near solid boundaries and another set near the edge of a shear layer.
Boussinesq eddy-viscosity approximation	A hypothesis which says that the turbulent stresses are related to the mean velocity gradients in almost the same way that the viscous stresses are related to the complete velocity gradients.
Capacity factor	The actual electricity production divided by the maximum possible electricity output.
Computational cost	The amount of resources required to run a simulation.
Contour	An outline, boundary or border, usually of curved shape.
Emissivity	The amount of radiation emitted or absorbed by a body compared with that of a black body under identical conditions.
Enclosure	An area that is surrounded by a barrier.
External flow	A flow where an unbounded fluid is flowing over a surface.
Gauss theorem	Theorem which relates the flux of a vector field through a closed surface to the divergence of the field in the volume enclosed.
Internal flow	A flow bounded by a solid.
Laminar flow	Fluid motion characterised by smooth layers of fluid.
Law of the wall	The law of the wall is one of the most famous empirically-determined relationships in turbulent flows near solid boundaries.
Reynolds number	Reynolds number, in fluid mechanics, a criterion of whether fluid flow is absolutely steady or on the average steady with small unsteady fluctuations.
Shear stress	A stress which is applied parallel or tangential to a face of a material.
SL 620	A type of insulation material.
Smoothing reactor	A component which reduce harmonic currents and transient over currents or current ripples in DC systems. These reactors are necessary in order to smooth the direct current wave shape, reduce losses and improve system performance.
Solar radiation	Radiant energy emitted by the sun from a nuclear fusion reaction that creates electromagnetic energy.
Stated Policies Scenario	Reflects how the current policies will impact the energy sector in the coming years.
Streamline	A line that is tangent to the velocity of fluid flow.
Streamwise	In the direction of a stream.
Subcooled	Lowered the temperature of a fluid, compared to the temperature in the enclosure.
Thermal plume	Thermal plumes are generated by fluid rising above an heat source.
Thermal stratification	The formation of different temperatures in certain areas of an enclosement.
Valve	A component containing thyristors.

List of Figures

List of Figures in the Appendices

List of Tables

1 Introduction

Planning larger constructions requires consideration of several aspects in order to achieve a well-functioning system. Room temperature is an important parameter in this regard. Industrial constructions often contain equipment with a high amount of heat emission. Standards have been developed to ensure that equipment and people can operate efficiently in different environments. On many occasions, it is an advantage to investigate how the indoor climate will function before building the construction. Evaluating the indoor climate from manual calculations is often time consuming and complicated. The time necessary to evaluate an indoor climate can be significantly reduced by the usage of computational fluid dynamics (CFD).

Computational fluid dynamics is a tool that computers use to perform numerical flow analysis. With the help of CFD, it is possible to examine how a prospective system operates before being built. A CFD analysis can expose flaws in the system, so these can be improved before the construction begins, thence achieving a more cost efficient project. For this thesis, numerical flow analysis will be completed on parts of the ventilation system installed on an offshore converter platform. The converter platform is a part of the Dogger Bank project. The analysis will be performed in two different systems on board the platform, an auxiliary transformer room and a valve hall. The purpose of the analyses is to ensure that the room temperature is within the design temperature, and to study if the planned ventilation system will function as intended.

1.1 Offshore wind power

Offshore wind has developed to be one of the most dynamic technologies in the energy sector. The development of offshore wind is increasing rapidly. In 2010, there was an installed capacity of 3GW in the world, which expanded to 23GW by 2018. The annual deployment has been increasing by nearly 30% each year, which is more than any other source of electricity, except solar photovoltaics (PV). During 2019 there were more than 5 500 offshore wind turbines connected to the power grid. This increasing growth is a result of the rising political support and the technological innovation.

The expanding growth of the offshore wind industry has been nurtured in European countries. Especially by countries that borders the North Sea. In these parts, there are high quality wind resources, as well as relatively shallow water levels. This provides exceptionally good conditions for the development of offshore wind technologies. In 2018 more than 80% of the total global installed offshore wind capacity was located in Europe. In the United Kingdom there were an installed capacity of roughly 8 GW, which was a third of the world total. The offshore wind produce 8% of electricity generation in the United Kingdom, which is more than twice as much as solar PV.

Offshore wind is set to expand significantly within the next two decades. In the Stated Policies Scenario, offshore wind is set to grow 13% each year. The economic ambitions within wind power are an important factor that plays a role in further development. By 2040, it is estimated that global offshore wind is on track to become a trillion dollar business. And within the next decade, it is set to become a competitor to fossil fuels. It is estimated that offshore wind will account for 10% of investment in renewable-based power over the next two decades. Reducing the losses in the transmission lines by investing in innovation will contribute to a further development, but also make it more cost efficient. [1]

1.2 Dogger Bank

The Dogger Bank project is an offshore wind farm, which is set to become the largest in the world. The installed capacity of the wind farm is going to be 3,6GW when fully functional. The development of the wind farm is separated into three phases, where each of the three phases is planned to install up to 200 wind turbines. The project is a cooperation between SSE Renewables, Equinor and Eni. The distribution between them is respectively, 40%, 40% and 20% of the stakes for Dogger Bank A and B. Dogger Bank C is divided equally between SSE Renewables and Equinor. When fully functional, the offshore wind farm will be capable of providing between $4, 5 - 6$ million British homes with electric power. [2, 3]

The production line from offshore wind to the British power grid is illustrated in Figure 1.1. The first part of the process is extruding energy from the wind, by using wind turbines. This energy is transported as high voltage alternating current (HVAC) to an offshore converter platform. The current is converted to high voltage direct current (HVDC) for long distance transportation to be more cost efficient. When the current reaches the shore it is converted back to HVAC at an onshore converter station. Furthermore, the HVAC then passes through an adjacent main substation before entering the National grid. [4]
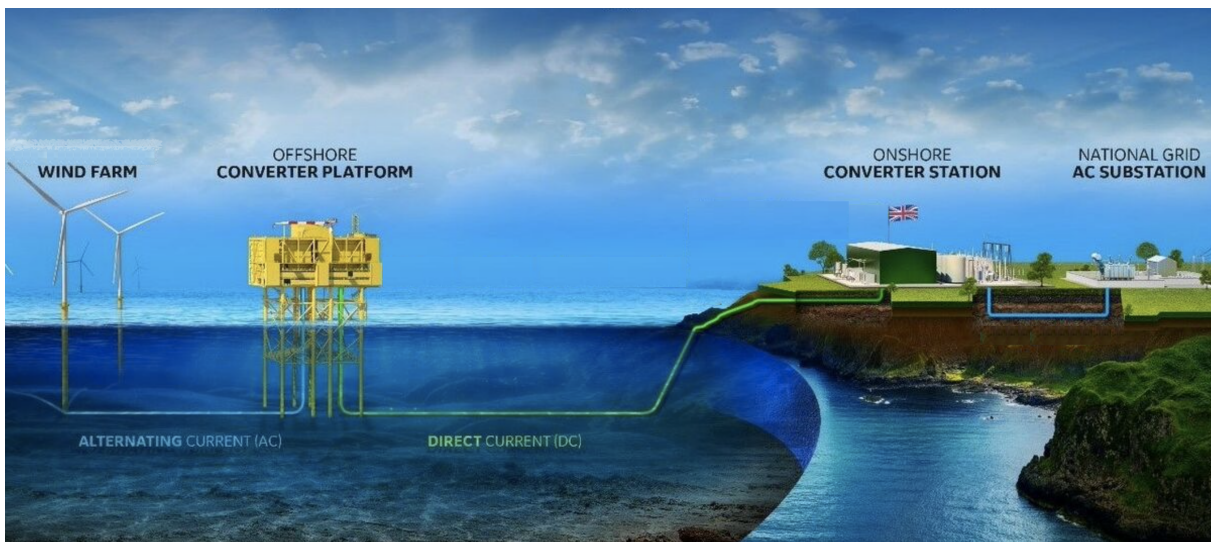
Figure 1.1: *Illustration of the power production line of the Dogger Bank project. The figure is modified. [5]*

Dogger Bank is a sandbank that cover a vast extent of the North Sea. The sandbank is located in a part of the North Sea that covers territories belonging to the United Kingdom, Germany, Denmark and the Netherlands. The area is around 130 kilometres from the coast of Yorkshire in the United Kingdom. The sandbank consists of areas where the sea level is shallower than other parts of the sea. Moreover, there is also better wind conditions at this part of the sea compared to land based. As a result, the Dogger Bank area is well suited for offshore wind. [2, 6]

The assembly of the wind turbines will be done with the biggest jack-up installation vessel in the world, the Voltaire. The vessel has a lifting capacity of 3000 tonnes and is one of few vessels that are capable of performing the assembly of the Haliade-X 13MW wind turbines. These are the wind turbines which will be installed for the Dogger Bank project. These turbines are the largest in the world, ranging 240 meters high with a rotor diameter of 220 meters. These giant turbines can produce enough electricity to provide an English home for over two days with a single revolution. The manufacturer of the Haliade-X, GE Renewables, estimates the capacity factor of the turbine to be approximately 60%. [3, 7, 8]

The Dogger Bank project will require three offshore converter platforms. The construction and design of these platforms are outsourced to Aibel and ABB. In addition to the converter platforms at sea, the project also includes construction of onshore cable installations and landfall onshore. Furthermore, offshore cable installation, inter-array cables and the wind turbines must be built as well. The installations offshore are not designed to be manned, with the exception of occasional maintenance work. The platforms will normally be manned from shore, and maintenance needs are covered by service operation vessels. [2, 9]

1.3 Thesis objective

The thesis is written in collaboration with Aibel, which is a leading service company within the energy sector. They provide engineering, construction, modifications and maintenance services. Aibel is currently working on the design, engineering and construction of several converter platforms for use in offshore wind projects. There are large amounts of energy involved in these platforms. Part of this energy will be lost as heat from the equipment on board. In the design of the platforms, parts of this heat must be managed by the platform's ventilation system. It is of great interest to ensure that the ventilation systems are correctly designed for the amount of heat, so that temperature requirements for personnel and equipment on the platform are maintained.

Aibel wishes to conduct CFD calculations of various rooms on their platform. The results from these calculations provide an indication on how the ventilation system operates and if the temperatures are within the design limits. The simulations are complex and extensive, and will provide an insight to the systems of high interest. These systems are an auxiliary transformer room and a valve hall. The results can either be compared with previous simulations, or used in future work. The purpose of the thesis is to:

- Conduct a literature study on numerical flow calculations. Both in general and in regard to the CFD applications.

- Conduct CFD calculations of two rooms on Aibel's platform to estimate the temperatures.

- The simulations will be based on the platform's ventilation design. Thus it is required to be familiarised with the ventilation system, and use relevant information about the platform and the rooms to correctly simulate room temperature.

- Evaluate simulation setups so that the simulations are satisfactorily accurate and relatively quick to perform (choice of simulation models, turbulence models, choice of mesh, et cetera).

2 Theory

CFD calculations require a considerable amount of knowledge within various fields of engineering. These disciplines include fluid- and thermodynamics, a general understanding of indoor climate, HVA/C systems and skills within relevant computer software. In this section, theory and relevant aspects are presented to elucidate these subjects in a scientific sense. The theory presented will later be used in methodology and discussed along with the results.

2.1 Indoor climate

The indoor atmospheric conditions, where equipment and people are located, is often referred to as indoor climate. The parameters which affect the indoor climate are important to regulate. Indoor climate is ventilated to establish desirable conditions for equipment, ensure comfort for people and prevent corroding and mold growth. The indoor environment is composed of seven different parameters, which affect how people perceive the indoor environment. The seven parameters are; acoustic, actinic, aesthetic, atmospheric, mechanical, psychosocial and thermal.

In this thesis, the thermal indoor environment will be the most essential parameter. Usually, the four most important parameters are the acoustic-, atmospheric-, actinic- and the thermal environment. The acoustic environment is important in terms of noise, the atmospheric in regards to indoor air quality, and the actinic in the regard of solar radiation. The thermal indoor environment is affected by temperature, flow rate and humidity. The humidity affects the perception of the ambient temperature. Air flow, or draft, in environments where people are located should not have a velocity that gives an experience of discomfort. Moreover, it is crucial that the temperature is adapted to suit the environment. [10, 11]

Every modern construction is required to provide a satisfying indoor climate. When dealing with large enclosures, often found in industrial environments, it is usual to encounter complications related to energy and air flows. These complications involve unwanted thermal stratification, local overheating, draughts and other unwanted air flows. To avoid these problems it is mandatory to plan and acquire a well-functioning ventilation system. HVA/C is an abbreviation of heat, ventilation and air-conditioning. The purpose of HVA/C systems is to control temperature, humidity, supply of outside air for ventilation, filtration of airborne particles and air flow in occupied space. These systems are applied to a wide range of buildings, from homes to industrial plants or offshore platforms.

To achieve full air conditioning there are seven processes required. The processes are heating, cooling, humidifying, dehumidifying, cleaning, ventilating and air movement. Heating and cooling are processes where thermal energy is either added or removed from an enclosure. Humidifying and dehumidifying are done by adding or subtracting water vapour to obtain the desired humidity. Cleaning is done to maintain or improve the air quality by removing particulates and biological contaminants. The ventilating process shall maintain or increase the air quality. Furthermore, diluting the gaseous contaminants in the air by exchanging the air between the outdoors and the conditioned space. The last process, air movement, is to circulate and mix the air in the conditioned space to achieve satisfactory ventilation. [12]

HVA/C systems will be affected by external factors such as the outdoor climate. Therefore, this must be considered during the design of a HVA/C system. The level of influence will vary by the location, because it is considerably more challenging to design an efficient HVA/C system on an offshore platform compared to a standard building. To reduce the influence of the outdoor climate, thermal insulation is commonly used. Thermal insulation material will reduce the heat flow through a wall. If the building is warm, the cooling will be slowed down, and if the space is cold it will reduce the heat gain. Insulation will simply reduce the heat transfer, but not prevent it completely. For instance, if a warm surface is surrounded by a cold space, both components will eventually achieve temperature equilibrium because of the heat transfer between them.

HVA/C systems are designed to meet certain criteria. An example is design temperatures, which is set to ensure the proper environment for equipment and personnel. To guarantee that the temperature do not exceed the design temperature, either measurements or simulations can be performed. The temperature measurements should be performed in various parts of the enclosure, such as near the heat sources, and by the inlets and outlets. It is recommended to measure temperature at a point that is located half the component height above the mass center of the component. Simulations for worst case scenario will usually have high surface temperatures on components with high emission. Thus the measurements are done at a set distance above the components. The HVA/C system operates as intended when all these measurements are within the temperature limit.

Ventilation is a way to regulate the temperature, humidity and the degree of pollution related to the indoor climate. Within the subject of ventilation, a distinction is made between comfort ventilation and process ventilation. Comfort ventilation aims to achieve optimal room climate for people, while process ventilation is adapted to industrial processes. Within process ventilation, the three most common methods are point ventilation, general ventilation and displacement ventilation. In point ventilation the contaminants are removed where they are formed, by leading it away in a duct system. For general ventilation, the room is supplied with a large amount of air. This causes the concentration of dust, vapour and gases to remain at an acceptable level.

Displacement ventilation is a principle where subcooled air is supplied into a room at low velocity near the floor. Simultaneously, warm air is extracted near the ceiling, hence a piston effect will be generated. The principle is illustrated in Figure 2.1, and as visualised there will be developed an upper- and a lower zone. When this kind of system works optimally, cool and clean zones with a low amount of contaminants are developed at floor level. As the heat rises, the warm and contaminated air will be extracted by the outlet in the upper zone. An inconvenience of displacement ventilation systems is that the lower zone is often perceived as cold and annoying by humans due to the constant draft. [13, 14]
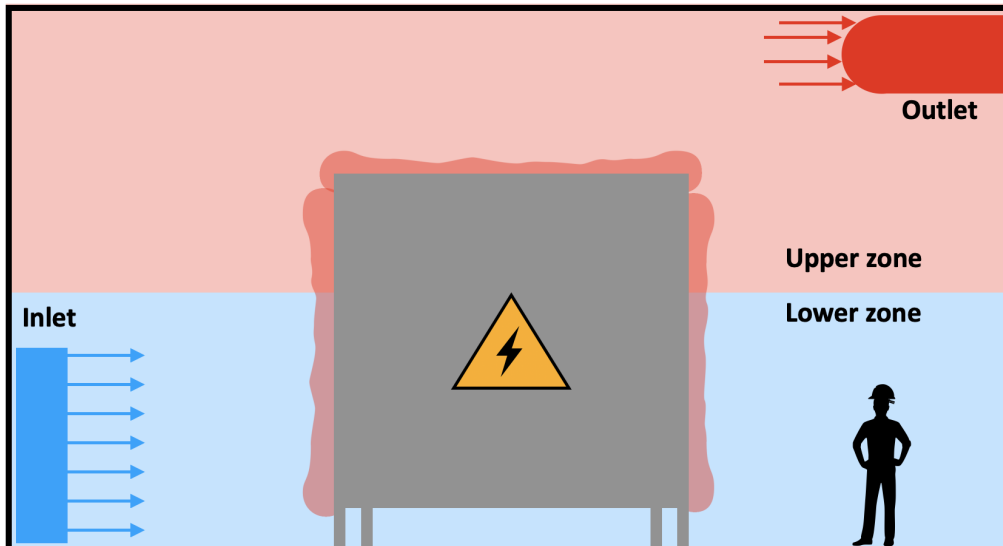
Figure 2.1: *Illustration of displacement ventilation system. Air is supplied near the floor, extracted at the ceiling and the heat source displaces the heat upwards due to buoyancy. Consequently, two different temperature zones are established.*

2.2 Computational fluid dynamics

Fluid dynamics is a branch of physics that concern fluid movement. Solving fluid- and thermodynamic calculations can be done using three different methods; experimental, theoretical and computational. The experimental method is the most realistic one, but it is costly and resource demanding. The theoretical method is simple and provides general information, often using mathematics. However, this method is limited by linear problems and difficult to implement when the calculations become more advanced. For these problems, computational fluid dynamics is the better choice. CFD calculations solves complicated physics and has no limitations in linearity. Although computers handle most of the calculations, it is vital to have a basic understanding of the theory and limitations of CFD to conduct the calculations. [15–18]

The finite volume method is a common technique used in CFD. This method can be used on all differential equations that can be written in the divergence form. Volume integral in the partial differential equation containing a divergence term is converted to a surface integral using Gauss's theorem, known as the divergence theorem. These terms are evaluated as fluxes on the surface of their respective finite volumes. The finite volume method is a conservative method because the flux entering the volume is identical to the amount leaving. [19]

When examining thermal fluids, they are characterised by governing equations based on the conservation law for the fluids physical properties. The three basic laws that govern this are; conservation of mass, conservation of momentum and conservation of energy. The conservation of mass is the continuity equation, while conservation of momentum is Newton´s second law, and conservation of energy is the first law of thermodynamics. Basically, these principles state that energy is conserved within a closed system. In addition, the momentum, mass and energy are constant parameters. [20]

Conservation of Mass

The continuity equation is shown in Equation 2.1. The equation presents how the transport rate of a quantity of mass that enters a system is equal to the amount leaving the system, plus the accumulation of mass within the system. In the equation ρ is the density, $\vec{v}$ is the velocity vector and ∇ is the gradient operator.

$$\frac{\partial \rho}{\partial t} + \rho \left(\nabla \cdot \vec{v} \right) = 0 \tag{2.1}$$

In cases where the fluid flow is assumed to be incompressible and the density is constant, the equation for continuity may be simplified. This is because the first part of the equation is neglected. In those circumstances, the gradient operator multiplied by the velocity vector is equal to zero. Thus, the equation can be rewritten as Equation 2.2. [20]

$$\frac{\partial \rho}{\partial t} = 0 \rightarrow \nabla \cdot \vec{v} = \frac{\partial u}{\partial x} + \frac{\partial v}{\partial y} + \frac{\partial w}{\partial z} = 0 \tag{2.2}$$

Conservation of Momentum

The conservation of momentum, which is presented by Newton´s second law, is often referred to as Navier-Stokes equation, shown in Equation 2.3. This equation is a cornerstone in fluid mechanics, and describes how pressure, velocity, temperature, and density of a moving fluid are related to each other. The equation can in theory be solved for any given flow by using calculus, but this is time consuming. Thus, it is more beneficial to solve these equations computationally. The static pressure is symbolised as p, while $\bar{\bar{\tau}}$ is the viscous stress tensor and $\vec{g}$ is the body accelerations acting on the continuum. [21]

$$\frac{\partial}{\partial t}(\rho \vec{v}) + \nabla \cdot (\rho \vec{v} \vec{v}) = -\nabla p + \nabla \cdot (\bar{\bar{\tau}}) + \rho \vec{g} \tag{2.3}$$

In situations where the fluid flow is assumed to be incompressible with a constant viscosity coefficient, the Navier-Stokes equation can be simplified, as shown in Equation 2.4. In the equation the viscosity coefficient is symbolised with μ. [20]

$$\frac{\partial}{\partial t}(\rho \vec{v}) + \nabla \cdot (\rho \vec{v} \vec{v}) = -\nabla p + \mu \nabla^2 \vec{v} + \rho \vec{g} \tag{2.4}$$

Solving Navier-Stokes equations for high Reynolds numbers can be time consuming. Therefore, the alternative method Reynolds-average can be implemented to simplify Navier-Stokes equation and make it more time-efficient. The Reynolds-averaged Navier-Stokes (RANS) equations control the transport of the average flow rates. RANS based modelling greatly reduces computational cost and resources, and is therefore widely used for practical applications. The Reynolds-Stress is the component of total stress in a fluid, which is found using RANS to account for the turbulent variations. [22–24]

Conservation of Energy

The conservation of Energy is presented by the first law of thermodynamics. This law states that the sum of the heat added to a system, dQ, plus the work done within the system, dW, equals to the energy change in the system, dE_t. This can be written mathematically, as presented in Equation 2.5. [20]

$$dE_t = dQ + dW \tag{2.5}$$

2.3   Heat transfer

One important distinction within heat transfer calculations is that heat and temperature are two different parameters. Heat is a quantity often measured in kWh, and heat flow is the movement of heat measured in watt. Contrarily, temperature is commonly measured in °C or K. Furthermore, temperature can be defined differently. One definition is static temperature, which is defined as the temperature that would be shown by a measuring instrument that has no relative velocity to the fluid stream being measured. [25, 26]

Heat transfer can occur by three different forms; conduction, convection and radiation. The three different forms are illustrated in Figure 2.2. From the figure it is visualised how the conduction is a heat flow process by molecular transportation. This can be along or through a material, as well as from one material to another. The material receiving the heat must be in contact with the warmer material. Radiation is a process where the heat is transmitted as energy across space. Convection is a process that occurs only in liquids and gases. Therefore, any solid material needs to be in contact with the fluid to lose or gain heat by convection. Convection happens because a temperature difference will change the density in different parts of the fluid. [25]
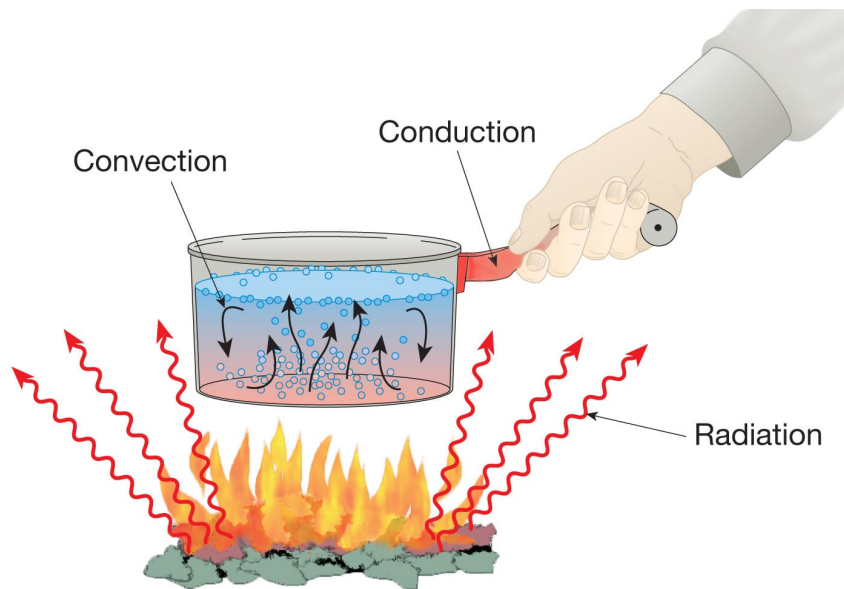
Figure 2.2: *Three different forms of heat transfer; convection, conduction and radiation. [27]*

Natural convection is a phenomenon which is a consequence of temperature differences across the space in an enclosure or heat transfer at surfaces. Natural convection happens without any external influence. Some substances, such as air, have a density heavily dependent on their temperature. Hot air has a lower density than cold air, and consequently hot air will rise in a cooler environment. Natural convection occurs because of buoyancy effects in gases. The buoyant force is an upward force that a fluid exerts on a body immersed in it. The density of a fluid is proportional to the buoyant force, thus the effects from gases can be neglected in many cases. Even though it can be neglected in many cases, the effect is essential for natural convection. This phenomenon is especially relevant for analysis of HVA/C systems, where subcooled air is supplied to cool a heated room. [24, 28]

The natural convection is important to take into account when performing CFD calculations to secure the most accurate result. It is especially important when doing CFD simulations of a room with a buoyancy-driven ventilation, which is the basic principle for displacement ventilation. CFD simulations in ANSYS Fluent accounts for the natural convection by setting the air density to incompressible-ideal-gas. This setting is calculating the density of air by using the ideal gas law for an incompressible flow, as shown in Equation 2.6. In the equation, p_{op} is operating pressure, R is the gas constant, M_w is molecular weight and T is temperature. [29, 30]

$$\rho = \frac{p_{op}}{\frac{R}{M_w} \cdot T}$$ (2.6)

The heat radiation energy is similar to radio- and light waves, thus it can take place without an intermediate medium for it to transfer, as well as across a vacuum. All bodies will emit radiant energy. The amount is decided by the temperature difference between radiating and receiving surfaces, the distance between the surfaces and the emissivity of the surfaces. Emissivity is the amount of radiation emitted or absorbed by a body in comparison to a black body in identical conditions. A black body is defined as a perfect absorber and radiator of energy, with non reflecting power. The emissivity is usually in the range of $0, 8 - 1$ for surfaces in constructions, where one is the value of a black body. [25, 31, 32]

Throughout thermal calculations the heat flux is a central parameter. This value is defined as the rate of heat energy transfer through a given surface. The heat energy can be expressed either per surface area, W/m^2, or as the total heat energy through the surface, W. Instances where more advanced analyses are required, the heat generation rate can be used. The heat generation rate is expressed as W/m^3. If the body being analysed is a solid, the ratio of total heat generation rate to the exposed surface area is equal to the average wall heat flux. [24, 33]

Another essential parameter associated with heat transfer calculations is the thermal transmittance, also known as U-value or heat transfer coefficient. The U-value is used to describe an element of structures ability to transmit heat under steady-state conditions. The value indicates how much heat that will flow through an area per time, per difference in temperature between the structure and the individual environments it intervenes with. In other words, it indicates the heat insulating trait of a material. U-value is expressed as $W/(m^2 \cdot K)$. [25]

2.3.1 Radiation Models

For systems including a heat source, which establishes high surface temperature, it is necessary to include heat transfer from radiation. Calculations involving radiation are complicated, thus radiation models that simplify the mathematics are indispensable. According to a study conducted by Menchaca-Brandan et al. regarding heat transfer calculations it was established that radiation had a significant impact. In the study, the temperature difference in the surrounding air was $2 - 4°C$ lower when radiation was ignored in simulations of a room with natural ventilation. Furthermore, the heat source was $17°C$ warmer when the radiation heat transfer was ignored. These results show the importance of radiation models in CFD simulations to gather accurate results. Consequently, it is important to consider which radiation model is the most suitable to utilise. The most common radiation models are:

- Discrete ordinates model (DO)
- Discrete transfer method (DTRM)
- Monte Carlo model (MC)
- P-1
- Rosseland
- Surface to surface (S2S)

A parameter that is often used to decide radiation model is the optical thickness. Optical thickness is defined as the absorption coefficient multiplied by the average length of the radiation beam. For optical thickness of zero, the S2S model is recommended. In cases where there are some uncertainties, the DO model is a convenient choice, due to the wide range of applicable cases. The DO model can be used for every value of optical thickness, and in cases with localised heat sources it is recommended by ANSYS user guide. The heat source is localised when all the generated heat comes from one or a few heat sources. [32, 34]

Considering the DO model is suitable for systems with localised heat sources, it is a fitting model for HVA/C systems with displacement ventilation. When the DO model is activated, it calculates the radiative transfer for a limited amount of discrete solid angles, each related with a vector direction fixed in the global Cartesian system. The level of accuracy with these discrete angles can be decided in CFD simulation programs. [35]

In addition to the recommendation from ANSYS user guide, the DO model has been used with satisfying results in previous studies. Some studies have also used P-1 or the DTRM models, but these particular models have limitations compared to the DO model. Regarding the P-1 model it typically estimates the radiation heat fluxes higher than they are in reality. The DTRM model needs a large amount of rays to get a reasonable result, thus the computational cost increases in comparison to the DO model. Therefore the DO model is confirmed as the most appropriate radiation model when a heat source is involved. [36–39]

2.4 Fluid flow distribution

Achieving a complete understanding of fluid flow distribution inside an enclosure is near impossible. In every realistic situation, the fluid flows are three dimensional. Moreover, fluid flow is dependent on numerous factors, making it difficult to obtain an accurate description of the distribution. Air distribution in a ventilated enclosure is a function of different factors, such as supply air jets and thermal plumes. Other important parameters are streamlines and turbulence. Obtaining a basic understanding of how these parameters affect air flow is imperative when designing an efficient ventilation system.

Supply air jets are used to distribute the incoming air, and to heat or cool the occupation zone. A free jet is produced when a fluid enters a large enclosure that is fully occupied by the same fluid in a relatively calm condition. A free air jet has two distinct features. Firstly, the jet will spread out into the enclosure in the shape of a cone. Secondly, the air velocity will gradually decrease with an increasing distance from the inlet. These features are illustrated in Figure 2.3. The air jet trajectory is affected by the air mass rate, the shape of the diffuser and objects in the enclosure. Simultaneously, when the air jet is used for cooling, it will have a downward curve when entering because of having higher density than the surrounding air. [40]
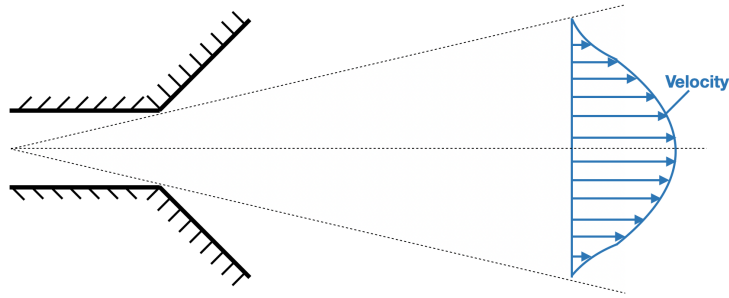
Figure 2.3: *The velocity and shape of a free air jet entering an enclosure.*

Thermal plumes are generated over objects that have a higher surface temperature than the surroundings. Example of such objects are industry equipment. The presence of such heat sources disturbs the equilibrium of air inside the enclosure, resulting in a continuous replacement of air. As a result of buoyancy, hot air jets are created above the heat sources. The maximum velocity of these jets is just above the heat source. Temperature gradients in the enclosure will emerge due to thermal plumes. When designing systems that takes advantage of this effect, such as displacement ventilation, it is necessary to determine the amount of air that creates the preferred temperature gradient. [40, 41]

Fluid flow can be described by Eulerian's description, named after the Swiss mathematician Leonhard Euler. In this description there is a defined finite volume that is a control volume, also called a flow domain. Fluid flows in and out of this domain. In the Eulerian description, the fluid particles are not observed individually, but rather as field variables that are functions of time and space within the flow domain. For example, the velocity field variable, $\vec{V}$, can be defined as a function of location, x, y, z, and time, t, as shown in the Equation 2.7. [24]

$$\vec{V} = \vec{V}(x, y, z, t) \tag{2.7}$$

Streamlines are excellent indicators of the instantaneous direction in which the fluid moves through a flow field. The streamline is the path that is traced out by a massless particle moving along the flow. As written by Yunus A. Çengel and John M. Cimbala in their book of Fluid Mechanics: *A streamline is a curve that is everywhere tangent to the instantaneous local velocity vector.* Streamlines cannot be directly observed, unless there is a steady flow field, but they are suitable to illustrate the fluids movement in a flow domain.

The mathematical definition of a streamline is presented in Equation 2.8. In combination with Figure 2.4 the equation can be interpreted where $\vec{V}$ is the velocity vector, and u and v are the decompressed directional velocity vectors in the x and y direction. $\vec{dr}$ is the arc length, and dx and dy are the directional arc length in the x and y direction. Furthermore, dr is the magnitude of $\vec{dr}$ and V is the speed, the magnitude of velocity vector, $\vec{V}$. Due to the figure being two-dimensional dz and w are not included, but this would be the arc length and the velocity in z direction. [24, 42]

$$\frac{dr}{V} = \frac{dx}{u} = \frac{dy}{v} = \frac{dz}{w} \tag{2.8}$$
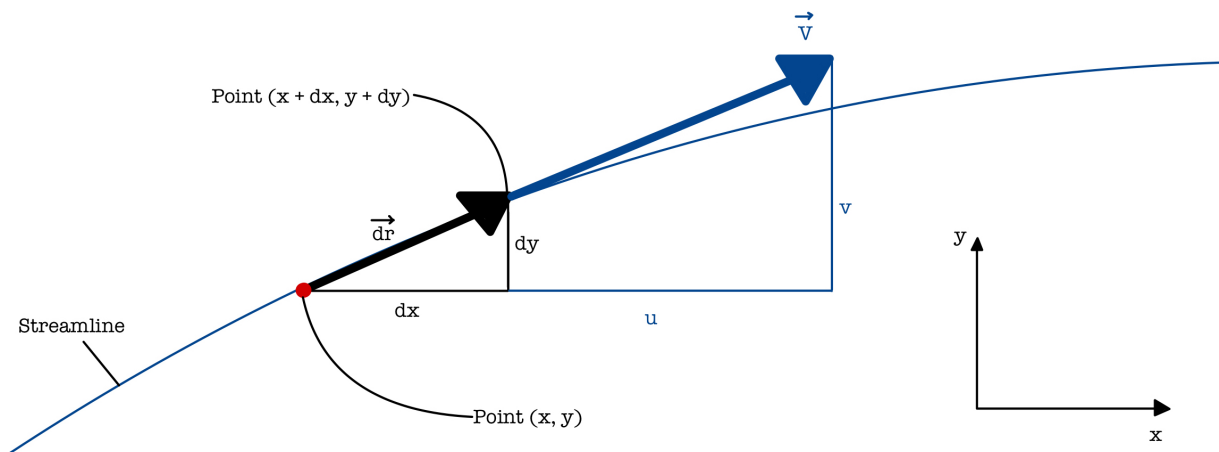
Figure 2.4: *Two dimensional flow where the arc length $\vec{dr} = (dx, dy)$ along a streamline is everywhere tangent to the local velocity vector $\vec{V} = (u, v)$. [24]*

2.4.1 Flow disruption

A basic understanding of how the extraction arrangements affect the flow pattern in an enclosed space is of much relevance when examining the design of ventilation systems. Most fluid flows are turbulent, and it is therefore vital to have a basic understanding of the influence that turbulence applies to the wall shear stress. Turbulence is a very complicated matter, consequently turbulence relied experiments and the empirical correlation are developed for various situations. [24]

Turbulent currents are characterised by rapid disordered oscillations in areas of the liquid. These oscillations run throughout the fluid and are called eddies. The oscillating currents are shown in Figure 2.5. From the figure it is visible how the currents cover a larger area over time. As a consequence of these oscillations, an additional mechanism for velocity and energy transfer is emitted. A consequence of turbulent flow is that mass, momentum and energy are transported faster relative to a laminar flow. Thus, turbulent flow is associated with high values of friction, heat transfer and mass transfer coefficients. [24]
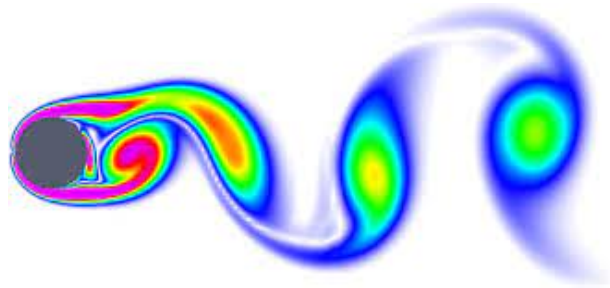
Figure 2.5: *Illustration of eddies which occur behind a solid cylinder. [43]*

Coandă effect is a phenomena discovered by the Romanian aerodynamics pioneer Henri Coandă. This phenomena refers to the situation where a fluid flow connects to a surface. Even if the surface changes direction, the fluid flow will remain connected to the surface. When this phenomena occur, a negative pressure will develop between the air pressure and the surface. Subsequently, the air velocity will slowly decrease, and the air will reach further into the enclosure. This affects the air throw length, which is a term used to describe how far into an enclosure the air travels. The Coandă effect will cause the air to circulate in an enclosure, which leads to a more effective mixture of air. The Coandă effect is illustrated in Figure 2.6. From the figure it is visible how swirls of air occur near the surface area. This is due to the negative pressure which occur. This negative pressure is the same that is causing diffusers to become dirty, since dust particles are drawn back towards the diffuser. [44]
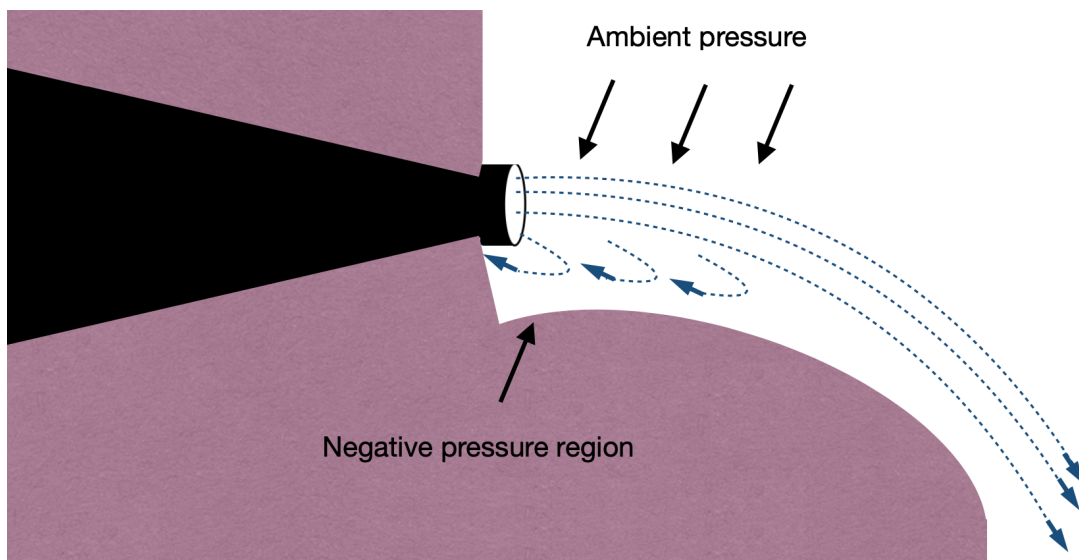
Figure 2.6: *Coandă effect occur due to the curved wall on one side of jet. This effect creates a negative pressure region which influence the air trajectory.*

Figure 2.7 illustrates a ventilated room where eddy and Coandă effect arise in an enclosure. The fluid flow enters the system on the right side of the figure. It is visible how the fluid follows the surface of the wall, as a result of the Coandă effect. Furthermore, this adhesion leads to development of eddies. The size of the inlet will influence the extent of eddies that occur in the enclosure. Eddies will increase in size with narrower inlets. The inlets placement will affect the size, amount and location of eddies. Thus it is essential for the ventilation system to evaluate the inlets location for its purpose. On the other hand, the location of the outlet will have a small impact on the eddy development, but instead plays an important role in extracting the air. If the outlet is located close to the ceiling, it will be effective for extracting warm air, as the warm air rises due to a lower density. [40]
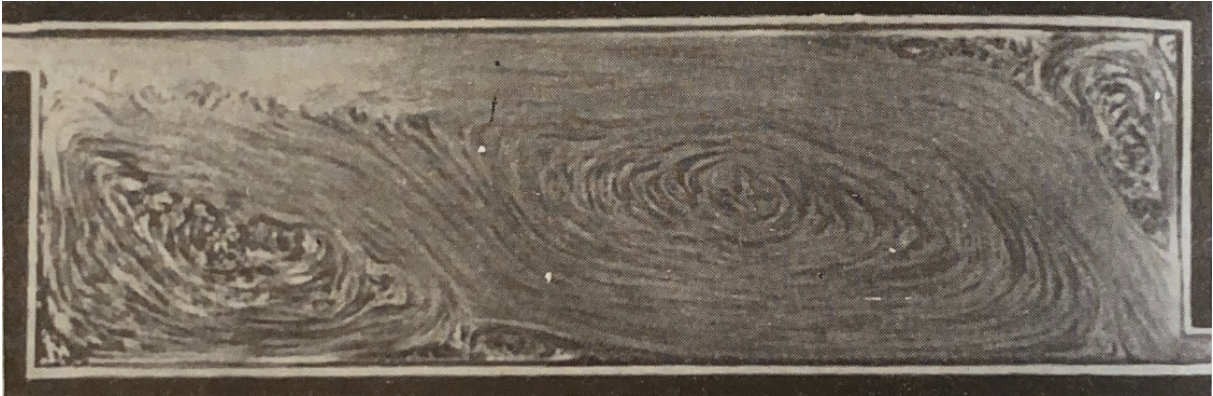

Figure 2.7: *Air circulation in an empty enclosure, where air is supplied at floor level and extracted by the ceiling. The air distribution is affected by the eddy and Coandă effect. [40]*

2.4.2 Turbulence models

Calculating turbulent flow is often a very complicated procedure. A precise simulation of a turbulent flow is usually not possible due to computer limitations. Consequently, different turbulence models are used to simulate turbulent flows. There are a variety of turbulence models with different level of complexity. An ideal turbulence model capture the essence of the relevant physics and provide accurate results, with the least amount of computational cost. [24, 45]

The most common turbulence models are called RANS Eddy-Viscosity models. These models are classified by the number of transport equations used. The transport equations can be time-averaged, ensemble-averaged or manipulated in other ways to make the simulations easier computationally. Fewer equations leads to more approximation of variables. There is no conclusion on which turbulence models are the most suited for various problems. Thus, before simulating it is a necessity to consider the turbulence model based on the preconditions of the problem. [46]

A relevant law regarding turbulent flow near solid boundaries is the law of the wall. This law describes the behaviour of both internal and external flows near walls. An external flow is an unbounded fluid flowing over a surface and an internal flow is a fluid bounded by a surface. For these kinds of flows the streamwise velocity near the wall will vary logarithmically with the distance from the surface. [45]

By observing high Reynolds number turbulent boundary layers, an approximate description of turbulence statistics on the near-surface is revealed. The observation shows that the effect of the fluid´s inertia and the pressure gradient are relatively small close to the surface. Therefore there are two primary mechanisms that impact the flow near the surface in a turbulent boundary layer. These two mechanisms are the rate at which momentum is transferred to the surface, and the molecular diffusion of momentum. The rate at which the momentum is transferred to the surface is given per unit area per unit time, thus it is equal to the local shear stress. In addition to this, the observation indicates that the details of eddies far from the surface are of little importance to flow statistics near the wall.

The local shear stress will vary near the surface, but the variation with distance from the surface, y, is fairly slow. Therefore, the surface shear stress, τ_w, can be used instead of the local shear stress. Turbulence behave the same way in gases and liquids, and therefore the two dimensional quantities, τ_w/ρ and kinematic viscosity, ν, are set as the primary dimensional quantities. Due to the dimensions of the quantities, a velocity scale, u_τ can be defined as shown in Equation 2.9. The velocity scale is also known as the friction velocity, and represents the velocities close to a solid boundary. [45]

$$u_\tau = \sqrt{\frac{\tau_w}{\rho}} \tag{2.9}$$

A typical velocity profile for a turbulent boundary layer can be described with a dimensionless velocity, u^+, and a dimensionless distance, y^+. They are defined as shown in Equation 2.10 and 2.11. In the equation the U is the mean velocity in x direction.

$$u^+ = \frac{U}{u_\tau} \tag{2.10}$$

$$y^+ = \frac{u_\tau \cdot y}{\nu} \tag{2.11}$$

Figure 2.8 illustrates how a turbulent boundary layer is divided into three distinct regions. These regions are called the viscous sublayer, the log layer and the defect layer. Even though the log layer is marked as an own distinct layer in the figure, it is not. It is marked as a distinct region for simplicity. In reality it is a region where the sublayer and defect layer merge, thus it is a overlap region. This is the area where the velocity is accurately represented by the law of the wall. The dotted linear function in the plot represents the law of the wall. By comparing it to the velocity profile, it reveals that the law of the wall is only applicable for y^+ values in excess of around 30 and up to around 600. It is applicable in this range because of the overlap between the law of the wall and the velocity profile. [45]

During CFD simulations the y^+ values should be located in the log layer in the interval $30-300$. The most desirable part of the interval is y^+ values close to the lower boundary. Adjustments of the y^+ values for simulation purposes are done in the mesh. When setting up a mesh it should be made to prevent y^+ values around $5-30$ to stay away from the buffer layer. It is also possible to use enhanced wall treatment, which require the y^+ values to be within the range of $1-5$. The y^+ values decreases with finer mesh, therefore some caution must be taken to avoid the range of $5-30$. [47]
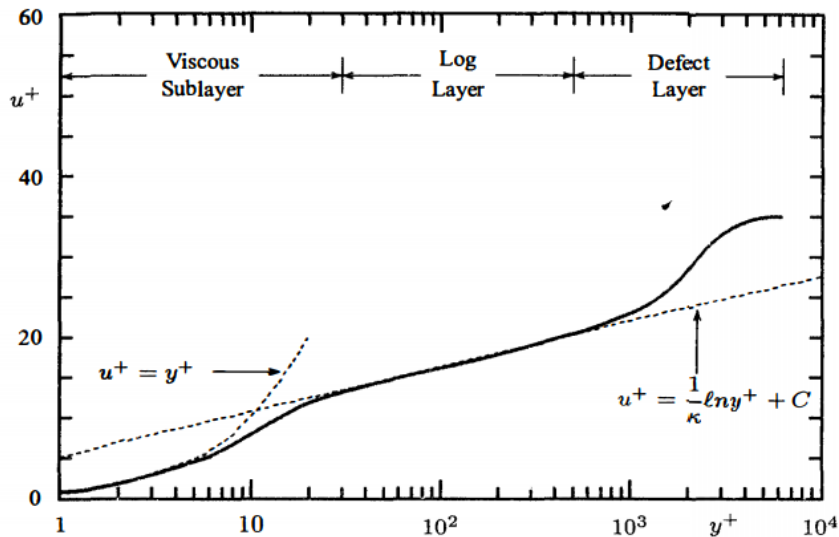
Figure 2.8: *Three distinct regions in a typical boundary layers velocity profile. The plot visualises u^+ as a function of y^+. The dotted linear line represents the law of the wall and the solid line is the velocity profile. [45]*

Two-equation models

Two-equation models are turbulence models which are based on the equation for the turbulence kinetic energy, and they retain the Boussinesq eddy-viscosity approximation. To achieve a better understanding of two-equation models, there are some important quantities that need to be defined. The first one is called the specific turbulence kinetic energy, κ. The quantity is the kinetic energy of the turbulent fluctuations per unit volume, and is proportional with the trace of the Reynolds-stress tensor. Another important quantity is the dissipation per unit mass, ϵ. The last highly relevant quantity is the specific dissipation rate, ω. In addition to providing computation of κ, the two-equation models provide the turbulence length scale or equivalent. Due to this, the models can be applied to predict properties of a turbulent flow, although there are no prior knowledge of the turbulence structure. [45]

$\kappa - \epsilon$ models

The $\kappa - \epsilon$ model is the most common two-equation model with a large number of variants. Originally, the standard $\kappa - \epsilon$ model was developed for flows with high Reynolds number. For models with flow consisting of low Reynolds number, it is often used wall functions to connect the near-wall flow and the outer-wall free stream. With wall functions the standard $\kappa - \epsilon$ model is capable of predicting airflow and turbulence reasonably well. [45, 48]

$\kappa - \omega$ models

The $\kappa - \omega$ models use the dissipation per unit turbulence kinetic energy, in addition to the specific turbulence kinetic energy as parameters. These models have had an increasing usage in the last decades. The strengths of the $\kappa - \omega$ models are the accuracy in attached boundary layers, mildly separated flows and backward-facing steps. Furthermore, it is applicable to both free shear and wall-bounded flows due to the models quality in the prediction to free shear flow spreading rates. [45, 48]

In the matter of predicting equilibrium adverse pressure flows, the $\kappa - \omega$ models are superior compared to the $\kappa - \epsilon$ models. In addition, the $\kappa - \omega$ models are less robust in wake region and free-shear flows. Due to the superiority of the $\kappa - \omega$ models near walls, an integrated model was developed to obtain the best attributes from both models. This model is called shear stress transport (SST) $\kappa - \omega$ model. When this model is activated, it will use a $\kappa - \omega$ model near wall boundaries, and in the regions far from walls, it is transformed to a model equivalent to a $\kappa - \epsilon$ model. This is visualised in Figure 2.9. The type of model on a given time is controlled by blending functions, which decide what model is most appropriate for that specific time. [45]
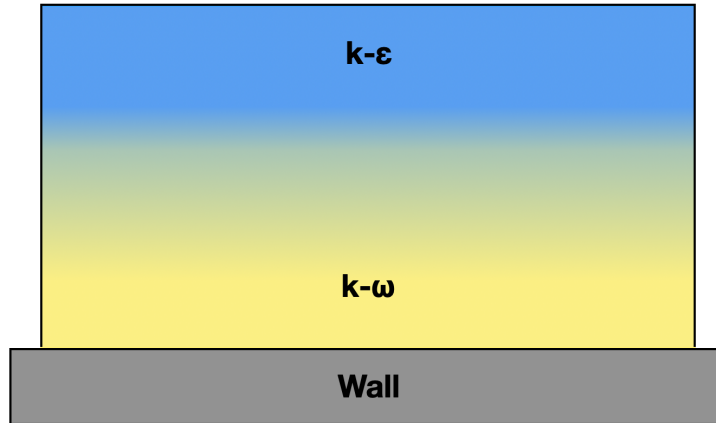
Figure 2.9: *Illustrates how the SST turbulence model is an integrated model between $\kappa - \omega$ and $\kappa - \epsilon$.*

The best possible turbulence model for a given simulation is difficult to establish. The only way to determine if the chosen model is correct, is to either compare the results to real life measurements or by doing a literature study. Real life measurements are impossible to obtain in many circumstances, thus calculations and literature studies of similar cases are often the only possible method of deciding a turbulence model.

In situations where there are one or a few localised heat sources, combined with displacement ventilation, it appears that the $SST \kappa - \omega$ model provides the most accurate result. A similar environment was simulated with standard $\kappa - \epsilon$, realisable $\kappa - \epsilon$, RNG $\kappa - \epsilon$, S $\kappa - \omega$ and SST $\kappa - \omega$ as turbulence models. The simulations gave an average deviation from measurements on respectively $7,0\%$, $7,9\%$, $5,6\%$, $4,9\%$ and $4,2\%$. In another simulation performed in a similar environment the SST $\kappa - \omega$ model had an average deviation of $4,42\%$, which was the lowest value compared to the other considered turbulence models. These results indicate that the SST $\kappa - \omega$ model has the most reliable results for a room with displacement ventilation and a heat source. [29, 49]

2.5 Meshing

The partial differential equations, which control fluid flow and heat transfer, are normally not susceptible to analytical solutions. For that reason, flow domains are divided into smaller subdomains through a process called meshing. These subdomains are commonly named elements. Two dimensional elements consist mainly of squares and triangles, while in three dimensions, tetrahedron, hexahedron, polyhedron, wedge and pyramid are common. The three dimensional elements are illustrated in Figure 2.10.


Figure 2.10: *The most common types of three dimensional mesh elements.*

Each element type has several variations, which specify the quantity of nodes they contain. Some of these are called Tet4, Hex8, Wed6 and Pyr5. The number is referring to the amount of nodes which the element consists of. The computer uses these elements as control volumes where various mathematical equations are calculated. Meshing will greatly impact the final solution accuracy, and it is therefore vital to ensure that the mesh is adequate for the analysis. The number of nodes and elements is a good measurement of how accurate the mesh is. Each node is a specific location in the computational domain. An element is a small volume that is created when nodes are connected together. More nodes and elements provide a more precise simulation, although an overly defined mesh will have a negative impact on the computational cost. [24, 50]

Ordinarily, mesh is classified into two different forms; structured- and unstructured mesh. These different forms of mesh are illustrated in Figure 2.11. Structured mesh consists of elements with the same size and form, and is visualised in Figure 2.11a. This kind of mesh makes it possible to easily identify the nodes and elements. Structured mesh consists of hexahedric elements for three dimensional purposes, and quadrilateral for two dimensional. Unstructured mesh, visualised in Figure 2.11b, consists mainly of tetrahedrons for three dimensional purpose, and triangles for two dimensional. The unstructured type of mesh will have varying size and shape. Furthermore, this mesh provides a more accurate replication of the actual geometry, but it requires more computational cost. Finite volume method solvers has the advantage that it easily allows for unstructured meshes. [51].
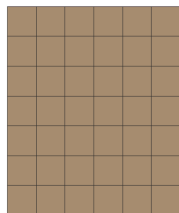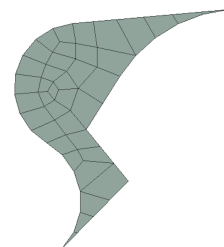
(a) *Structured mesh.*   (b) *Unstructured mesh.*

Figure 2.11: *An distinction within mesh grids. Structured mesh includes elements with equal size and shape, while unstructured mesh contains elements with varying size and shape.*

A good quality mesh is dependent on well-defined and coherent geometry. A good geometry is free from sharp outcropping and distinct features, which often create skewed and inaccurate meshing. To achieve good mesh quality it is often necessary to neglect geometry that do not affect the results. Furthermore, an enclosed geometry ensures that the solver can distinguish between different types of solids and fluids. Most meshing programs have ways of reviewing the mesh to ensure that it is sufficient. Reviewing the mesh means that each element is studied independently in terms of size and shape. A good mesh contribute to a more accurate solution and faster simulation. Two important parameters to inspect are orthogonal quality and skewness.

Skewness is a measure of how ideal the shape of a face or an element is, measured in the interval $0-1,00$. In Figure 2.12 it is visible how a skewness between $0-0,25$ is an Excellent skewness that indicates a good quality mesh. On the other side of the spectrum, it is suggested that a skewness between $0,98-1,00$ is an Unacceptable result that indicates an inadequate mesh. Skewness is the difference between the cell shape and the shape of an equal cell with a corresponding volume. A large skewness will reduce the accuracy of the results. In general, the rule is that the maximum skewness for a triangular/tetrahedral network in most streams should be below $0,95$, and with an average value that is less than $0,33$. At a maximum value above $0,95$ it can lead to difficulties in reaching convergence. [52]
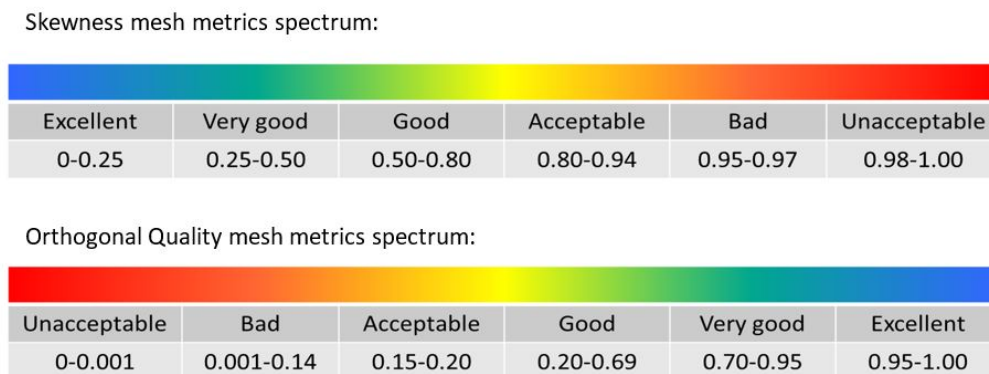
Skewness mesh metrics spectrum:

Excellent	Very good	Good	Acceptable	Bad	Unacceptable
0-0.25	0.25-0.50	0.50-0.80	0.80-0.94	0.95-0.97	0.98-1.00

Orthogonal Quality mesh metrics spectrum:

Unacceptable	Bad	Acceptable	Good	Very good	Excellent
0-0.001	0.001-0.14	0.15-0.20	0.20-0.69	0.70-0.95	0.95-1.00

Figure 2.12: *Skewness and orthogonal quality categories. [53]*

Mesh orthogonality is a concept that represents how close the angles between adjacent element surface or element edges are in relation to an optimal angle. Depending on the topology of the geometry. Orthogonal quality is a measure of how satisfactory mesh orthogonality is designed. This quality is measured in the interval of $0-1,00$. According to ANSYS learning manual, which is presented in Figure 2.12, a value of $0-0,001$ is in the range of Unacceptable and a value of $0,95-1,00$ is in the range of Excellent.

The mesh quality of a topology will vary over a curved object, as visualised in Figure 2.13. Figure 2.13a and 2.13b visualises the variation of skewness and orthogonal quality respectively. For both of the figures, the red colour illustrates a bad quality mesh, with high skewness and low orthogonal quality. The blue colour illustrates a good quality mesh, with low skewness and a higher orthogonal quality. The figures show that curved geometry needs to have a finer mesh compared to a straight surface to obtain desired mesh quality, according to the skewness and orthogonal quality. [50]
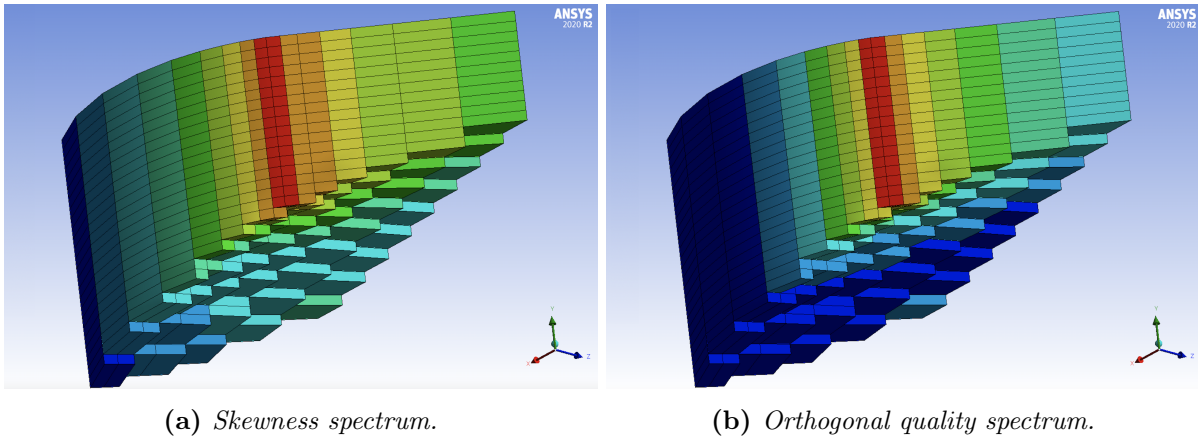
(a) *Skewness spectrum.*   (b) *Orthogonal quality spectrum.*

Figure 2.13: *Change in skewness and orthogonal quality over a curved object, caused by the angular differences.*

To improve skewness and orthogonal quality element sizing at critical points, such as face sizing, can be implemented. This allows a finer mesh in certain parts of the domain by lowering the element size. Figure 2.14 depicts how face sizing is used to create a finer mesh on one of the faces, as well as how the face sizing impact bigger parts of the domain and not just the face. Creating a finer mesh is important close to the boundaries and near points of interest. The reason for this is to ensure that the simulation executes precisely and converges. In other parts of the domain, the mesh can be coarser to save computational cost.
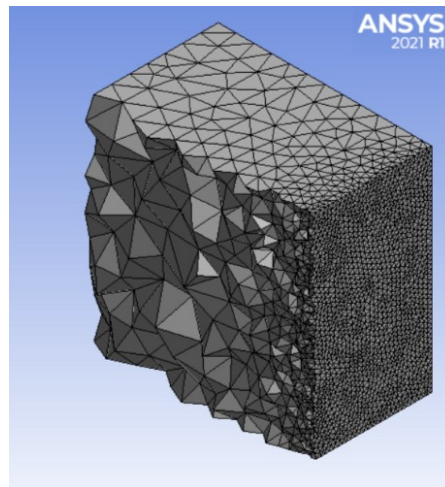

Figure 2.14: *Illustration of how the face sizing function changes the element sizes through parts of the cube and not only the applied face.*

Simulations should be performed with a different number of elements to determine the ideal number of elements for an accurate result. This is called a mesh independence study. A mesh independence study is done by first creating a good quality mesh and then run a simulation with it. Afterwards, the process is repeated multiple times with continually increasing mesh fineness until the results are satisfactory. The results are satisfactory when the deviation between the simulation results are within a tolerance limit, often $1-5\%$. The mesh with the least amount of nodes and elements, which still provides results within the deviation criteria is the optimal mesh. Namely because this is the mesh that provides accurate results at the lowest possible computational cost. [54]

2.6 Boundary conditions

To separate fluid domains from solids in the computational domain it is important to implement boundaries. One vital boundary is that of a wall, which is used to contain a fluid. At solid wall boundaries, either the wall temperature or the wall heat flux must be specified. The wall heat flux is defined as the rate of heat transfer from the wall to the fluid. However, if both of these parameters are specified it will be overspecified. Hence, if for instance the wall temperature is specified by the user, the program will compute the heat flux, and vice versa. [24]

In regard to defining the boundary conditions there are not always a recognised heat flux through the wall. In these instances there will continuously be a heat transfer either from or to the fluid domain from external spaces. When modelling heat transfer through walls in ANSYS Fluent there are five distinct thermal boundary conditions to select. In addition to the fixed heat flux and fixed temperature there are convective, radiation and a combined radiation and convection model. To use the convective heat transfer the input values are the heat transfer coefficient and the free stream temperature, which is the temperature outside the domain. The input for the radiation heat transfer model is external emissivity and external radiation temperature. For the combination of the two, all four input values are indispensable. [55]

Two other essential boundaries are inlet and outlet. They govern the amount of fluid that enters and leaves the computational domain. These boundaries are mainly specified by velocity or pressure. If the inlet or outlet is specified by velocity, the velocity of the fluid flow along the face of the boundaries is stated. Additionally, if it is a pressure inlet the total pressure along the inlet face is specified. Furthermore, with a pressure outlet it is the static pressure along the outlet face that must be specified. In circumstances where pressure outlets are utilised, the atmospheric pressure is often applied. [56]

During CFD calculations there are a number of challenges that occur while trying to achieve a setup to work as intended. The first challenge appear when modelling the inlet and outlet. To achieve air flow through the inlets and outlets, they need to be in the outer boundary of the fluid domain. For instance, if the inlet is placed within the outer walls, then the stream will not enter the fluid domain. This problem is visualised in Figure 2.15. The figure shows how the air flow is trapped inside the inlet and outlet, instead of flowing into the room. [24, 56]
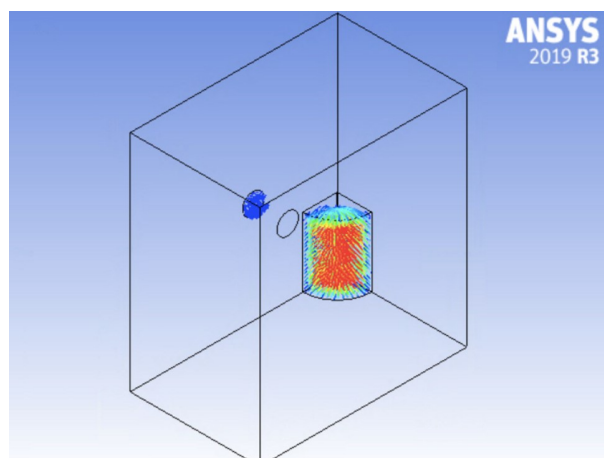

Figure 2.15: *Poorly modelled inlet and outlet, where the air is not supplied or extracted within the domain.*

Another specification that needs considering is the cell zone conditions. When a radiation model is activated it is important to activate the participating in radiation for each domain. If the fluid domain is not participating it is equivalent of having no radiation model activated. In addition to activating the radiation model the operating conditions needs to be specified. When simulating with the air density set as incompressible ideal gas, it is necessary to specify the operating density of the fluid domain. The cell zone condition is where the heat source parameters are set. [32]

2.7 Sources of error during CFD

CFD is a great tool for analysing problems that are near impossible to solve without computational help. However, CFD analyses can only provide an approximation to a problem and it can be difficult to evaluate if the results from the analysis are accurate compared to reality. Consequently, it is important to be aware of the different sources of error that affect the simulation results. Some of these errors are related to computational limits.

One of the errors is the rounding error, which is due to the difference between the exact value of a number, and the value it is stored as in the computer. The error is caused by computers calculating numbers to a certain numerical precision. Computers cannot store a number with infinitely many decimals, hence a small source of rounding error will occur. Rounding errors can cause large length scales and variable ranges, as well as high grid aspect ratios. In ANSYS, this source of error can be reduced by using the double precision solver. Double precision uses 64 bit to represent a number, while the ordinary single precision solver uses 32 bit. Hence, the disadvantage of implementing double precision is that it requires more storage space. [57, 58]

Truncation error is a source of error that occurs due to the difference between the partial derivation in governing equations and their discrete approaches. In the event of rapid changes in cell volume between adjacent cells, it will develop larger truncation errors. The truncation error is directly a function of the grid quality and flow gradient. Hence, this defect can be adjusted by improving the smoothness by refining the mesh. Truncation errors occur to keep the computational cost down, and is therefore an expected error to a reasonably degree. [50, 57]

The number of iterations is closely related to residuals. Residual error is a measure of how far from the regression line the data points are. It is preferable to have a low residual root-mean-square (RMS) error. For many instances a residual RMS error of $10^{-4} - 10^{-5}$ is sufficient. When the residuals have reached this set tolerance limit, the solution have converged. However, in many incidents the solution converges slowly and requires several thousand iterations. If the residuals become stationary, the total heat transfer rate can be used to validate if the simulation is converged. If the value is close to zero or below, the simulation have converged. [59]

Residuals, convergence and computational errors are closely related. Another important term in this regard is stability. Numerical stability imply that an error is not allowed to grow as the calculation proceeds from one iteration to another. If a simulation has poor stability it can often lead to what is called a floating point error. This error message occurs when the computer must do something that is mathematically impossible, such as division by zero. This is equivalent to the solution diverges, which is the opposite of convergence. [57]

3 Methodology

This section will regard the working process of the thesis and how the results were obtained and analysed. First, an introduction to the different software and their main functionality will be provided. Furthermore, it will be elaborated how the simulation was conducted. Mainly, this include how the geometry was modelled, the meshing strategy and parameter setup for the two simulation scenarios.

3.1 Software

Several software were required during this thesis. A literature study and skill development in the various software had to be carried out to obtain the results. NavisWork was used in order to obtain the geometry from data provided by Aibel. Afterwards, the geometry was modelled in the computer-aided design (CAD) software; SolidWork, ANSYS- DesignModeler and SpaceClaim. Each software have different strengths within modelling. Furthermore, ANSYS- Mesh, Fluent and CFD-post were used to execute the simulations and process the results.

NavisWork

NavisWork is a three dimensional design review software made by the Sheffield based company NavisWork, and was purchased by AutoDesk in 2007. NavisWork is used for project review to evaluate and improve coordination. NavisWork combines design- and construction data in one simple model. NavisWork also opens up the possibility of merging data from different subject areas to gain a better understanding of the complete system. [60, 61]

SolidWorks

SolidWorks is a complete three dimensional software tool which is offered by Dassault Systèmes SolidWorks Corp. It is a CAD software which was founded in 1993, and published in 1995. The software uses the principle of parametric design. SolidWorks software supports different three dimensional files, thus it is possible to use SolidWorks together with other simulation programs, such as ANSYS. [62, 63]

ANSYS

ANSYS was founded by Swanson Analysis System Inc. in 1971, and one year after its founding, the software was launched. The ANSYS package contains a variety of simulations and CAD software for engineering problems. Among these are; ANSYS- Fluent, CFX, DesignModeler, SpaceClaim, Mesh and Post-processing. All the different software are accessible from ANSYS Workbench which enables the user to perform several tasks from one interface. [64, 65]

3.2   Geometry

The geometry of the two systems were evaluated through NavisWork, and replicated through various CAD software. Simplifications were made to make the modelling phase easier and reduce the computational cost. The simplifications mainly included removing unnecessary components that had a negligible effect on the simulation results.

3.2.1   Auxiliary transformer room

The first system that was analysed in the thesis is a relatively small room containing an auxiliary transformer. The purpose of the transformer is to supply low voltage for different alternating current power systems. The auxiliary transformer room is modelled with a combination of SolidWorks and DesignModeler in ANSYS. The dimensions of the systems are listed in Table 3.1. Besides the transformer, the room also consists of one inlet and one outlet. The HVA/C system is based on displacement ventilation, where the inlet is placed near the floor and the outlet near the ceiling. The geometry model is shown in Figure 3.1. The room is simplified when modelled to keep the computational cost down. Hence, only the objects that affect the HVA/C system significantly are included in the model. Components like speakers, cables and fire extinguishers were neglected.

Table 3.1: *Dimensions for the auxiliary transformer room.*

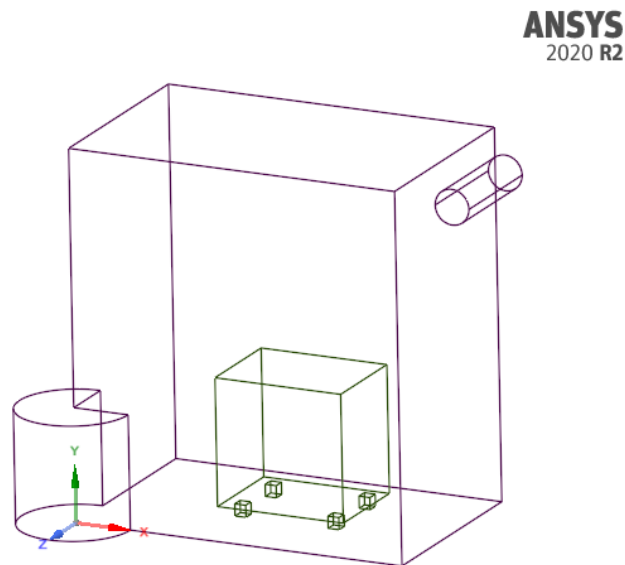| Geometry	Value
Height room	6, 50 m
Length room	6, 00 m
Width room	3, 75 m
Transformer volume	8, 98 m^3

Figure 3.1: *Geometry model of the auxiliary transformer room.*

3.2.2 Valve hall

The second system is a valve hall, which is one of the biggest rooms on the converter platform. For comparison, the valve hall is approximately 100 times bigger than the auxiliary transformer room. The purpose of the valve hall is to finalise the conversion from alternating current to direct current. The valve hall contain twelve valves and a smoothing reactor that act as the main heat sources. The valve hall is modelled on the same principle as the transformer room. Since the valve hall is considerably larger and more complex, even more geometry was disregarded during modelling. The dimensions for the valve hall are listed in Table 3.2, and the complete geometry is shown in Figure 3.2. The valves and smoothing reactor are modelled as twelve cubes and one cylinder respectively. The components legs were neglected in the model to save computational cost. Additionally, there are eight inlets on floor level and eight outlets in the ceiling.

Table 3.2: *Dimensions for the valve hall.*

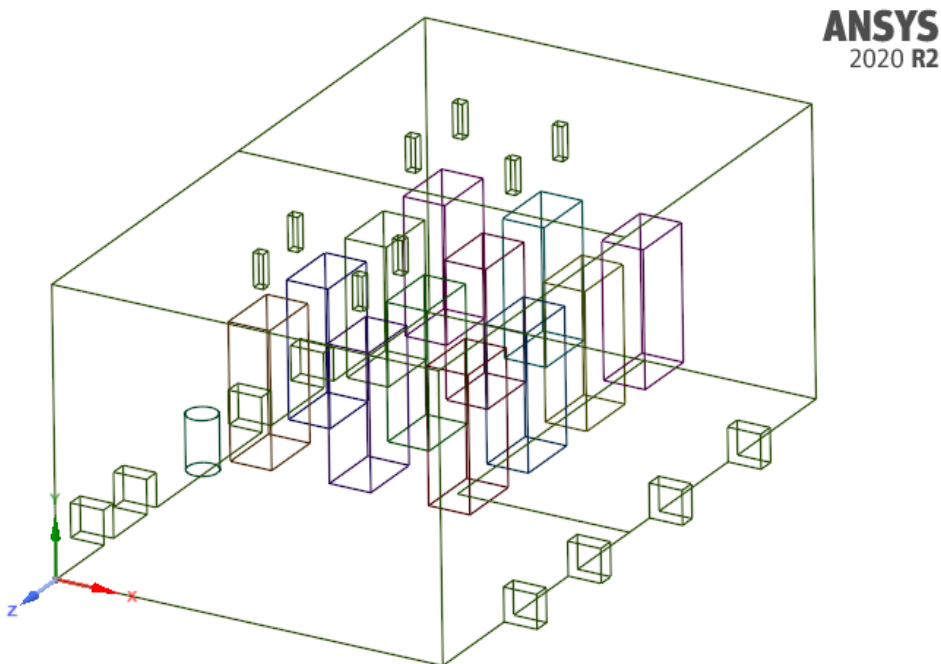| Geometry	Value
Height room	$16,90$ m
Length room	$39,00$ m
Width room	$23,40$ m
Volume of valves	$960,00$ m^3
Volume of smoothing reactor	$8,14$ m^3

Figure 3.2: *Geometry model of the valve hall.*

3.3 Meshing

The process of creating the mesh for the simulations in this project consisted of three steps. Firstly, a mesh was generated through ANSYS Mesh and an independence study was conducted to establish the necessary number of nodes and elements. Secondly, the elements were redistributed in the simulation domain to guarantee that calculations run smoothly and precisely in areas of importance. Thirdly, the mesh was reviewed to ensure that important parameters, such as skewness, orthogonal quality and y^+ values were within tolerable limits.

The mesh independence study was done by changing the number of elements and study how this affected the simulation results. In the independence studies it is examined how the mesh affects the average air temperature inside the two different systems. To create a mesh that provides accurate results, face sizing was used on the inlet, outlet, heat sources and the walls. Concurrently, the mesh remains coarser in areas with less gradients, where temperature and airflow are more static. The element distribution for the two rooms is listed in Table 3.3. Noncritical surfaces are represented by Fluid domain in the table. The valve hall has a significantly coarser mesh, because the room is larger and more complex compared to the auxiliary transformer room.

Table 3.3: *The element size used for the different sections of the systems.*

Section \ System	Auxiliary transformer room	Valve hall
Fluid domain	300 mm	750 mm
Inlet	70 mm	200 mm
Outlet	130 mm	200 mm
Smoothing reactor	–	500 mm
Transformer/Valves	70 mm	750 mm
Walls	250 mm	280 mm

The mesh distribution for the auxiliary transformer room and valve hall is shown in Figure 3.3 and 3.4 respectively. The figures show a section plane of the two mesh domains and they visualise how the composition of elements is greater around the heat sources, the inlet and outlet. Consequently, the mesh is finer near the boundaries and coarser in other parts of the domain. The main reason for this is to ensure that the simulation yields accurate results in important parts of the domain.
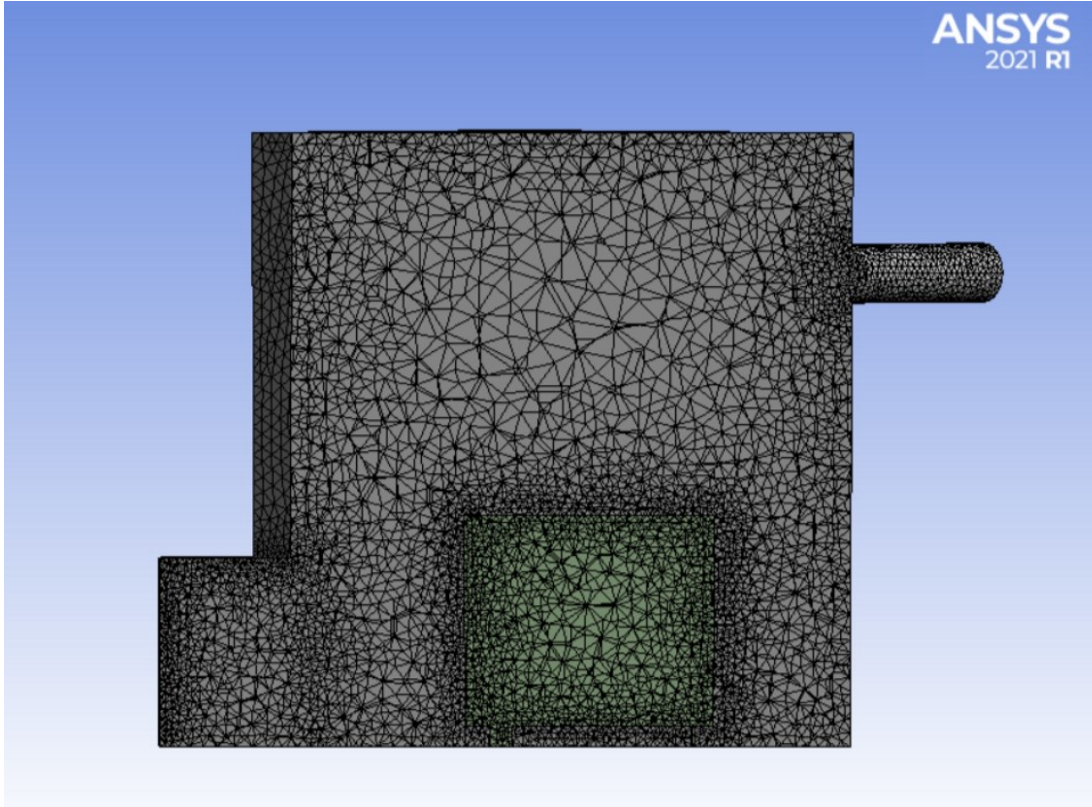
Figure 3.3: *A section plane of the mesh, which shows the mesh distribution across the auxiliary transformer room.*
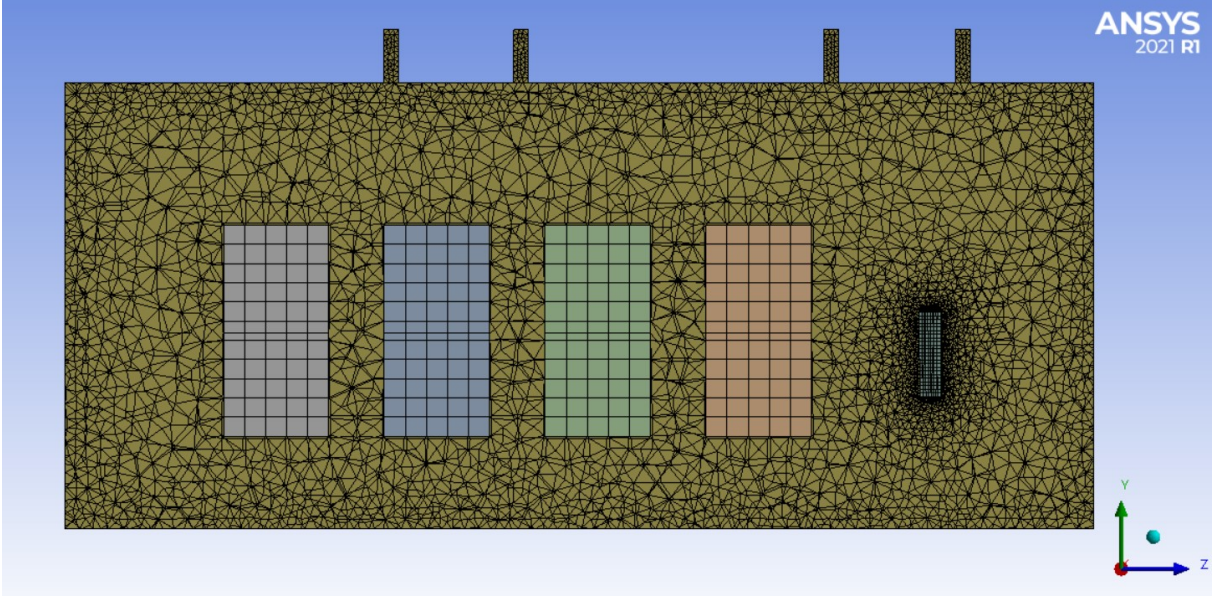

Figure 3.4: *A section plane of the mesh, which shows the mesh distribution across the valve hall.*

3.4 Setup

For both systems it is of interest to establish if the planned HVA/C system is capable of maintaining the temperature beneath the design limit. To review these issues it is accounted for the worst case scenario. Hence, the CFD simulation is conducted with maximum outdoor temperature, adjacent rooms are at their highest design temperature and the emission from electric equipment is set at maximum, with an extra 15% safety margin. Consequently, the scenarios that are simulated in this thesis will hardly ever occur.

To achieve a correct simulation, it is imperative that the input values used in the simulation program represent the reality. The parameters regarding boundary conditions, as well as turbulence- and radiation models will be listed in this section. Furthermore, it will be provided a short explanation of specific parameters. Most of the parameters are based on data provided by Aibel, hence they are established and cannot be altered. The most important parameters from Aibel include the inlet mass flow rate, design temperature, as well as the heat emission from equipment.

3.4.1 Auxiliary transformer room

For the CFD simulation of the auxiliary transformer room several parameters were established, as presented in Table 3.4. The inlet air temperature is based on the summer maximum design temperature of $26,0°C$. This inlet temperature is not the same as the outdoor maximum temperature, which is $23,9°C$. The temperature difference occurs because there is an assumed temperature increase in the fan section inside the platform. Moreover, the inlet design temperature reflects the air temperature at ceiling level and because the air is supplied at floor level the actual temperature will be lower in reality. The mass flow rate is a result of air flow calculations provided by Aibel. The heat source emission is calculated based on the net electric heat equipment emission and the volume of the transformer. The auxiliary transformer acts as an heat source, and the design temperature limit for the room is $40,0°C$.

Table 3.4: *Boundary conditions for the auxiliary transformation room.*

Boundary condition	Parameter
Inlet	
Type	Mass flow inlet
Mass flow rate	$1,8$ kg/s
Inlet air temperature	$26,0$ °C
Outlet	
Type	Pressure outlet
General	
Fluid	Air as incompressible ideal gas
Viscous model	SST $\kappa - \omega$
Emission from transformer	$3\,202,0$ w/m^3
Radiation model	Discrete Ordinates method
External emissivity	$0,9$
Internal emissivity	$0,9$

In addition, the table includes some specifications related to radiation- and turbulence models. The DO radiation model was selected because it is the recommended model for systems that include localised heat sources. In addition, the optical thickness was approximated to a value greater than zero, thus the S2S model was excluded. For turbulence model, the SST $\kappa - \omega$ was chosen because studies show that this model has the lowest deviation when simulating a HVA/C system with displacement ventilation. Emissivities were set to $0,9$ because some of the calculations regarding the provided U-values were calculated with an emissivity of $0,9$. Furthermore, an emissivity of $0,9$ is regularly used in circumstances where this value must be approximated.

The specifications needed to model correct walls in the auxiliary transformer room are listed in Table 3.5. The table includes the total U-value for the different walls, their construction materials and their respective thickness. Lastly, the temperatures of the adjacent rooms are listed. All of these values are included in the ANSYS setup to achieve an accurate simulation of the heat transfer through the walls.

Table 3.5: *Wall parameters for the auxiliary transformer room.*

Surface	U-Value $[W/m^2 \cdot K]$	Material 1	Thickness 1 [mm]	Material 2	Thickness 2 [mm]	Adjacent temperature [°C]
Ceiling	$0,51$	Steel	10	SL 620	60	$45,0$
Floor	$3,84$	Steel	10	—	—	$23,9$
Wall east	$0,51$	Steel	5	SL 620	60	$35,0$
Wall north	$0,51$	Steel	5	SL 620	60	$35,0$
Wall south	$0,51$	Steel	5	SL 620	60	$35,0$
Wall west	$0,51$	Steel	5	SL 620	60	$40,0$

3.4.2 Valve hall

The setup for the valve hall was similar to the auxiliary transformer room. Henceforward, most of the parameters will be listed without any elaboration of why they are chosen due to the fact this was given in the previous section. The different parameters used for the valve hall setup are listed in Table 3.6. The table includes two values for heat source emission, one for the combination of all twelve valves, and one for the smoothing reactor. The reason behind the significant difference in emission, is because the smoothing reactor account for nearly half of the total heat emission. Furthermore, the volume of the smoothing reactor is very small in comparison to the combined volume of the valves. The design temperature limit of the system is $45,0$°C, and near the ceiling it is limited to $60,0$°C.

Table 3.6: *Boundary conditions for the valve hall.*

Boundary condition	Parameter
Inlet	
Type	Mass flow inlet
Mass flow rate	$6,0$ kg/s
Inlet air temperature	$28,0$ °C
Outlet	
Type	Pressure outlet
General	
Fluid	Air as incompressible ideal gas
Viscous model	SST $\kappa - \omega$
Emission valves	$79,0$ w/m^3
Emission smoothing reactor	$7\,061,0$ w/m^3
Radiation model	Discrete Ordinates method
External emissivity	$0,9$
Internal emissivity	$0,9$

The wall boundary conditions on the valve hall are more complex than the auxiliary transformer room. Due to the size of the valve hall, some of the surfaces have several adjacent rooms. Three of the walls, and a part of the ceiling are adjacent to the outdoor environment. The fourth wall has a adjacent room with a temperature of $35,0°$C. The challenges regarding boundary conditions stem from the floor and ceiling, because of different temperatures in the adjacent rooms. The solution was to divide the floor and ceiling in to two separate surfaces, which makes it possible to add different boundary temperatures, even though it increases the computational cost.

Table 3.7: *Wall parameters for the valve hall.*

Surface	U-Value $[W/m^2 \cdot K]$	Material 1	Thickness 1 [mm]	Material 2	Thickness 2 [mm]	Adjacent temperature [°C]
Ceiling east	0, 54	Steel	20	SL 620	60	23, 9
Ceiling west	0, 51	Steel	10	SL 620	60	50, 0
Floor east	0, 54	Steel	10	SL 620	60	35, 0
Floor west	0, 54	Steel	10	SL 620	60	45, 0
Wall east	0, 53	Steel	20	SL 620	60	23, 9
Wall north	0, 51	Steel	5	SL 620	60	35, 0
Wall south	0, 53	Steel	20	SL 620	60	23, 9
Wall west	0, 53	Steel	20	SL 620	60	23, 9

4 Results and discussion

The results will be presented and discussed continuously in this section. First, the meshing process will be presented. Secondly, it will be provided a thorough assessment of the temperature distribution inside the two enclosures. Penultimately, the air jets and streamlines will be analysed and presented. Lastly, different sources of errors will be discussed, and scenarios of interest to simulate if the thesis should be prolonged will be presented.

4.1 Results and discussion of the mesh

A good mesh provides accurate simulations with low computational cost. During the meshing process it has been completed a study concerning mesh independence, element quality and y^+ values. This was conducted to ensure and validate that the mesh was of good quality. This section will elaborate how the mesh has been optimised, and if the final mesh was satisfactory. In addition, the final mesh for the two systems will be presented.

4.1.1 Meshing of the auxiliary transformer room

Figure 4.1 shows the mesh independence study for the auxiliary transformer room. The number of elements ranges from approximately 15 000 up to 800 000. From roughly 400 000 elements and above, the air temperature reaches a stationary state. Fewer elements than 400 000 causes inaccurate simulation results. The mesh should thus consist of around 400 000 elements, which is the optimal combination between accuracy and computational cost.
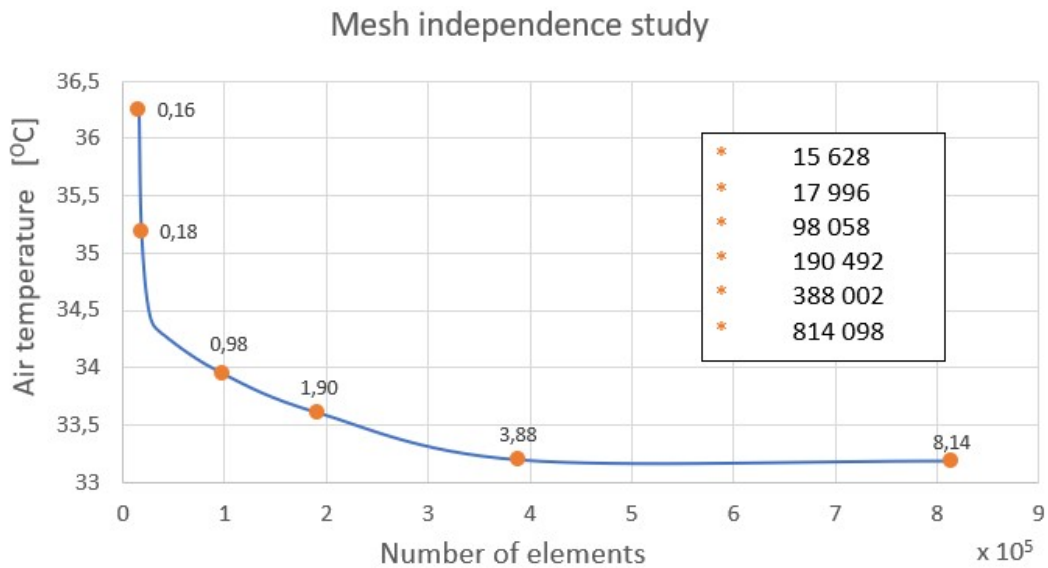
Figure 4.1: *Mesh independence study with air temperature as a function of the number of elements for the auxiliary transformer room. The graph reaches a stationary state around* 400 000 *elements.*

To achieve a well functioning mesh around critical sections, it was required to use the face sizing function in ANSYS Mesh. This resulted in various element size for different sections of the room, as previously presented in Table 3.3. The mesh for the auxiliary transformer room consists of 401 995 number of elements. These elements are reviewed in terms of orthogonal quality and skewness. Figure 4.2 visualises two section planes of the room. Figure 4.2a and 4.2b visualises orthogonal quality and skewness respectively. From the figures it is visible how both of these parameters are close to optimal for most parts of the room.
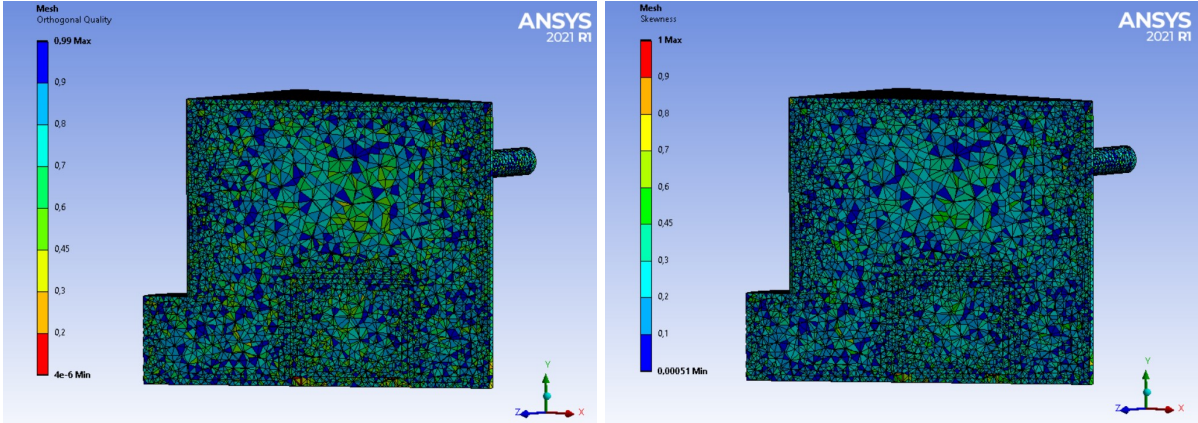
(a) *Orthogonal quality.*   (b) *Skewness.*

Figure 4.2: *Visualisation of the element metrics for a section plane in the auxiliary transformer room.*

Figure 4.3 presents the distribution of the orthogonal quality through a histogram. From the histogram it is visible that the orthogonal quality mostly ranges from $0,63 - 0,95$. The average orthogonal quality was calculated to be approximately $0,77$, which indicates an orthogonal quality in the category Very good. The distribution of the skewness is visualised through a histogram in Figure 4.4, and the skewness ranges mainly between $0,05 - 0,37$. The average skewness was calculated to $0,23$, which expressed a skewness of the category Excellent.
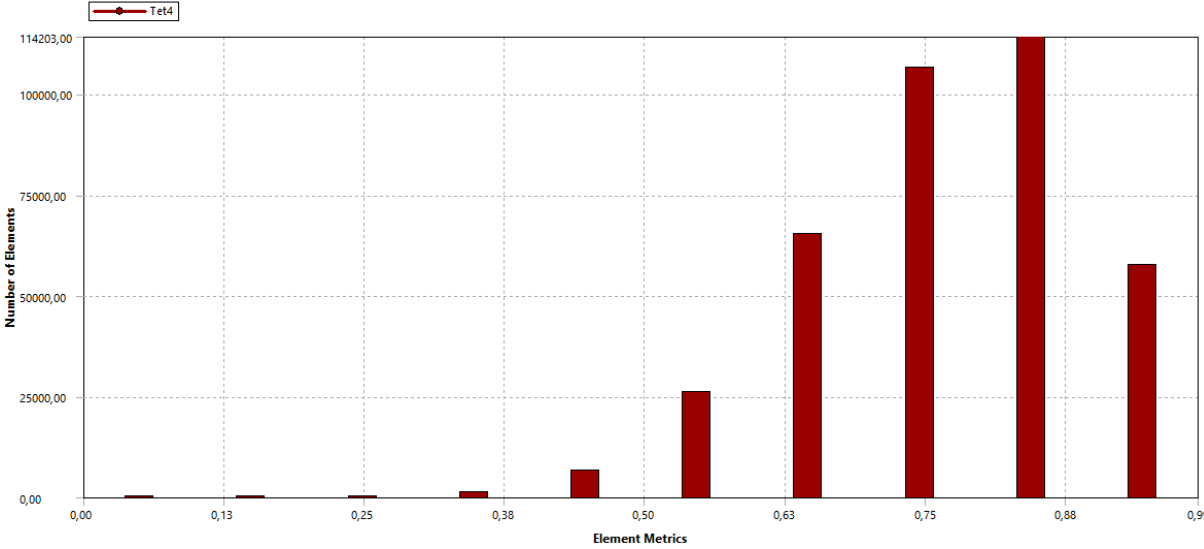
Figure 4.3: *Histogram of the orthogonal quality for the auxiliary transformer room. The x-axis is the orthogonal quality and the y-axis is number of elements.*
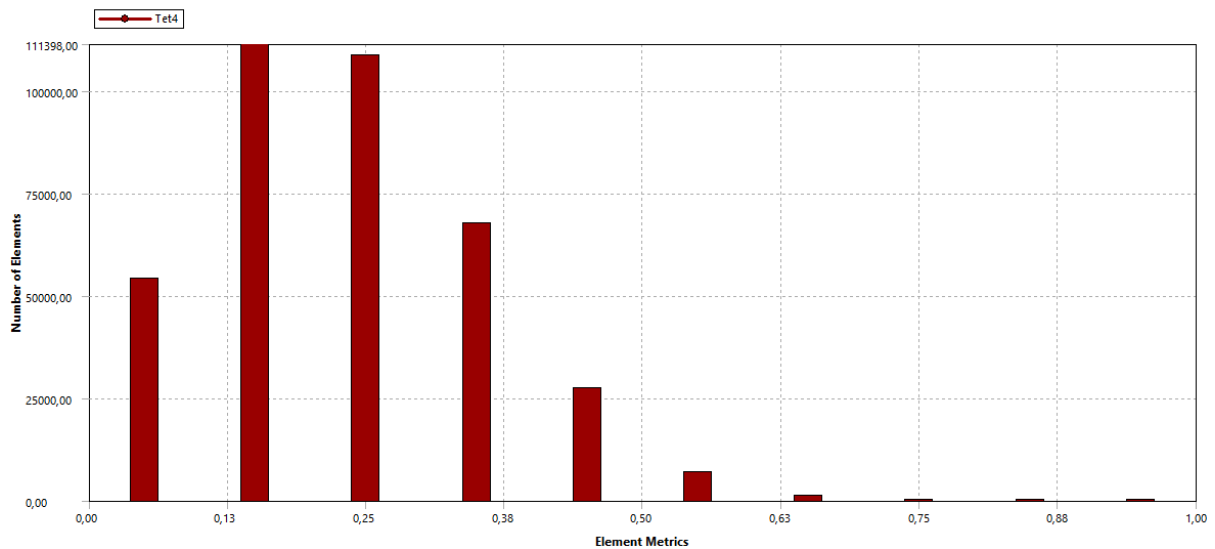
Figure 4.4: *Histogram of the skewness for the auxiliary transformer room. The x-axis is the skewness and the y-axis is number of elements.*

Figure 4.3 and 4.4 visualise the element type used for the meshing of the auxiliary transformer room. The room consisted unequivocally of Tet4 elements, which is a tetrahedron element with four nodes. Due to the simplicity of the geometry, no other element types were required. Moreover, it is visible from Figure 4.2a and 4.2b that the mesh consists of an unstructured grid. An accurate replication of a real geometry must include elements with varying size and shape, thus unstructured grid was well fitted for this purpose.

Additionally, the mesh can be validated by analysing the y^+ values on the walls surrounding the fluid domain. To achieve authentic simulations, the y^+ values must be in the interval of $30 - 300$. In order to identify the areas of the domain that do not fall within the desired interval, figures are cut to range. Cut to range means that surfaces, which is not within the desired interval will be invisible. As visualised in Figure 4.5 the majority of the walls are within the desired range for the simulation.
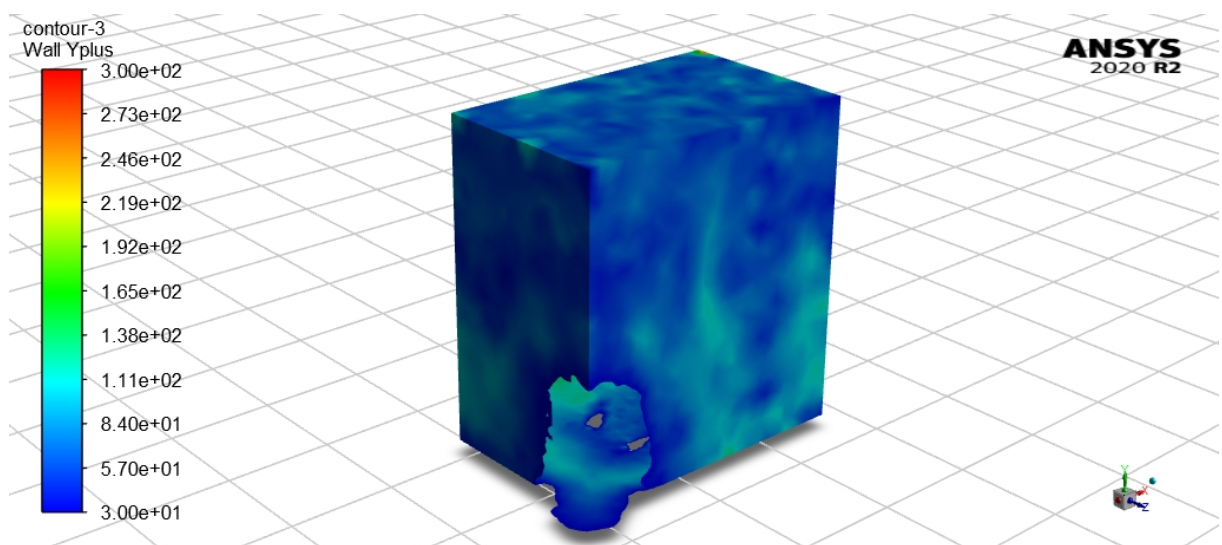
Figure 4.5: *Contour of wall y^+ values for the auxiliary transformer room, within the interval of $30 - 300$. All surfaces outside the interval are invisible.*

34

The dark blue colour in Figure 4.5 indicates y^+ values close to 30, which is the most preferable value for CFD simulations. Some parts of the walls have a light blue colour which corresponds to y^+ values of around 100. Although some parts of the surface have values up to 100, the majority of the surface area have y^+ values close to 30. Only parts of the walls located close to the inlet, and under the transformer legs are outside of this interval. These parts have y^+ values less than 30, but cover a negligible part of the total surface. The y^+ values under the legs are outside the interval, due to the small distance between the legs and the floor.

The y^+ values less than 30 around the inlet indicate a mesh too fine for the desired interval. The reason for a finer mesh in this area is to ensure that the simulation runs accurately. The fine mesh on the inlet will gradually become coarser before reaching the set element size of the walls. Therefore, the area surrounding the inlet automatically gets a finer mesh compared to the rest of the walls. The transition between the inlet and the walls is not immediate because of the curved shape on the inlet, which requires a finer mesh compared to plane surfaces. Although the y^+ values are out of range in the area, it is a necessary inaccuracy to assure correct air supply.

Besides assuring correct air supply, the parts of the walls outside of the desired range will have a low amount of air flow. The inlet will supply the air along the floor of the room, and therefore only a small portion of the stream will be in contact with these specific areas. Thus, the part of the walls with y^+ values less than 30 will not affect the results negatively because of the location and the necessity of fine mesh around the inlet. All things considered, the y^+ values in this case indicate a good mesh.

4.1.2 Meshing of the valve hall

The mesh independence study for the valve hall is displayed in Figure 4.6. This study includes a greater interval of elements, ranging from 80 000 up to 1 356 500 elements. Although, this test includes nearly three times as many elements, compared to the auxiliary transformer room, the graph is still not completely stationary. Nonetheless, it is opted to use 1 305 027 elements for the simulation, which is a compromise between accuracy and computational cost.
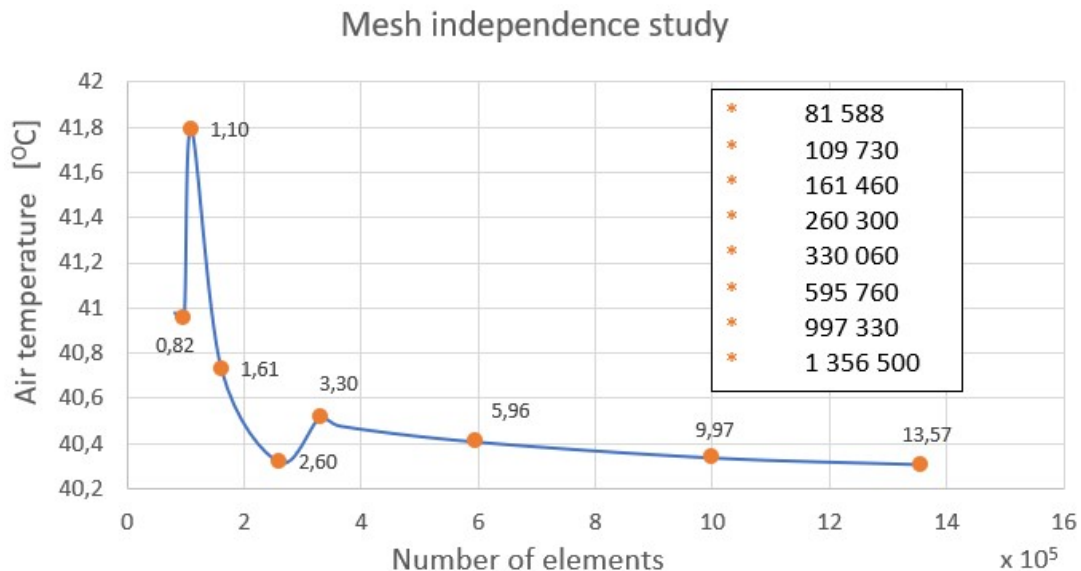

Figure 4.6: *Mesh independence study with air temperature as a function of the number of elements for the valve hall. The graph reaches a stationary state around 1 300 000 elements.*

The independence study for the valve hall caused faulty results with few elements. From an independence test it is expected a graph that is consistent, such as the independence test for the auxiliary transformer room. However, for the valve hall, the mesh study shows a big leap in air temperature with few elements. The reason for this is that the simulation ran unsteady with few elements, which caused inaccurate results. The results emphasise how important an independence study is to avert incorrect results.

The orthogonal quality of the valve hall can be evaluated by studying the graphic representation and the histogram in Figure 4.7 and 4.8 respectively. Most of the elements have an orthogonal quality between $0, 50 - 0, 95$. The average orthogonal quality for the valve hall was calculated to be approximately $0, 77$. This means that the average orthogonal quality was in the category of Very good. Conclusively, the orthogonal quality for the valve hall was within the desired range for an accurate simulation.

During the meshing phase, improvements had to be implemented around the smoothing reactor due to its curved shape. Hence, a mesh optimisation was performed around the component. This was done by using the face sizing function in ANSYS Mesh. The element size on the faces of the smoothing reactor were adjusted until the orthogonal quality reached a desirable value. The element size for different sections of the room was previously presented in Table 3.3. The fine mesh around the smoothing reactor is visualised in Figure 4.7. The figure displays a section plane of the domain, including four valves and a barely visible smoothing reactor. It is visible how the fine mesh on the smoothing reactor creates an increased amount of elements in the fluid domain around the component.
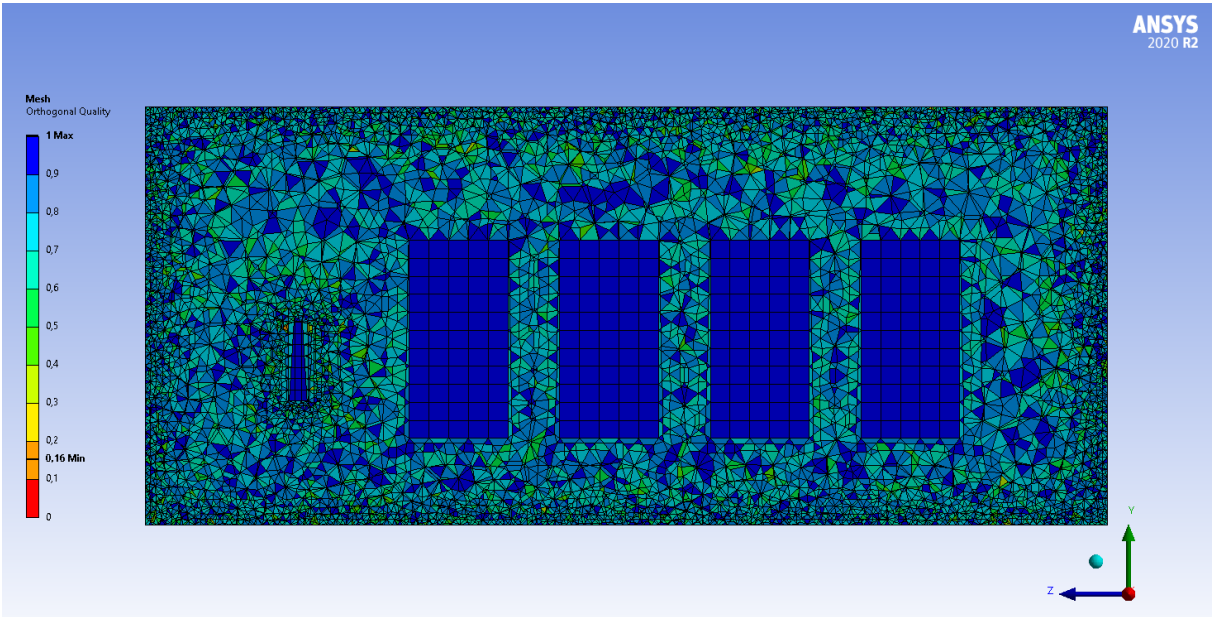

Figure 4.7: *Visualisation of the orthogonal quality of the elements for a section plane in the valve hall.*
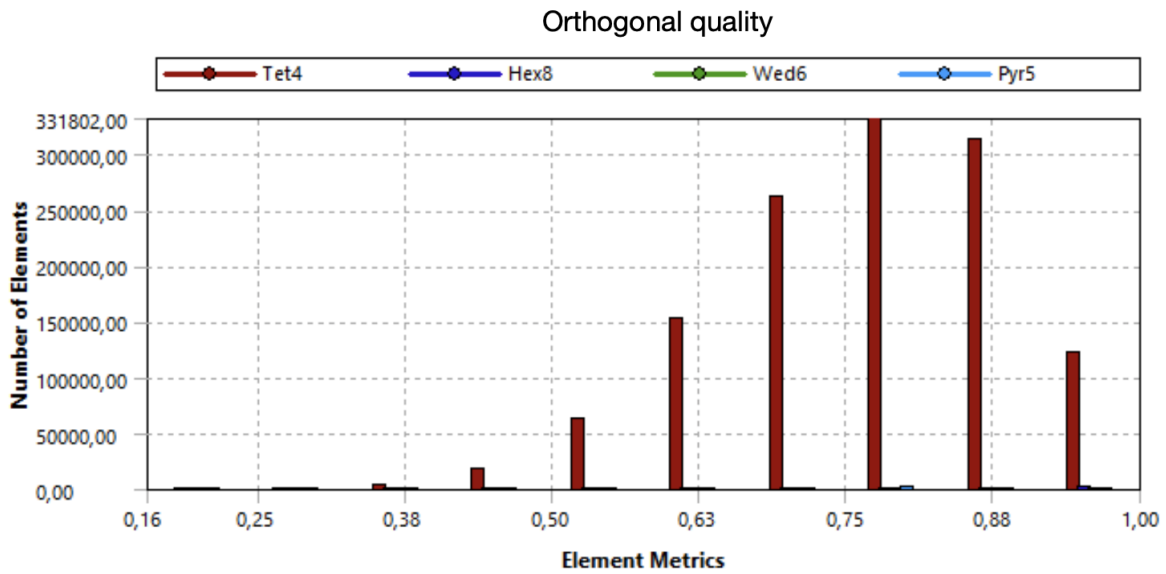
Figure 4.8: *Histogram of the orthogonal quality in the valve hall. The x-axis is the orthogonal quality and the y-axis is number of elements.*

Figure 4.9 presents the element skewness, jointly with Figure 4.10, it is possible to analyse the quality of the mesh in regard to skewness. The figures display that the element skewness are normally between $0, 04 - 0, 40$. The average skewness of the room is calculated to be approximately $0, 23$, which qualify for the category of Excellent. The average value provided a satisfactory result and indicated a good quality mesh. Figure 4.9 visualises how the skewness is approximately zero for the mesh at the valves. The reason for the excellent quality on the valves, is their geometric simplicity as boxes. This simplicity saved computational time due to a coarser mesh. There are no areas which were unsatisfactory, thus the mesh are excellent in terms of skewness.
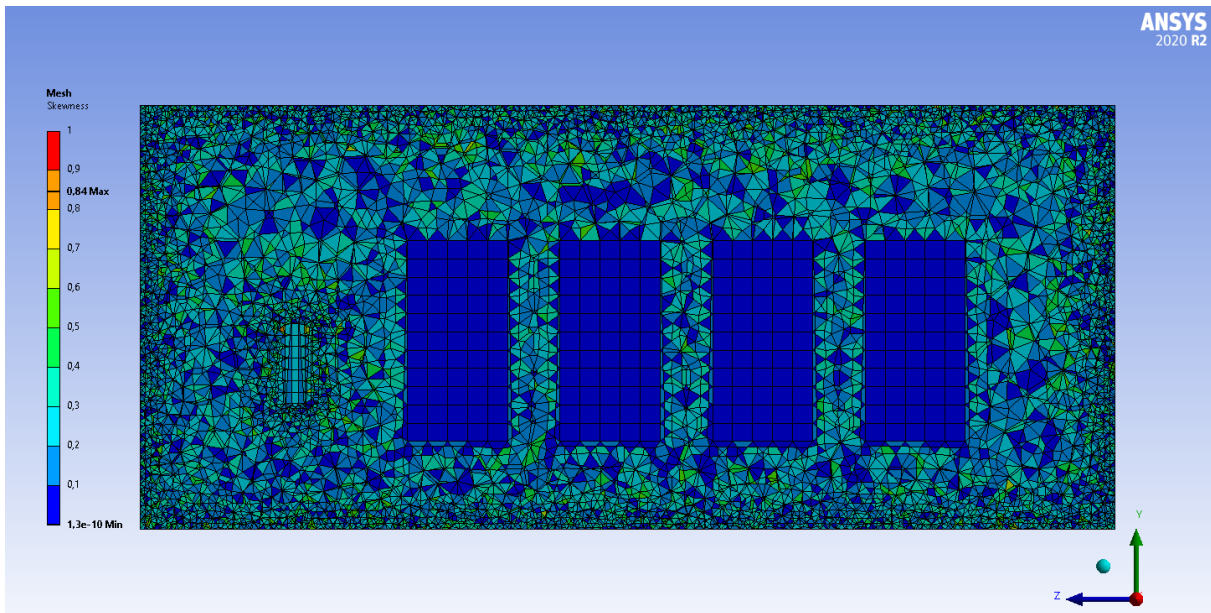
Figure 4.9: *Visualisation of skewness of the elements for a vertical section plane in the valve hall.*
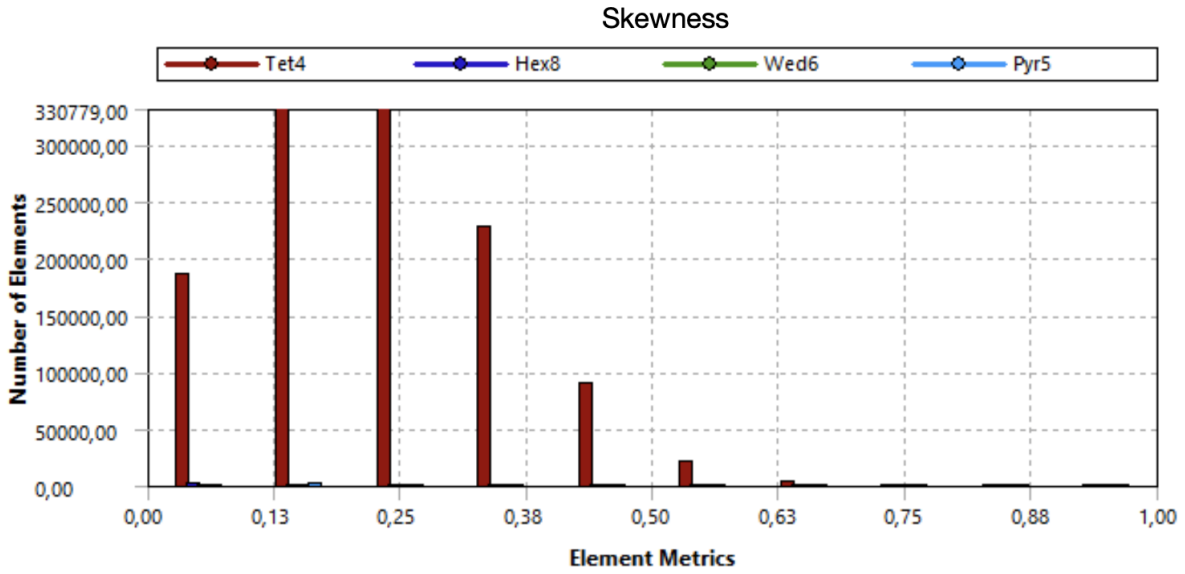
Figure 4.10: *Histogram of the element skewness in the valve hall. The x-axis is the skewness and the y-axis is number of elements.*

The histograms in Figure 4.8 and 4.10 show the element composition used in the meshing. Tet4 is the most common type of element for this enclosure, which is a tetrahedron element with four nodes. There is also a small amount of the Hex8, Wed6 and Pyr5 elements, which are hexahedron with eight nodes, wedge with six nodes and pyramid with five nodes respectively. Moreover, it is visible from Figure 4.7 and 4.9 that the mesh consists of both unstructured- and structured grid. The valves consist of structured grid, which simplify the element shapes. The simplification saves computational cost, as a consequence of coarser mesh. This area is also where the Hex8 elements are used, as shown in Figure 4.8 and 4.10. The rest of the room consists of unstructured grid. This grid leads to a more similar replication of the real life geometry, and in turn a more realistic simulation.

Furthermore, y^+ values were used to evaluate the quality of the mesh. Similarly to the auxiliary transformer room, the desired range for y^+ values is between $30 - 300$. Figure 4.11 visualises a contour of the y^+ values on the walls in the valve hall. The closest wall is made invisible to get a visual representation of the y^+ values for a larger part the room. The figure illustrates that the walls are within the desired range, and a large part of the surface is close to 30. Unlike the auxiliary transformer room, the elements around the inlets are within the y^+ values interval. This is a result of the modelling difference for the inlets. In the auxiliary transformer room the inlet is designed as a cylinder, but in the valve hall they are designed as cubes. Due to the cubic design, the transition from the inlets to the walls is more immediate.

38

An unforeseen discovery in Figure 4.11 is that the y^+ values are higher by the floor directly under the inlets and by the ceiling over the smoothing reactor. In these areas, the air velocity is higher than the surroundings, as visualised in Appendix D. One of the parameters used to calculate the y^+ values is the friction velocity. Thus, the y^+ values will increase on surfaces when the friction velocity is increased. Although the y^+ values increase in some areas, all the values are still within the desirable range. Therefore, both the element metrics and the y^+ values validate a good mesh.
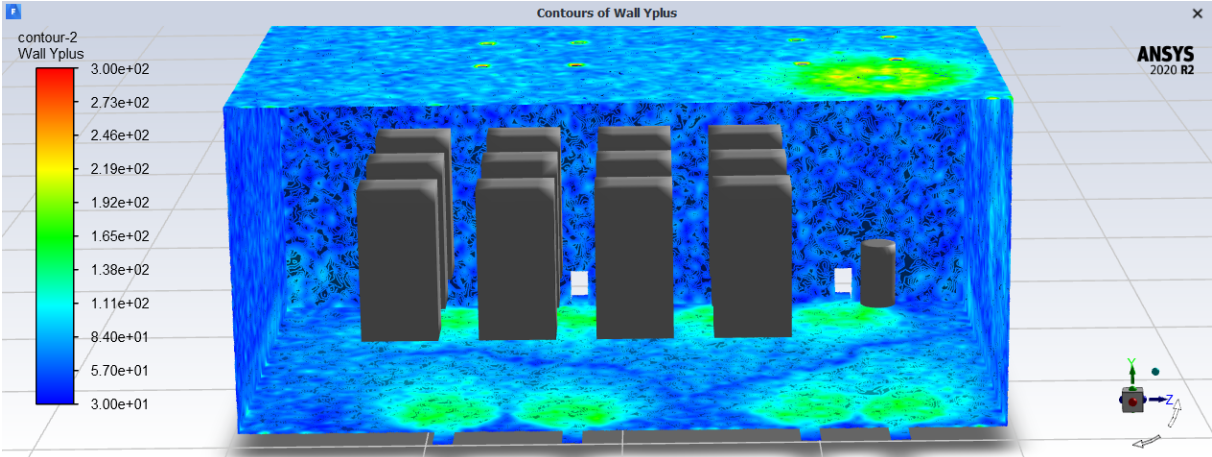
Figure 4.11: *Contour of wall y^+ values for the valve hall, within the interval of $30 - 300$. The closest wall is made invisible for visual purposes, even though all surfaces are within the desired range.*

4.2 Room temperature

One of the main purposes of this thesis was to examine if the planned HVA/C system would be capable of maintaining a temperature beneath the design limit. The working principle for the installed HVA/C system is displacement ventilation. This principle is well suited for the two systems, since they both have heat sources located in the lower zones. As a consequence, the low temperature air jets that enter the room near the floor will contribute, along with buoyancy, to displace the heat upwards. This establishes thermal stratification with a main composition of heat near the ceiling where it is extracted. Simultaneously, the occupation zone remains cool.

4.2.1 Auxiliary transformer room temperature

Figure 4.12 displays the temperature profile of the auxiliary transformer room. The display shows a distinct higher temperature above the transformer. The temperature ranges from $26,0$°C at the inlet to approximately $42,0$°C under the ceiling. Temperatures at key parts of the room are presented in Table 4.1. The temperatures in the table are all within the design limit, thus all the important areas of the room are adequately cooled down. The highest values in the table are above the transformer and by the outlet, which correlate well with the theory regarding natural convection and heat transfer.
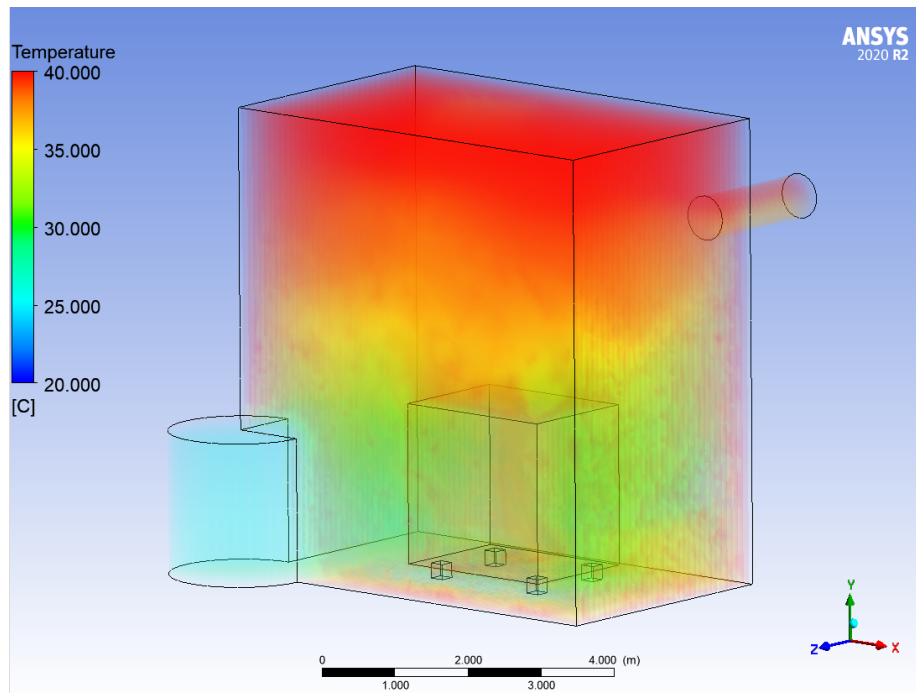
Figure 4.12: *Temperature gradient of the complete auxiliary transformer room, in the interval of* $20,0 - 40,0$°*C.*

The maximum temperature in the enclosure is marginally higher than the design limit of $40,0$°C. The room adjacent to the ceiling have a design temperature of $45,0$°C, which decreases the heat transfer through the ceiling. This in cohesion with warm walls from radiation make a temperature of over $40,0$°C realistic in the area under the ceiling. Ideally, the temperature under the ceiling should be within the design temperature, but the infringement is marginal. All the key parts of the room are within the limit in an absolute worst case scenario, and therefore the temperature against the ceiling is unproblematic.

Table 4.1: *Calculated temperatures at vital points in the auxiliary transformer room.*

Location	Temperature
Average	34, 96 °C
Inlet	26, 00 °C
Outlet	38, 15 °C
1, 13 m above transformer	36, 19 °C
1, 00 m beside transformer	31, 03 °C

It is of most interest to review the air temperature and airflow in the occupation zone. In this part of the room it is a relatively cool temperature. One hypothesis before simulating the auxiliary transformer room was that the part of the room close to the inlet would be significantly colder than the opposite side of the room. Appendix A shows the temperature in the auxiliary transformer room for different planes. The temperature distribution is relatively good, however it is visible that the room is warmer on the side leading away from the inlet in the lower part of the room. The temperature difference between the two sides of the transformer decreases in correlation with the height in the room. Hence, the hypothesis of a cooler temperature near the inlet seems correct for this simulation.

Figure 4.13 shows a temperature contour directly above the floor. The figure visualises a significant difference between the two sides in the room. The temperature on the opposite side of the inlet is approximately 13, 0°C warmer right above the floor. The reason for the significant difference is due to the inlets positioning. The chilled air jets from the inlet will become heated and displaced upwards before reaching the opposite corner. This leads to poorer cooling close to the floor in the areas far from the inlet. Towards the ceiling, the temperature distribution will even out.
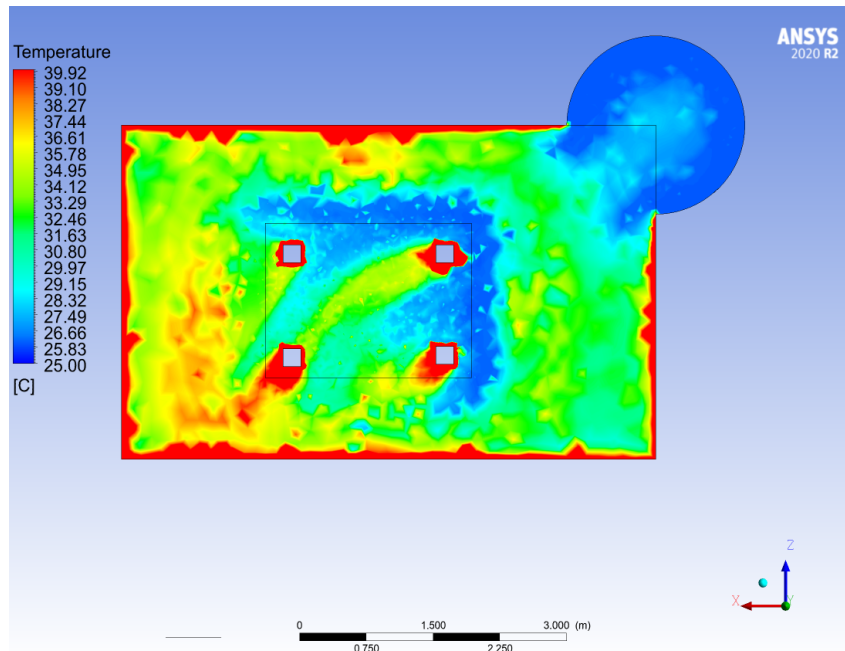
Figure 4.13: *Temperature gradient directly above the floor in the auxiliary transformer room, in the interval of* $25, 0 - 40, 0°C$

The simulation of the auxiliary transformer room resulted in wall temperatures that exceeded the design temperature. All of the heat emission from electric equipment is emitted from the transformer alone, in addition to an extra 15% as a safety margin. Because of a high amount of heat emission, the transformer surface becomes unrealistically warm. In reality, the transformer surface is around $60, 0°C$, which is less than half the temperature in this simulation. The surface temperature on the transformer in the simulation needed to be approximately $125, 0°C$ to emit the correct amount of heat.

The high surface temperature on the transformer will increase the thermal radiation emitted to the surroundings. Since the room is modelled empty, except from the transformer, all the radiation beams hit the walls directly. The walls are designed with insulation to protect the platform in case of fire, which leads to less heat transfer through the walls. The convection heat losses through the walls are further decreased by setting the adjacent rooms to their maximum design temperature. The adjacent rooms have approximately the same temperature as the transformer room. Consequently, the wall temperature will become relatively high due to unrealistically high thermal radiation and a low heat transfer loss through the walls.

To support the assumption that the warm walls is a consequence of high surface temperature on the transformer, a new simulation was performed. For this simulation the surface temperature of the transformer was set to $100, 0°C$ to further evaluate if the results from the main simulation are reasonable. The temperature for the new simulation is visualised in Figure 4.14. A lower surface temperature will reduce the radiative heat transfer, which leads to a slightly colder room. In addition, the wall temperature is significantly reduced. This indicates that the walls will be within a reasonable range in a real life scenario, with a transformer temperature of $60, 0°C$.

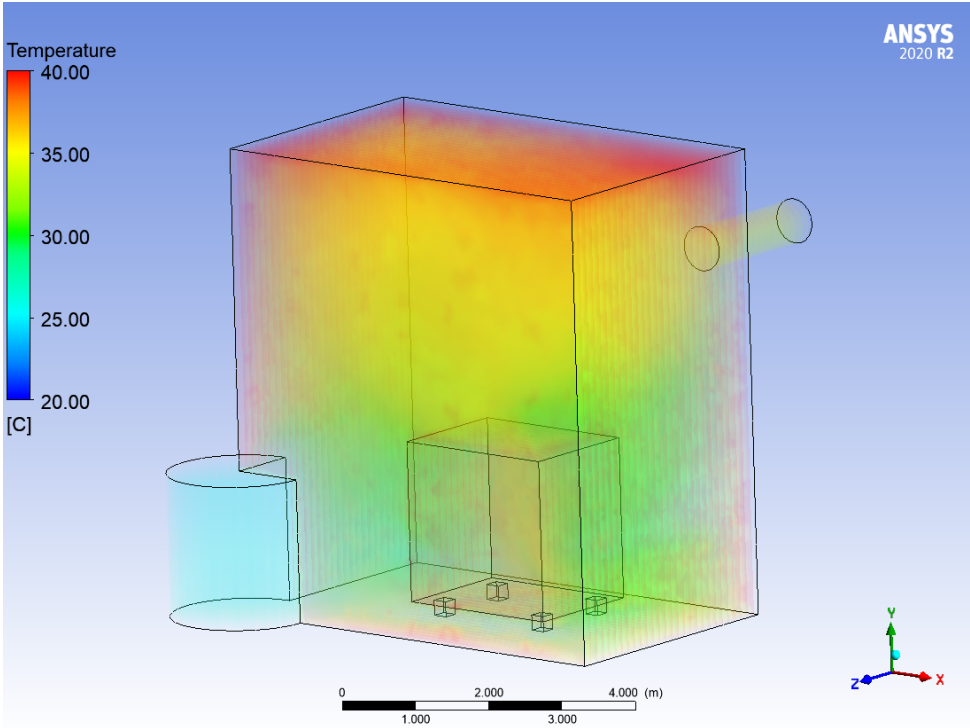**Figure 4.14:** *Temperature gradient of the complete auxiliary transformer room, in the interval of $20, 0 - 40, 0°C$. The transformer surface temperature is set to $100, 0°C$.*

The fixed temperature on the transformer is an indication of what could occur with a lower surface temperature. However, this is an unwanted way of interfering with the simulation. When the fixed temperature is enabled it prevents some of the input heat emission to affect the room. As a consequence of adjusting the surface temperature on the transformer, the heat emission will be adjusted by the ANSYS Fluent software. Hence, it is not recommended to add a fixed value when doing simulations with a given heat emission. When the simulation has enabled a fixed value, which is lower than the original temperature, it will no longer be a simulation of worst case scenario.

4.2.2 Valve hall temperature

The valve hall has a distinct thermal stratification which indicates that the HVA/C system functions well for this enclosure. Appendix B shows the temperature distribution in the valve hall for different planes. The temperature varies from $28,0°C$ by the inlets to approximately $45,0°C$ beneath the ceiling. The average temperature of the room is $40,1°C$, which is within the design limit of $45,0°C$. The temperature gradient of the room is provided in Figure 4.15.

The valve hall contains spots that are particularly warm. Mutual for all these warm spots are that they are located near the smoothing reactor. These are caused by radiation heat transfer from the smoothing reactor. The amount of radiation heat transfer increases along with the surface temperature. The surface temperature on the smoothing reactor is significantly higher than on the valves, thus the hot spots are only on the walls close to the smoothing reactor. Due to the high surface temperature used in the simulation, the warm spots are reasonable.
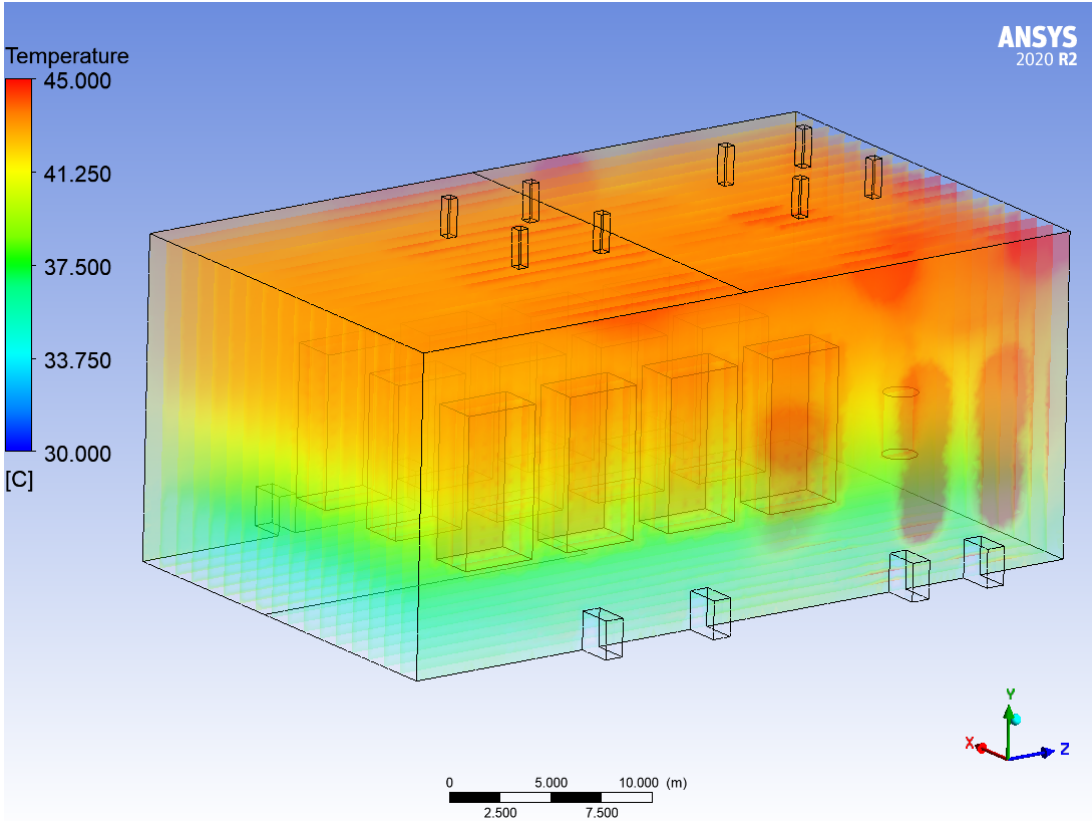
Figure 4.15: *The temperature gradient of the complete valve hall, within the interval of $30,0 - 45,0°C$.*

The design temperature is set to ensure the safety of the equipment in the room. Therefore, the temperature in the proximity of the valves and smoothing reactor was measured. The values are presented in Table 4.2. There is only one value for the valves due to a negligible temperature difference in the measured areas. The temperature distribution around the valves is visualised in Figure 4.16. The temperature measurements indicate that the temperatures around the valves are within the temperature limit.

Table 4.2: *Calculated temperatures at vital points in the valve hall.*

Location	Temperature
Average	40, 13 °C
Inlet	28, 00 °C
Outlet	43, 41 °C
1, 60 m above smoothing reactor	48, 33 °C
1, 00 m beside smoothing reactor	40, 29 °C
1, 00 m beside valves	40, 74 °C
4, 00 m above valves	43, 35 °C
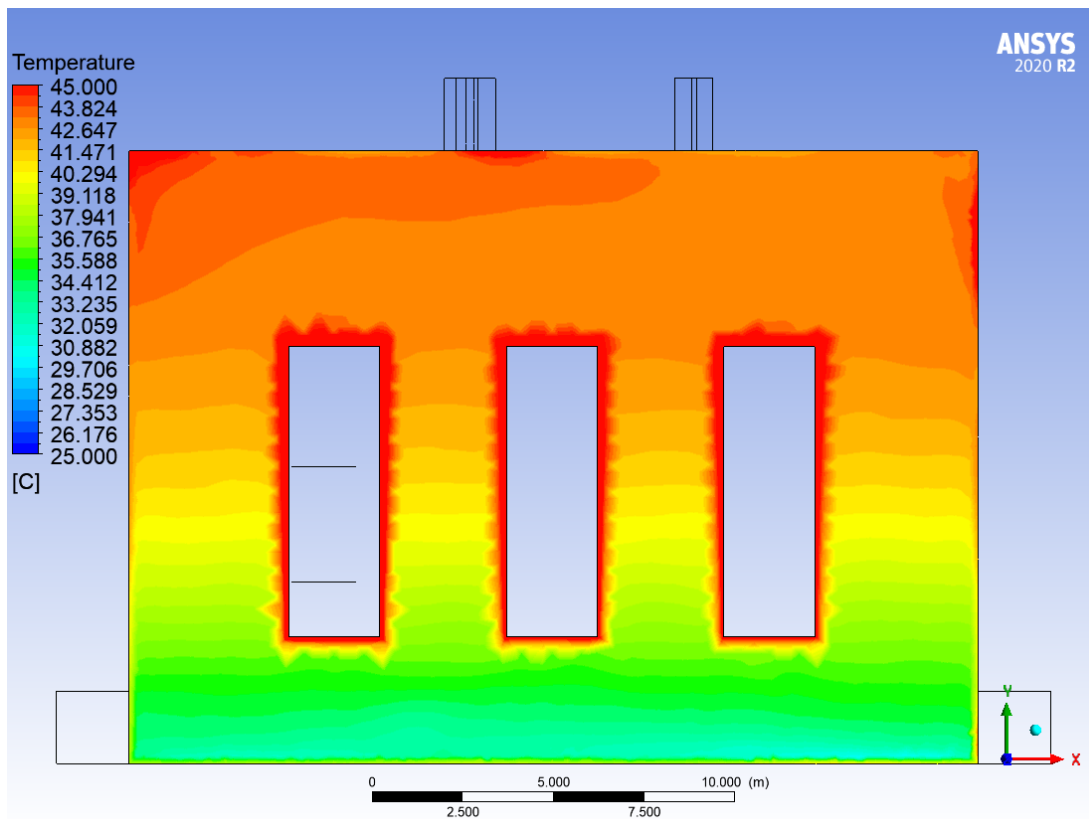
Figure 4.16: *Vertical section plane that shows the temperature gradient around the valves, in the interval of $25, 0 - 45, 0°C$.*

Contrastingly, the temperature over the smoothing reactor is some degrees warmer than the design temperature. Figure 4.17a shows that the area directly over the smoothing reactor is too warm. Hence, the scale was adjusted in Figure 4.17b to show a better picture of the temperature. A measurement done $1, 6\,m$ above the smoothing reactor yielded a temperature of $48, 3°C$, which is over the design temperature.

One possible reason for the high temperature, is the heat emission distribution from the components. In this simulation the heat emission from the smoothing reactor is $57,5$kW, which is 43% of the total heat emission in the system. The provided data from Aibel did not specify how much each component emits individually. A small adjustment of the heat emission from the reactor could make the air around it a few degrees colder.

The amount of heat emission from the smoothing reactor will create an extensive thermal plume, and naturally cause the surrounding air to increase in temperature. It is a relatively small component with a high emission, which leads to a high surface temperature. Furthermore, the high surface temperature will heat up the surrounding air. The air circulation above the smoothing reactor is not sufficient to maintain the temperature within the design limit. However, the deviation only exceeds with a few degrees.
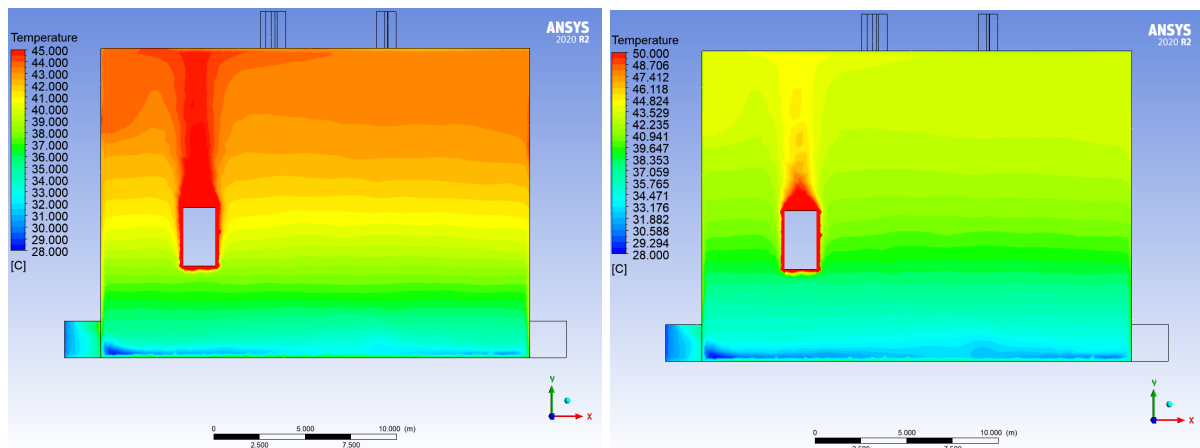
(a) *Temperature contour in the interval of $28,0-45,0°C$.* **(b)** *Temperature contour in the interval of $28,0-50,0°C$.*

Figure 4.17: *Two vertical section planes which show the temperature contour gradients around the smoothing reactor with different intervals.*

One of the objectives of this thesis is to examine how accurate the modelling must be to achieve a legitimate result. Consequently, the smoothing reactor was initially modelled as a solid cylinder to save computational cost with an easier mesh. Additionally, the valve hall was simulated with a hollow smoothing reactor to obtain a more realistic model. The main difference between a hollow and solid reactor was the temperature over the component. Figure 4.18 depicts the temperature contour in the same conditions as Figure 4.17b. The figure shows an increase in the temperature above the smoothing reactor. The increase in temperature is caused by the decreased surface area of the smoothing reactor in the modified model. The temperature over the smoothing reactor increased by $1,7°C$, which is an increase by $3,5\%$.

As a consequence of a decreased volume with a hollow smoothing reactor, the surface temperature on the component will increase. The simulations with a hollow smoothing reactor resulted in a deviation in the average room temperature of merely $0,03°C$, which is a negligible difference. In addition, the streamlines across the enclosure were approximately the same, except that some air jets passed through the smoothing reactor. Thence, there was no significant difference between the two simulations in regard to the valve hall as a system.
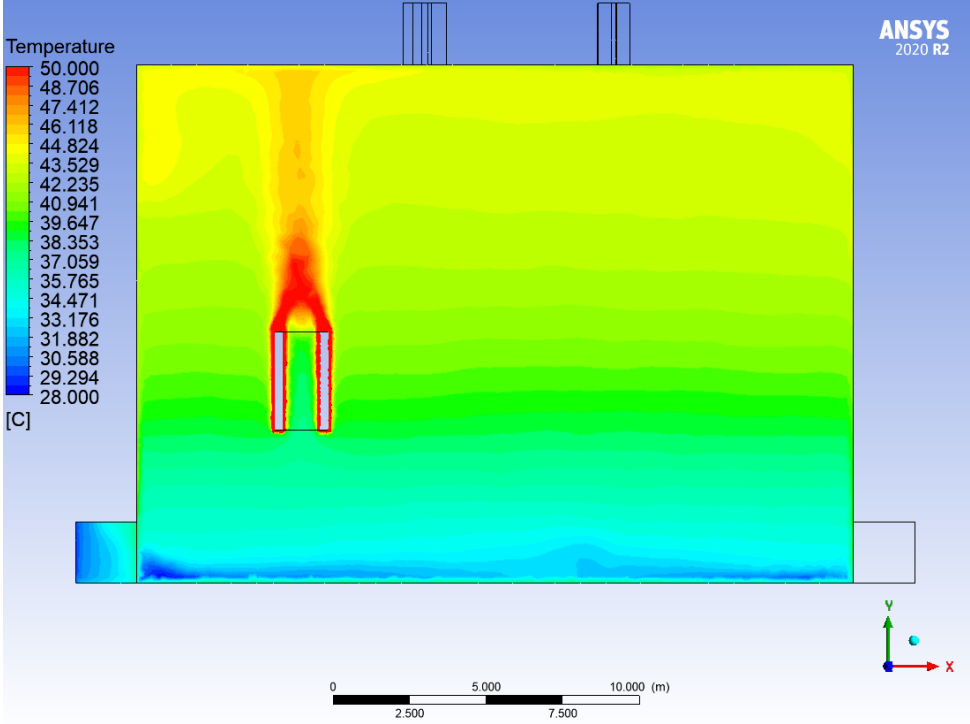
Figure 4.18: *Vertical section plane that shows the temperature contour over the hollow smoothing reactor, in the interval of $28,0 - 50,0°C$.*

4.3 Streamlines

Air distribution of the auxiliary transformer room and the valve hall is important when evaluating the ventilation system. Post processing functions in ANSYS were used to illustrate streamlines and to effectively obtain an accurate representation of the air supply. To achieve a clear overview of the streamlines, several figures are used to display the streamlines in different planes of the systems. Some of the figures will be presented and discussed in this section, while several others are attached in the appendices. Appendix C consists of streamline profiles for the auxiliary transformer room, and Appendix D contains streamline profiles for the valve hall.

4.3.1 Streamlines in auxiliary transformer room

Figure 4.19 includes streamlines for vertical and horizontal planes in the auxiliary transformer room. The inlet air jets are spreading out into the room in the shape of a cone, which lead to a well functioning air distribution and effective cooling of the transformer. Furthermore, the air jets have a downwards trajectory when entering the enclosure. The air velocity inside the enclosure ranges from $0 - 8, 28 \, m/s$, where the highest velocity occurs only through the outlet. The velocity in the room will mostly range between $0 - 1, 00 \, m/s$, with an average velocity of $0, 28 \, m/s$.
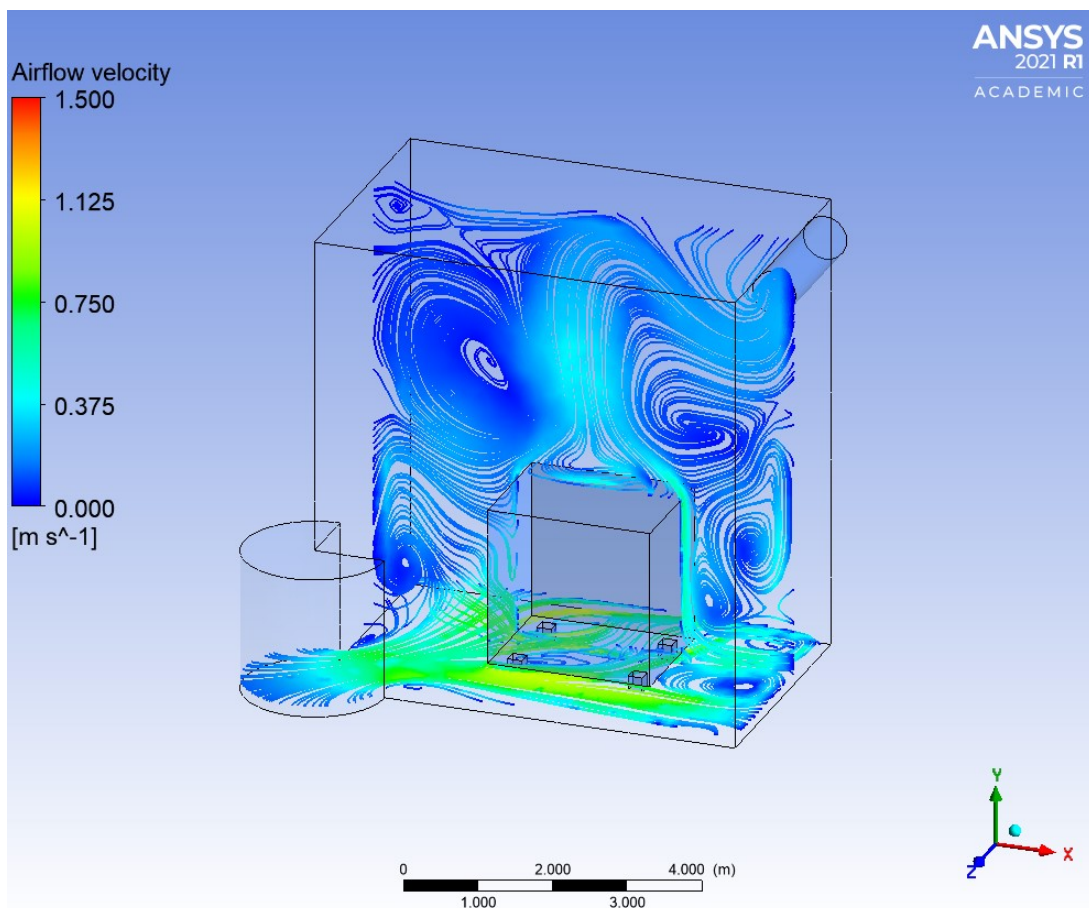
Figure 4.19: *Streamlines in the auxiliary transformer room for two separate planes. The airflow velocity is within the interval of $0 - 1, 50 \, m/s$.*

47

The air velocity in the auxiliary transformer room varies with the distance from the floor level. At the lower zones, the air velocity has a greater magnitude compared to the higher zones. One reason for this is due to the air jet velocity decreases in accordance with the distance from the inlet. Another reason is that the transformer disturbs the air jets natural trajectory, and as a result the air velocity increases near the transformer surface. Contrastingly, the velocity decreases above the component due to the empty volume, and therefore the fluid can move more freely.

Figure 4.19 visualises the circulation of the air inside the room and how eddies occur. The eddies that occur in the room will stir the air inside the room. This will ensure that the heat is distributed more throughout the room. Nevertheless, it is still a distinction between the upper and lower zones. The stirring is not beneficial considering it is working directly against the displacement ventilation principle. This is due to the mixing of the two temperature zones which counteracts the piston effect. As the geometry of the auxiliary transformer room is simplified, this simulation will contain less eddies compared to what would occur in reality. As a consequence of more eddies, the temperature in the system will be more distributed, thus the average temperature in the enclosure will increase. This is because the heat extracted in the outlet will be lower compared to what it would be with less eddies.

Underneath the transformer, the air velocity increases, which is shown in Figure 4.20. This is due to the pressure differences around the transformer unit. The fluid flow will follow the surface of a solid body even though the surface is curved. The fluid flow along the surface visualises the Coandă effect. As a consequence, a negative pressure is formed around the legs of the transformer. The negative pressure will act as a suction pressure and accelerate the air jets around these areas. The air distribution and air jet trajectories inside the auxiliary transformer room correspond well with theory concerning fluid flow inside an enclosure. This correlation, between theory and simulation, is an indication that the simulation results are accurate.
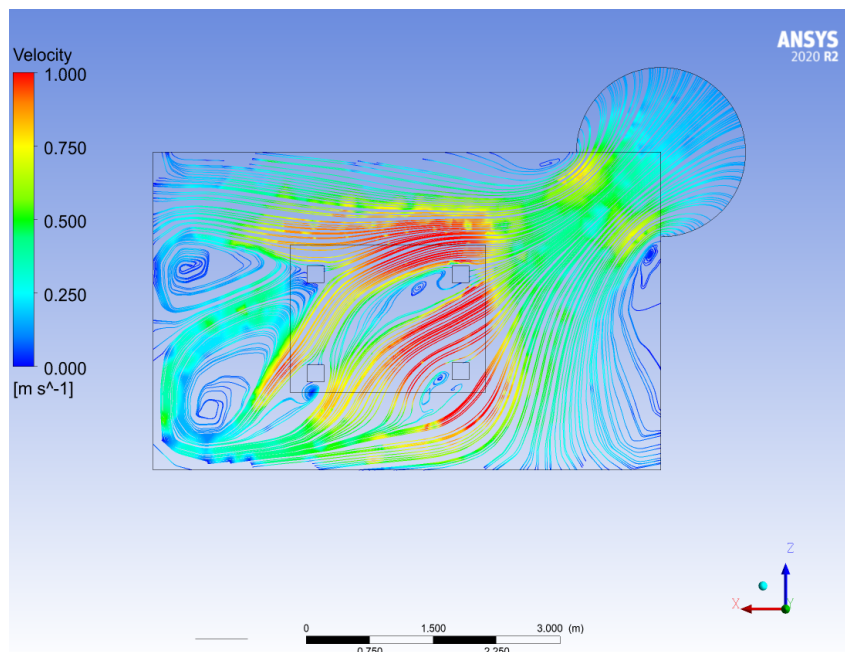

Figure 4.20: *Streamlines underneath the transformer in the auxiliary transformer room. The airflow velocity is within the interval of $0 - 1,00 \, m/s$.*

4.3.2 Streamlines in the valve hall

Figure 4.21 visualises the complexity of the air distribution inside the valve hall. From the figure it is visualised how the greatest velocities appear above the smoothing reactor and in the outlets. The air velocity in the room ranges from $0 - 3,58\,m/s$, and the highest velocity occur in the outlets. Most of the velocity ranges between $0 - 0,50\,m/s$. The average velocity in the room was calculated to approximately $0,11\,m/s$.

From Figure 4.21 it is visualised how the velocity increases around the smoothing reactor. The reason for this is due to the heat flows that occur around the component. As the heat rises, the velocity will gradually increase along the smoothing reactor and a thermal plume will form. In the figure it is visible how some of the outlets are placed near the smoothing reactor. This is beneficial for the ventilation system, as the warm air around the smoothing reactor has a short path to the outlets. This helps keeping the room temperature cool and within the limits. The air is distributed well around and in between the valves, which indicate that the ventilation system operates as intended in this part of the enclosure.
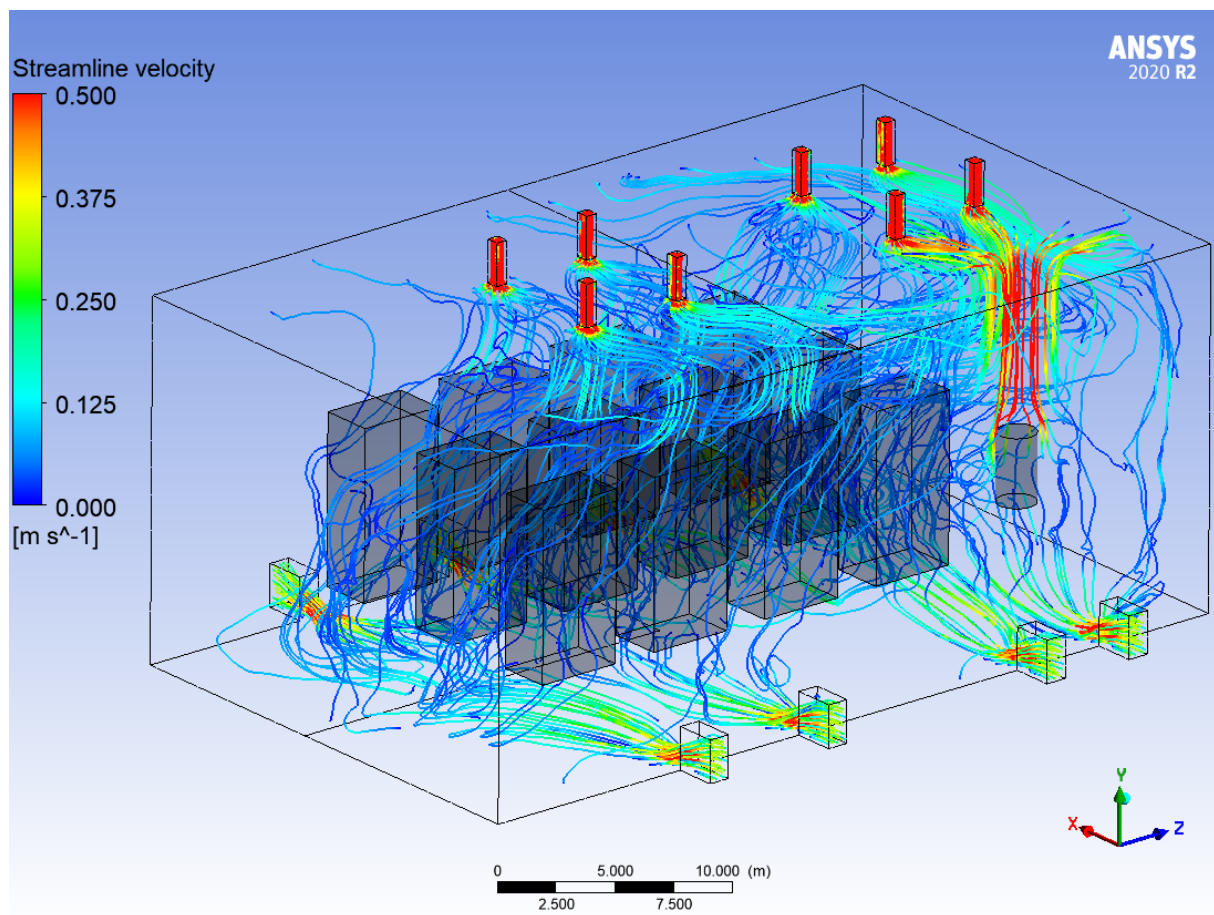
Figure 4.21: *Three dimensional streamlines in the complete valve hall. The airflow velocity is within the interval of $0 - 0,50\,m/s$*

Figure 4.22 shows a thermal plume above the smoothing reactor. The thermal plume will divide into streams of air close to the ceiling. The streamlines follows the surface of the ceiling due to the Coandă effect, which leads to formation of eddies. Considering the room has several outlets and the room itself has a large volume, the eddies will have a marginal effect on the temperature. Anyhow, these eddies will still lead to an air agitation in the room, which causes the temperature to mix to some extent. Another detail to notice in Figure 4.22 is the small swirls of air that is formed directly above the smoothing reactor. These swirls arise because of a negative pressure in this region, which causes some air to be drawn back to the reactor surface. The air trajectories towards the smoothing reactor will bring dust particles from the room to the top of the component. If dust gather on top of the warm component, it could become a fire hazard. Hence, this is something worth noting in terms of precautions regarding fire protection.
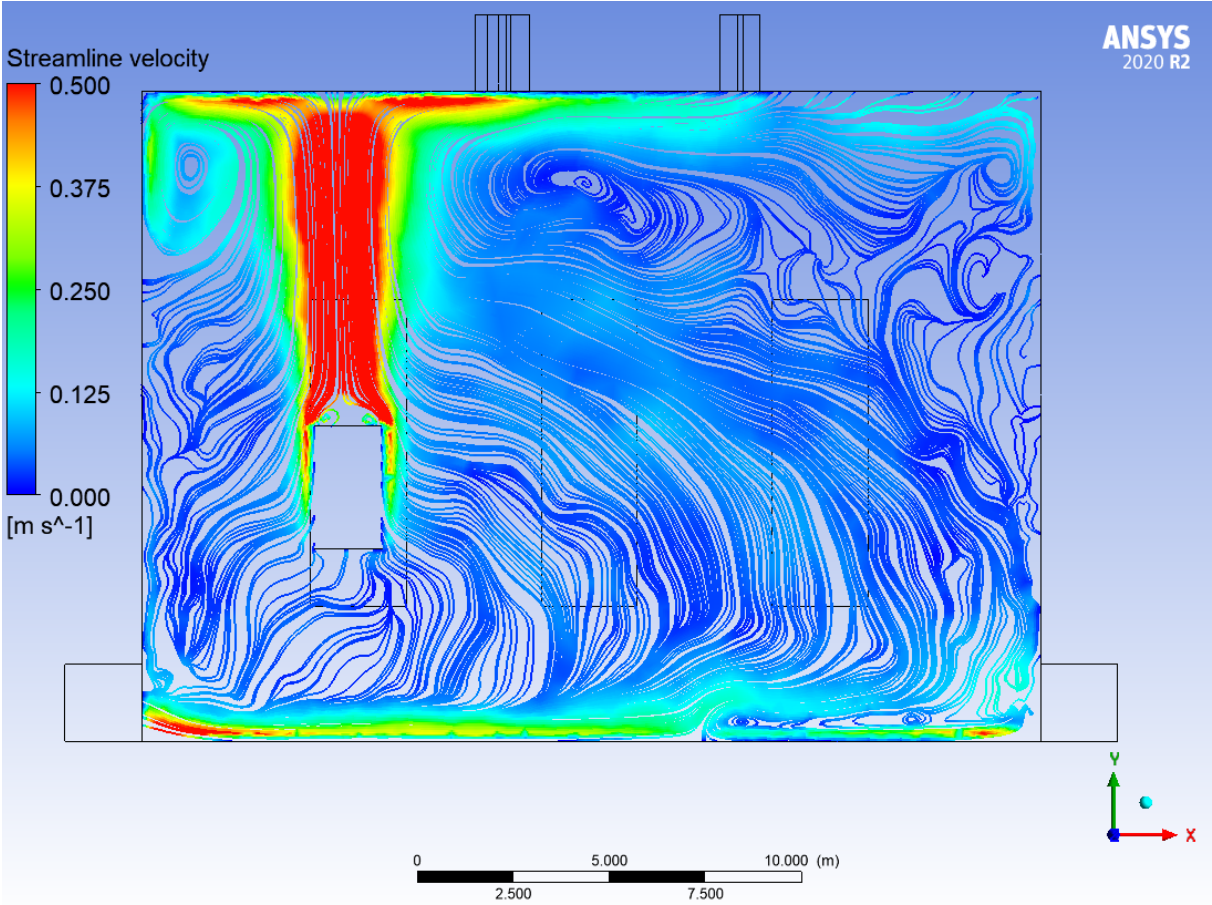
Figure 4.22: *Streamlines in a vertical plane in the valve hall. The airflow velocity is within the interval of $0 - 0,30\,m/s$. The thermal plume and eddies cause the air trajectory to be disrupted.*

4.4 Sources of error

When performing CFD analysis it is often difficult to validate the results. Hence, it is important to be aware of the different sources of error that can influence the simulation results. Many errors that are difficult to discover occur because of computational errors. This section will concern errors and mistakes associated with the simulations.

An example of an error that can occur is the number of iterations and convergence, which is a limiting factor associated with computational cost. An RMS error of $10^{-4} - 10^{-5}$ is sufficient to obtain a credible result. However, from Figure 4.23 it is visible that this is not the case for these simulations. The simulation of the valve hall shows an RMS error between 10^{-2} and 10^{-6} for the different residuals. Moreover, the figure shows a steady graph with no tendency for change. This suggests that it is difficult to decrease the RMS errors any further. There are multiple ways to lower the RMS error. The most effective is to increase the number of iterations, but this will increase the computational cost. Another way is to change the choice of algorithms in the setup, which also increases the computational cost.
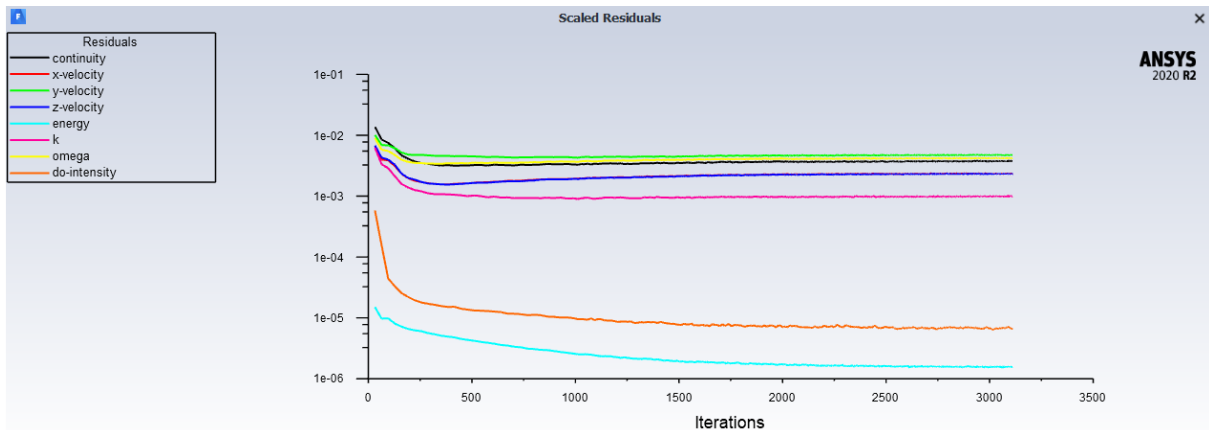
Figure 4.23: *Residuals from the valve hall. All the residuals and their associated colours are presented in the top left corner. The x-axis represents number of iterations, and the y-axis is the RMS error.*

Even though the residuals failed to reach the desired values, the convergence of the simulation was studied. The total heat transfer rate for both room were relatively close to zero, which indicates that the simulation had converged. Despite not being able to obtain any lower residual values, it was concluded that the results are not noticeably affected. The reason for this is that the graphs are stationary, which indicate that the minimum RMS error obtainable for these simulations are already reached and that the simulation has converged.

To minimise rounding errors the double precision solver was selected, even though this led to a higher computational cost. It emerged during the simulation process how this method was demanding more storage space. The function gave a more detailed result due to more precise calculations. In retrospect, the necessity of the function could have been evaluated for the purpose of the thesis. Results from double precision solver could have been compared to results from simulations with single precision solver. This could have elucidated if the single precision solver would have given an accurate result, or if the difference between the results would have been considerable.

In the auxiliary transformer room it was issues regarding truncation error. The legs of the transformer led to a difference between the partial derivation in governing equations and its discrete approach. The truncation error caused by the transformer legs led to mesh inaccuracies in areas of the floor directly beneath the legs. Both the skewness and orthogonal quality were classed as Unacceptable for these small surfaces. Adjusting the mesh in this area should have solved the problem, however this became unachievable due to an error during the geometry modelling phase. The error occurred because the legs and floor did not properly merge together, and as a consequence, the mesh was not able to separate between the boundaries. Furthermore, the y^+ ended up outside of the desired range and caused inaccurate temperatures in this specific area. For the purpose of the simulation, the same calculations could have been completed on a geometry without legs on the transformer.

A mesh that is too coarse can cause errors that are difficult to discover when inexperienced to CFD calculations. This issue was prominent when simulating the valve hall due to the complexity. During the analysis, coarse mesh caused the simulation to not initiate and run properly. More specifically, the mesh caused a floating point error. On many occasions, floating point errors are related to meshing, based on the fact that the subdomains are not sufficiently constructed for the constrained equations. However, it is possible that other mistakes cause floating point error, such as incorrect input within the setup.

4.5 Further work

CFD calculations consist of various processes, parameters and models. Due to the complexity, some elements have been prioritised to complete the thesis objective, while other elements have been simplified. There are several ways to extend the thesis scope, which could have been done with additional time. This subsection presents some suggestions on interesting topics to analyse further.

One disadvantage of CFD analysis is that it is nearly impossible to obtain results that fully resembles real life situations. However, with high performance computers it is possible to simulate situations with a minor deviation. For this thesis, computer performance has been a restricting factor. Hence, it would be enlightening to perform further simulations of these scenarios using a more advanced computer. This would enable finer mesh and a faster convergence due to increased computational power.

The geometry models of the systems were simplified to save computational cost. Firstly, the room will in reality have more contents. Secondly, the inlet and outlet are modelled with simple geometry and their position was adjusted slightly to connect them with the external domain. This was necessary to ensure air supply into the enclosure. Thirdly, all of the heat emissions are emitted from one or a few localised heat sources in this simulation. Realistically, it will also be heat dissipation from other sources, such as lighting and solar radiation. Consequently, it would be interesting to implement these changes to obtain an even more precise result, but this would require a significantly more advanced computer.

Furthermore, the simulation could be enhanced by adjusting the mesh to obtain y^+ values within the range of $1-5$. It would be interesting to compare the results from enhanced wall treatment and the values applicable to the law of the wall. To be able to compare them, a thorough study of enhanced wall treatment would be necessary. This information could have been used to determine the most suitable method for similar simulations.

The simulation scenario that the results are based on is highly unlikely. For instance, it would seldom occur that the ambient temperature and heat dissipation from the equipment are at maximum simultaneously. Arguably, it appears that the current HVA/C system is over-dimensioned. In this regard, it is of interest to analyse other scenarios and study if the HVA/C system still meet the criteria. Examples of such scenarios could be to lower the inlet mass flow, which would lead to a more cost efficient ventilation system.

The ventilation for the valve hall is designed with inlets on two separate sides of the room. By reducing the sides with inlets to one, the required space for the ventilation design would be decreased. The converter platform could therefore be designed moderately smaller, thus less material are needed for the construction. Consequently, the work hours and space needed for the construction would be reduced. All these factors are participating in making the construction of the platform more economical.

The possible challenges of the design are inadequate cooling of the equipment. A possible problem is that the air jets will have a velocity that is too agile to efficiently cool down the equipment facing the inlet. Furthermore the air stream might not cover the whole room, thus the equipment surfaces facing opposite side of the inlets could be overheated. To simulate this case the inlets needs to be redimensioned and the geometry needs to be adjusted. The air distribution and temperature in key areas should be evaluated closely in an eventual simulation.

There are countless adjustments that can be implemented in the simulation to slightly influence the results. However, it is impossible to verify that the simulations are fully realistic without doing real life measurements. Hence, to achieve a deeper understanding of how to optimise the simulations, measurements on either a functioning prototype, or the systems in operation would be incredibly insightful. Performing measurements on a fully functional valve hall and auxiliary transformer room, and then comparing the results with the CFD calculations is a good way to validate the results.

5 Conclusion

The objective of this thesis was to evaluate temperature distribution of two systems on a converter platform by performing CFD calculations. To accomplish a deeper understanding of the temperature distribution, the air flow around the rooms were researched. In addition, the setups and mesh were evaluated to ensure a satisfactorily accurate result.

The meshing process is a key part of the CFD calculations, and must be conducted thoroughly to provide accurate results. For both the auxiliary transformer room and the valve hall, a mesh independence study, a revision of the element quality and a study of y^+ values were implemented. Common for both systems were element qualities close to optimal, which ensured accurate and fast simulations. The element quality was reviewed in terms of skewness and orthogonal quality. The y^+ values were within the range applicable with the law of the wall. Due to the element quality and y^+ values, the mesh was concluded to be well executed for the simulations. One paramount difference between the two rooms was the number of elements required. The mesh independence studies established that the auxiliary transformer room needed approximately $400\,000$ elements to provide stationary results, while the valve hall was not completely steady with $1\,350\,000$ elements. Conclusively, it is indisputable that more complex simulations require a finer mesh.

The main purpose of the simulation was to evaluate if the temperature in the two rooms were within the design temperature limits. The average temperature in the auxiliary transformer room was $35, 0$°C and the highest temperature around the equipment was $36, 2$°C. The only infringement from the design temperature was located beneath the ceiling. The infringement was caused by the high radiative heat transfer from the transformer, which led to overheated walls. However, it was concluded that the warm walls would not be a problem in reality. The simulation of the auxiliary transformer room yielded temperatures within the desired range for every key area in the enclosure. Thus, the ventilation system inside the auxiliary transformer room worked as intended.

The average temperature inside the valve hall was $40, 1$°C, which is within the design temperature of $45, 0$°C. The temperature above the valves and in the outlets were both in excess of $43, 0$°C. Contrarily, the area above the smoothing reactor exceeded the design temperature, with a temperature of $48, 3$°C. When modelled as a hollow cylinder, the temperature was approximately $50, 0$°C above the smoothing reactor. The decreased volume of the smoothing reactor caused an increased surface temperature. Due to some imprecise values of the exact heat emission from the smoothing reactor, as well as a relatively small deviation from the design temperature, the valve hall´s ventilation is concluded as functional.

The air distribution inside the two enclosures clearly resemble a typical displacement ventilation system. Both systems have an distinct upper and lower zone with a beneficial thermal stratification. Furthermore, there were eddies formations in both the systems due to the Coandă effect. The eddies were concluded to be unproblematic, due to the fact that the temperature in the systems were within reasonable limits. The placement of the outlets around the smoothing reactor in the valve hall was evaluated to be beneficial for the purpose of leading the heat out of the enclosure.

Bibliography

[1] *World Energy Outlook 2019.* eng. World Energy Outlook. Paris: OECD Publishing, 2019. ISBN: 9264523278.

[2] *About The Dogger Bank Wind Farm Projects.* Dogger Bank Wind Farm. URL: https://doggerbank.com/about/ (visited on 04/02/2021).

[3] *Vindparken Dogger Bank tildeler rekordstor turbinkontrakt som skaper nye lokale arbeidsplasser - equinor.com.* URL: https://www.equinor.com/no/news/20200922-dogger-bank.html (visited on 04/02/2021).

[4] *Onshore | Dogger Bank Wind Farm.* URL: https://doggerbank.com/construction/onshore/ (visited on 12/02/2021).

[5] *Info graphic Sofia Windfarm (1200×675).* URL: https://dvzpv6x5302g1.cloudfront.net/AcuCustom/Sitename/DAM/078/Info_graphic_Sofia_Winfarm_Main.jpg (visited on 12/04/2021).

[6] *Dogger Bank - equinor.com.* URL: https://www.equinor.com/no/what-we-do/wind/dogger-bank.html (visited on 04/02/2021).

[7] *Dogger Bank Offshore Wind Farm | SSE Renewables.* URL: https://www.sserenewables.com/offshore-wind/projects/dogger-bank/ (visited on 04/02/2021).

[8] *Haliade-X offshore wind turbine | GE Renewable Energy.* URL: https://www.ge.com/renewableenergy/wind-energy/offshore-wind/haliade-x-offshore-turbine (visited on 04/02/2021).

[9] *Aibel.* URL: https://aibel.com/search/results?q=dogger+bank (visited on 02/04/2021).

[10] Yunus A. Çengel and Afshin J. Ghajar. *Heat and mass transfer : Fundamentals and Applications.* 5th ed. in SI units. New York: Mcgraw-Hill, C 2015. ISBN: 9789814595278.

[11] Leif I Stensaas. *Inneklimateknikk.* VVS-teknikk. Oslo: Gyldendal yrkesopplæring, 2000. ISBN: 8200451739.

[12] Robert McDowall. *Fundamentals of HVAC Systems.* Elsevier Science, 2007. ISBN: 978-0-12-373998-8.

[13] Halvor Røstad. *industriventilasjon.* In: *Store norske leksikon.* July 3, 2018. URL: http://snl.no/industriventilasjon (visited on 01/03/2021).

[14] Bent A. Børresen. *fortrengningsventilasjon.* In: *Store norske leksikon.* July 2, 2018. URL: http://snl.no/fortrengningsventilasjon (visited on 01/03/2021).

[15] Frank M White. *Fluid mechanics.* eng. 7th ed. McGraw-Hill series in mechanical engineering. New York: McGraw-Hill, 2011. ISBN: 9780073529349.

[16] *Definition of Hydrostatics.* URL: https://www.merriam-webster.com/dictionary/hydrostatics (visited on 04/02/2021).

[17] *Definition of Fluid Dynamics.* URL: https://www.merriam-webster.com/dictionary/fluid+dynamics (visited on 04/02/2021).

[18] Richard H Pletcher. *Computational fluid mechanics and heat transfer.* eng. 2nd ed. Series in computational and physical processes in mechanics and thermal sciences. Boca Raton, Florida: CRC Press, 1997. ISBN: 1591690374.

[19] Bastian E. Rapp. In: *Microfluidics: Modelling, Mechanics and Mathematics.* Ed. by Bastian E. Rapp. Micro and Nano Technologies. Oxford: Elsevier, 2017. ISBN: 978-1-4557-3141-1.

[20] *What is CFD | What is Computational Fluid Dynamics?* SimScale. URL: https://www.simscale.com/docs/simwiki/cfd-computational-fluid-dynamics/what-is-cfd-computational-fluid-dynamics/ (visited on 09/02/2021).

[21] *Navier-Stokes Equations*. URL: https://www.grc.nasa.gov/www/k-12/airplane/nseqs.html (visited on 02/05/2021).

[22] *ANSYS FLUENT 12.0 Theory Guide - 4.2.1 Reynolds-Averaged Approach vs. LES*. URL: https://www.afs.enea.it/project/neptunius/docs/fluent/html/th/node45.htm (visited on 08/03/2021).

[23] *ANSYS FLUENT 12.0 Theory Guide - 4.2.2 Reynolds (Ensemble) Averaging*. URL: https://www.afs.enea.it/project/neptunius/docs/fluent/html/th/node46.htm (visited on 08/03/2021).

[24] Yunus A Çengel. *Fluid mechanics : fundamentals and applications*. eng. 3rd ed. Boston: McGraw-Hill, 2013. ISBN: 9780073380322.

[25] John Willoughby. *Plant Engineer's Reference Book*. Ed. by Dennis A. Snow. Second Edition. Oxford: Butterworth-Heinemann, 2002. ISBN: 978-0-7506-4452-5.

[26] Bjørn Pedersen. *varme*. In: *Store norske leksikon*. Oct. 27, 2017. URL: http://snl.no/varme (visited on 12/05/2021).

[27] *Heat transfer types. jpg (1400×1020)*. URL: https://clqtg10snjb14i85u49wifbv-wpengine.netdna-ssl.com/wp-content/uploads/2020/04/heat-transfer-methods-1.jpg (visited on 07/05/2021).

[28] De-Ling Liu. *Developments in Surface Contamination and Cleaning*. Ed. by Rajiv Kohli and Kashmiri L. Mittal. Oxford: William Andrew Publishing, 2010. ISBN: 978-1-4377-7830-4.

[29] Sara Gilani et al. "CFD simulation of stratified indoor environment in displacement ventilation: Validation and sensitivity analysis". In: *Building and Environment* 95 (2016). ISSN: 0360-1323.

[30] *ANSYS FLUENT 12.0 User's Guide - 8.3.5 Incompressible Ideal Gas Law*. URL: https://www.afs.enea.it/project/neptunius/docs/fluent/html/ug/node289.htm (visited on 03/02/2021).

[31] *Emissivity - an overview | ScienceDirect Topics*. URL: https://www.sciencedirect.com/topics/engineering/emissivity (visited on 09/02/2021).

[32] M. Alejandra Menchaca-Brandan et al. "The influence of radiation heat transfer on the prediction of air flows in rooms under natural ventilation". In: *Energy and Buildings* 138 (2017). ISSN: 0378-7788.

[33] *Heat Flux - an overview | ScienceDirect Topics*. URL: https://www.sciencedirect.com/topics/chemical-engineering/heat-flux (visited on 09/02/2021).

[34] *ANSYS FLUENT 12.0 Theory Guide - 5.3.9 Choosing a Radiation Model*. URL: https://www.afs.enea.it/project/neptunius/docs/fluent/html/th/node118.htm?fbclid=IwAR1lkI3wHPrVOxZfstthVU8sDl5l63z1XobG30ktPSeN4IWaGiOtRcd7DpM (visited on 06/04/2021).

[35] *ANSYS FLUENT 12.0 Theory Guide - 5.3.6 Discrete Ordinates (DO) Radiation Model Theory*. URL: https://www.afs.enea.it/project/neptunius/docs/fluent/html/th/node115.htm?fbclid=IwAR2cJBJMogP-Lq58RUaOpqotvvUXBjpIWwjkDLqXNg8cN77yuuO2UDN5MXQ (visited on 06/04/2021).

[36] Adnan Ploskić and Sture Holmberg. "Heat emission from thermal skirting boards". In: *Building and Environment* 45.5 (2010). ISSN: 0360-1323.

[37] Ran Gao et al. "Comparison of indoor air temperatures of different under-floor heating pipe layouts". In: *Energy Conversion and Management* 52.2 (2011). ISSN: 0196-8904.

[38] C. Teodosiu, F. Kuznik, and R. Teodosiu. "CFD modeling of buoyancy driven cavities with internal heat source - Application to heated rooms". In: *Energy and Buildings* 68 (2014).

[39] C. Teodosiu, N. Niculiţă, and R. Teodosiu. "Computational fluid dynamics based modeling of a linear heat source". In: *Energy and Buildings* 68 (2014).

[40] V. V Baturin. *Fundamentals of industrial ventilation.* eng. 3rd enl. ed. Vol. 8. International series of monographs in heating, ventilation and refrigeration. Oxford: Pergamon Press, 1972. ISBN: 0080158285.

[41] Per Kvols Heiselberg et al. *Ventilation of Large Spaces in Buildings: Analysis and Prediction Techniques.* English. R / Institut for Bygningsteknik R9803. Department of Mechanical Engineering, Aalborg University, 1998.

[42] *Definition of Streamlines.* URL: https://www.grc.nasa.gov/WWW/K-12/airplane/stream.html (visited on 12/04/2021).

[43] *Eddies flow image (328×154).* URL: https://encrypted-tbn0.gstatic.com/images?q=tbn:ANd9GcRRajhqzsxbynZCceifxuSGo98l7Rb5AW5BK9Y2ifygzgBg9iPIXHkNlN7On_n5vzZ3Mds&usqp=CAU (visited on 12/04/2021).

[44] *Fluidics and the Coanda Effect.* URL: https://media.lanecc.edu/users/driscolln/RT112/Air_Flow_Fluidics/Air_Flow_Fluidics8.html (visited on 12/04/2021).

[45] David C. Wilcox. *Turbulence Modeling for CFD.* Third edition. DCW Industries, Inc., 2006. ISBN: 978-1-928729-08-2.

[46] *ANSYS FLUENT 12.0 User's Guide - 12.2 Choosing a Turbulence Model.* URL: https://www.afs.enea.it/project/neptunius/docs/fluent/html/ug/node407.htm (visited on 03/03/2021).

[47] *ANSYS FLUENT 12.0 User's Guide - 12.3.1 Near-Wall Mesh Guidelines.* URL: https://www.afs.enea.it/project/neptunius/docs/fluent/html/ug/node410.htm#sec-guidelines-wf (visited on 09/03/2021).

[48] Zhiqiang John Zhai et al. "Evaluation of Various Turbulence Models in Predicting Airflow and Turbulence in Enclosed Environments by CFD: Part 1—Summary of Prevalent Turbulence Models". In: *HVAC&R Research* 13.6 (2007).

[49] S. Gilani et al. *CFD simulation of temperature stratification for a building space: Validation and sensitivity analysis.* 2013. URL: https://www.scopus.com/inward/record.uri?eid=2-s2.0-84886668884&partnerID=40&md5=edd302b91d16c3ca7a2baf527b16db84 (visited on 02/02/2021).

[50] *ANSYS Fluent User's Guide.* In: Release 15.0. Nov. 2013. URL: http://www.pmt.usp.br/academic/martoran/notasmodelosgrad/ANSYS%20Fluent%20Users%20Guide.pdf (visited on 04/04/2021).

[51] *Meshing in FEA: Structured vs Unstructured meshes.* OnScale. Section: Simulation. Apr. 1, 2020. URL: https://onscale.com/blog/meshing-in-fea-structured-vs-unstructured-meshes/ (visited on 09/04/2021).

[52] *ANSYS FLUENT 12.0 User's Guide - 6.2.2 Mesh Quality.* URL: https://www.afs.enea.it/project/neptunius/docs/fluent/html/ug/node167.htm (visited on 12/03/2021).

[53] *Mesh quality recommendations, padt-ansys-cfd-meshing-f03.jpg (933×361).* URL: https://i0.wp.com/www.padtinc.com/blog/wp-content/uploads/2017/04/padt-ansys-cfd-meshing-f03.jpg (visited on 08/04/2021).

[54] *Recommendations on how to create a high quality mesh for accurate CFD.* en. 2018. URL: https://www.simscale.com/blog/2018/03/tips-high-quality-mesh/ (visited on 04/02/2021).

[55] *ANSYS FLUENT 12.0 User's Guide - 7.3.14 Wall Boundary Conditions.* URL: https://www.afs.enea.it/project/neptunius/docs/fluent/html/ug/node250.htm#sec-wall-shell-conduction (visited on 10/03/2021).

[56] *ANSYS FLUENT 12.0 User's Guide - 7.3 Boundary Conditions.* URL: `https://www.afs.enea.it/project/neptunius/docs/fluent/html/ug/node236.htm` (visited on 02/05/2021).

[57] J.C. Tannehill, D.A. Anderson, and R.H. Pletcher: *Computational Fluid Mechanics and Heat Transfer.* Taylor & Francis, Washington, DC, 1997. ISBN: 1-56032-046-X.

[58] *ANSYS FLUENT 12.0 User's Guide - 26.13.1 Monitoring Residuals.* URL: `https://www.afs.enea.it/project/neptunius/docs/fluent/html/ug/node812.htm#144585` (visited on 12/04/2021).

[59] Leif Rune Hellevik. *Numerical Methods for Engineers.* URL: `https://folk.ntnu.no/leifh/teaching/tkt4140/._main000.html` (visited on 08/03/2021).

[60] *NavisWorks | AutoDesk.* URL: `https://www.autodesk.no/products/navisworks/overview` (visited on 09/04/2021).

[61] *Beyond Design: the Construction and BIM blog.* Beyond Design: the Construction and BIM blog. URL: `https://beyonddesign.typepad.com/posts/` (visited on 12/04/2021).

[62] *SolidWorks: 3D Modeling Software with parametric construction.* Sculpteo. URL: `https://www.sculpteo.com/en/glossary/solidworks-definition/` (visited on 01/03/2021).

[63] *Company Information.* URL: `https://www.solidworks.com/sw/183_ENU_HTML.htm` (visited on 01/03/2021).

[64] M.A. Wahab. *The Mechanics of Adhesives in Composite and Metal Joints: Finite Element Analysis with ANSYS.* DEStech Publications, 2014. ISBN: 978-1-60595-096-9.

[65] *About ANSYS.* URL: `https://www.ansys.com/about-ansys` (visited on 09/03/2021).

A Appendix A: Temperature contour for the auxiliary transformer room

A.1 Horizontal temperature contour
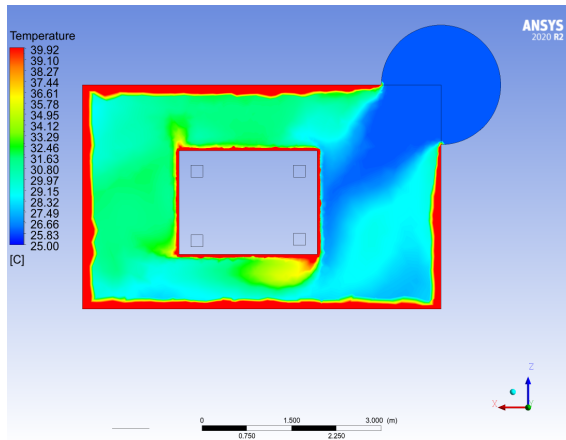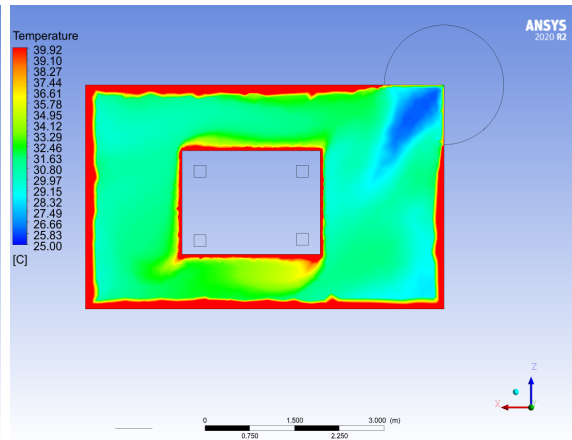
(a) *Distance from the floor = 1m.*

(b) *Distance from the floor = 2m.*
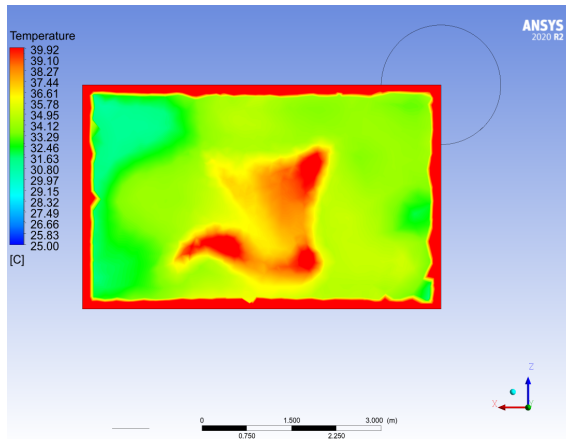
(c) *Distance from the floor = 3m.*
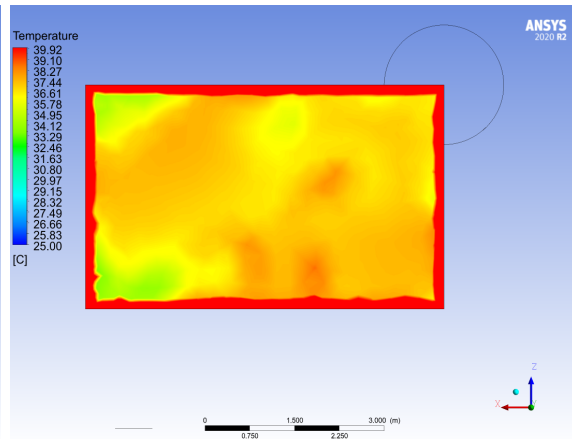
(d) *Distance from the floor = 4m.*
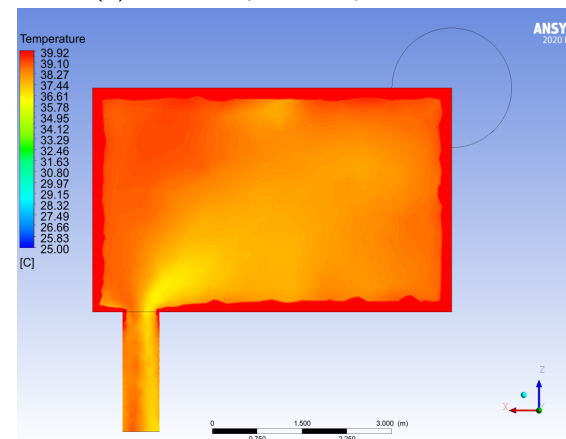
(e) *Distance from the floor = 5m.*
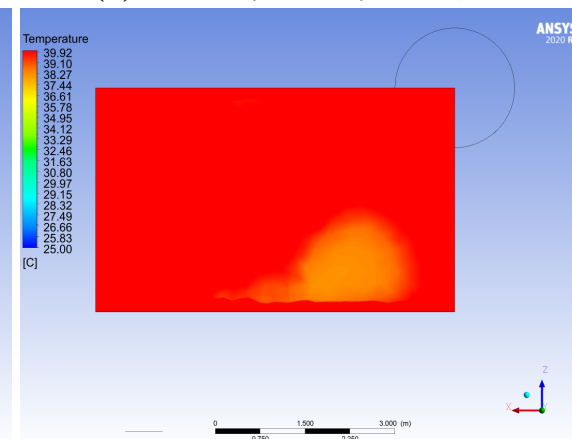
(f) *Distance from the floor = 6m.*

Figure A.1: *Horizontal temperature contour in the interval $1 - 6\,m$.*

A.2 Vertical temperature contour
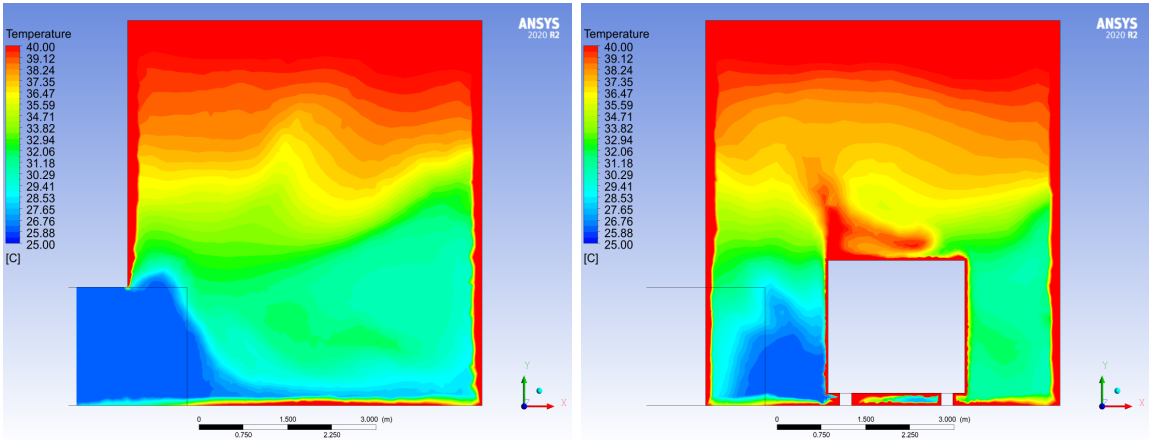
(a) *Distance from the east wall = 0,5m.*

(b) *Distance from the east wall = 1,5m.*
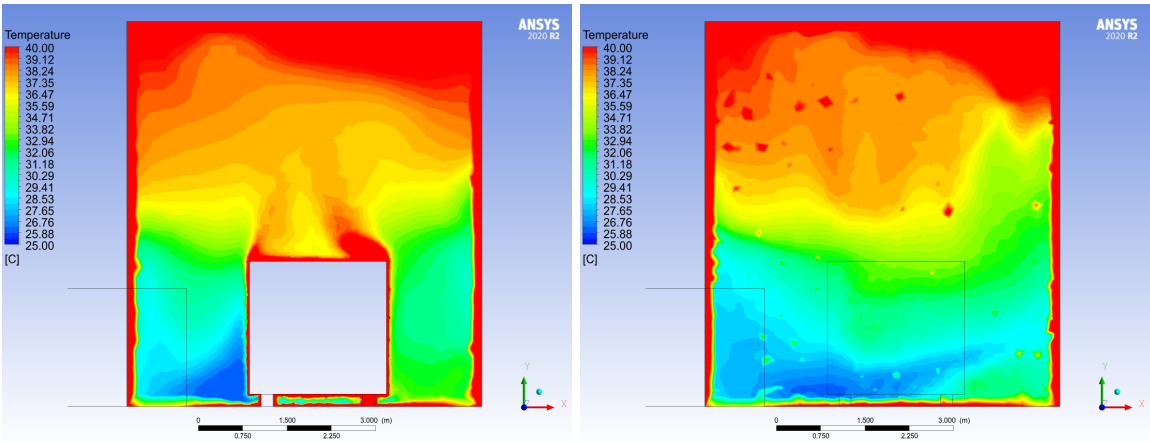
(c) *Distance from the east wall = 2,5m.*

(d) *Distance from the east wall = 3,5m.*

Figure A.2: *Vertical temperature contour in the interval $0,5 - 3,5\,m$.*

B   Appendix B: Temperature contour for the valve hall

B.1   Horizontal temperature contour
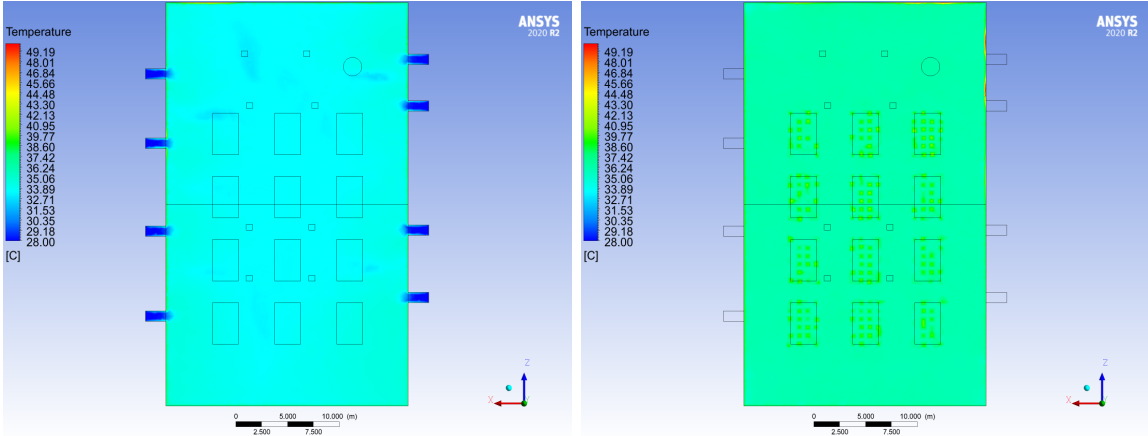
(a) *Distance from the floor = 1m.*

(b) *Distance from the floor = 3m.*
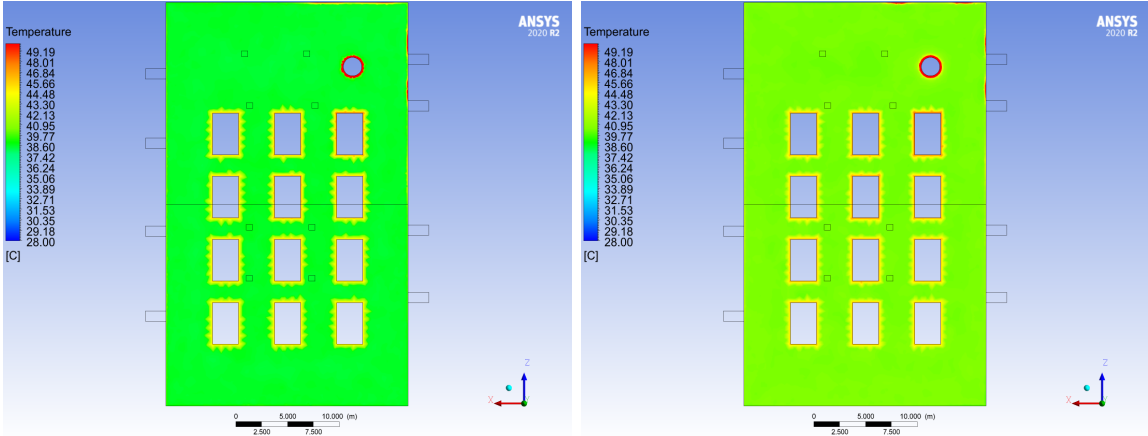
(c) *Distance from the floor = 5m.*

(d) *Distance from the floor = 7m.*
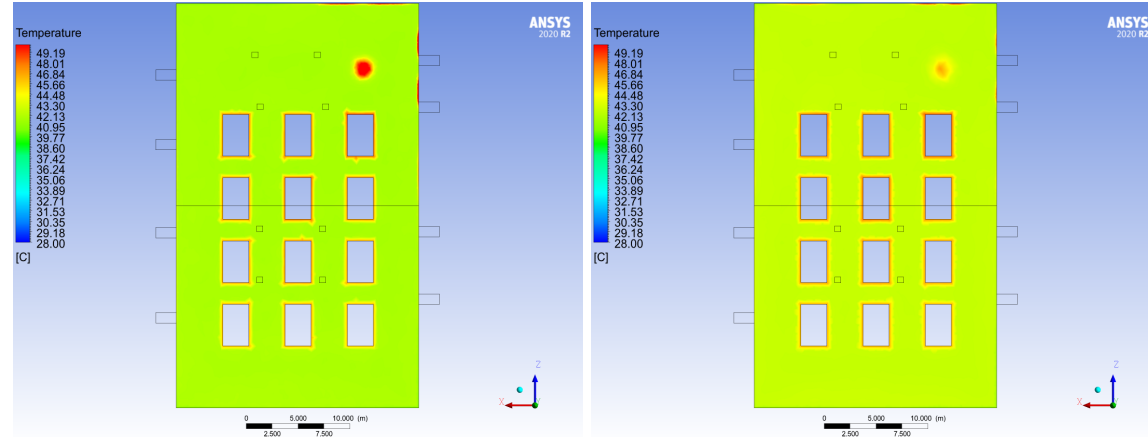
(e) *Distance from the floor = 9m.*

(f) *Distance from the floor = 11m.*

Figure B.1: *Horizontal temperature contour in the interval $1 - 11\,m$.*
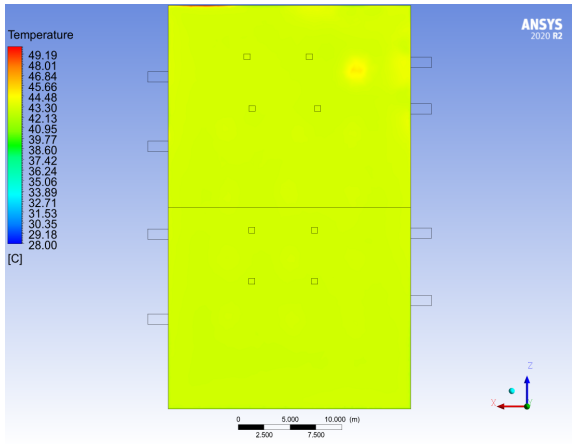
(a) *Distance from the floor = 13m.*
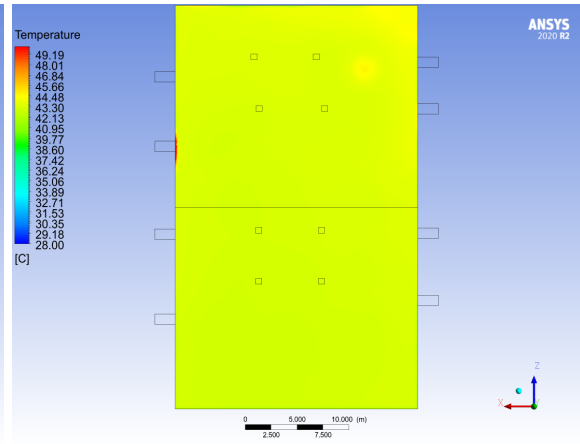
(b) *Distance from the floor = 15m.*

Figure B.2: *Horizontal temperature contour in the interval* $13 - 15\,m$.

B.2   Vertical temperature contour
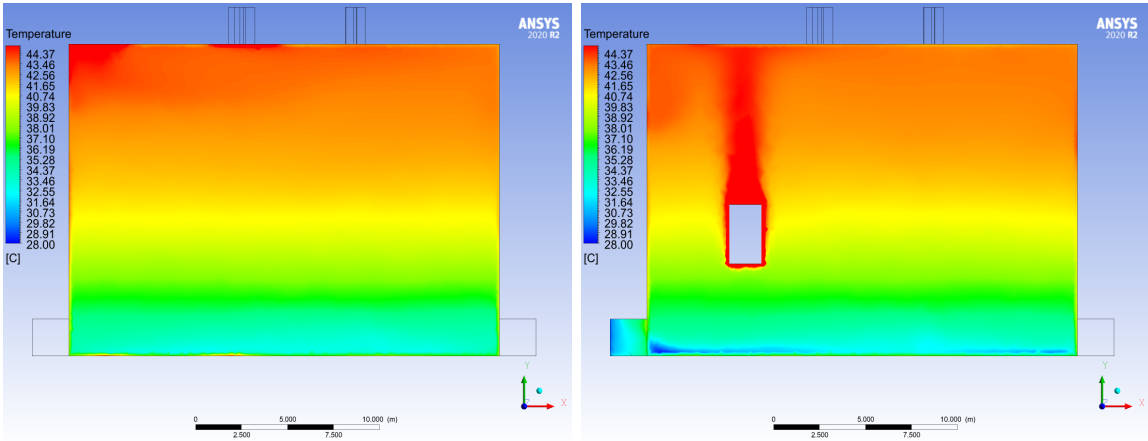
(a) *Distance from the east wall = 2m.*

(b) *Distance from the east wall = 6m.*
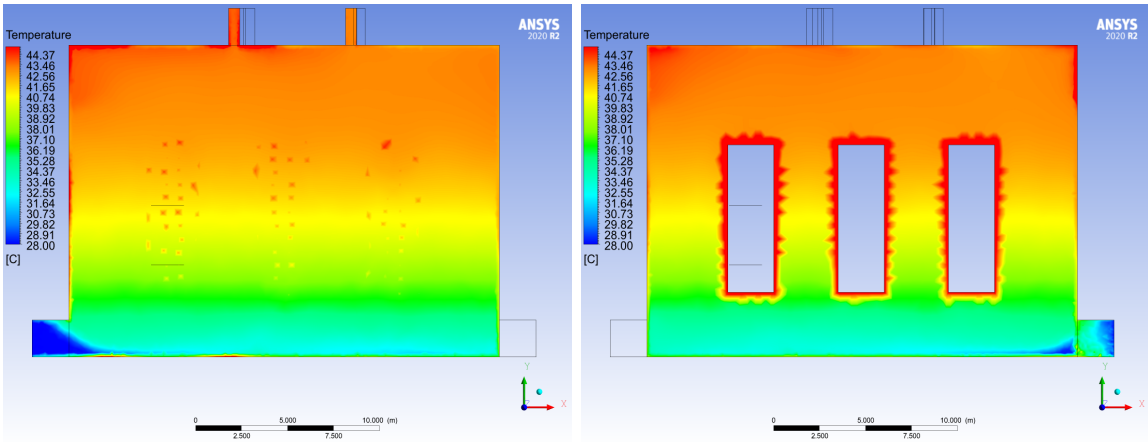
(c) *Distance from the east wall = 10m.*

(d) *Distance from the east wall = 14m.*
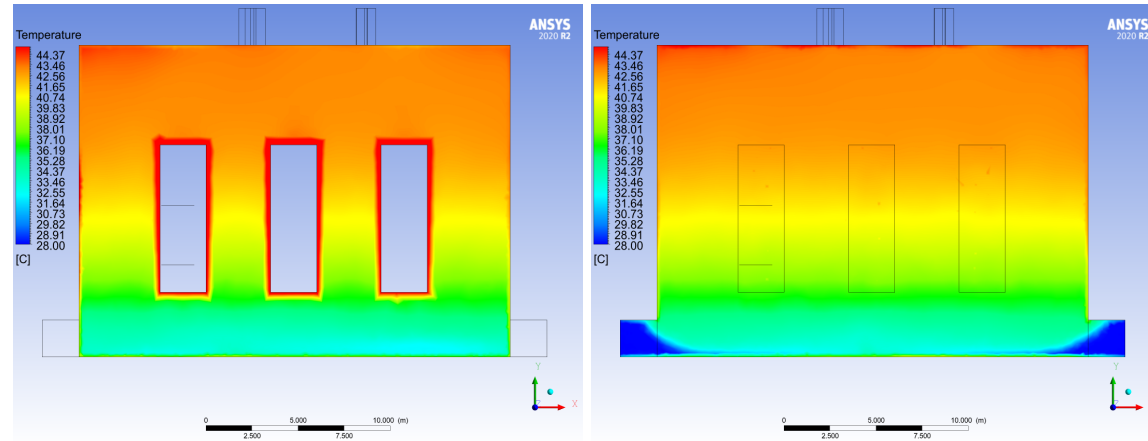
(e) *Distance from the east wall = 18m.*

(f) *Distance from the east wall = 22m.*

Figure B.3: *Vertical temperature contour in the interval* $2 - 22\,m$.
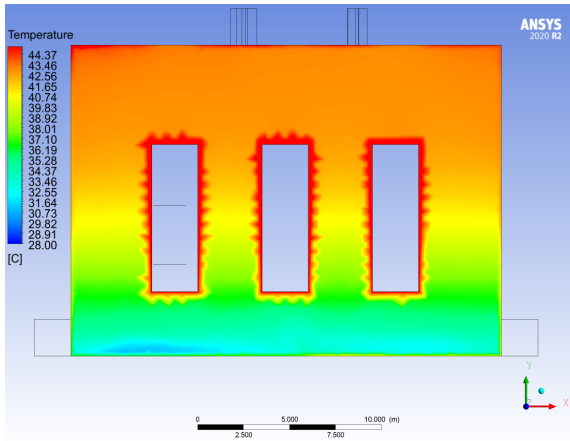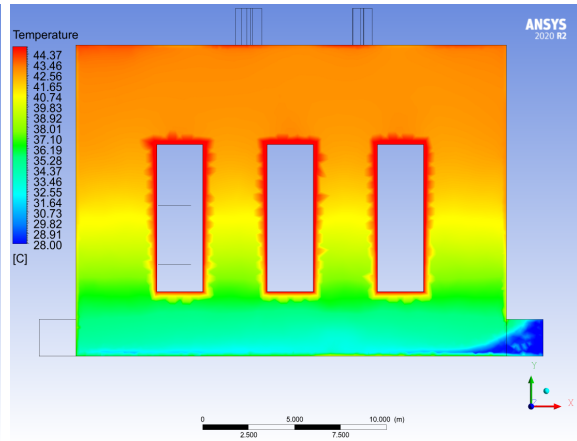
(a) *Distance from the east wall = 26m.*

(b) *Distance from the east wall = 30m.*
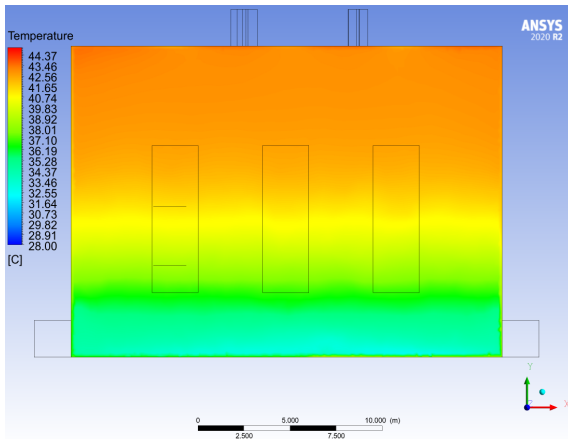
(c) *Distance from the east wall = 34m.*
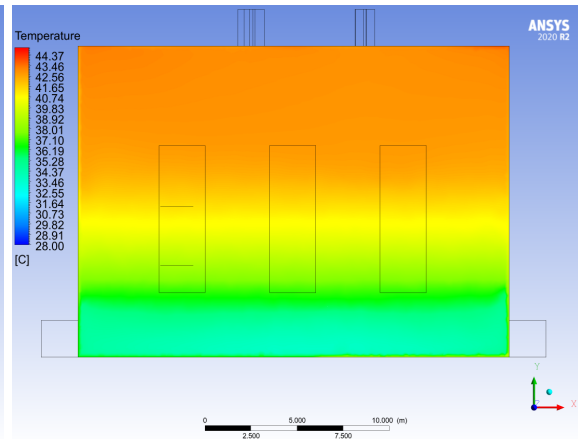
(d) *Distance from the east wall = 38m.*

Figure B.4: *Vertical temperature contour in the interval* $26 - 38\,m$.

C Appendix C: Streamline profiles for the auxiliary transformer room

C.1 Horizontal streamline profiles

(a) *Distance from the floor = 1m.*

(b) *Distance from the floor = 2m.*

(c) *Distance from the floor = 3m.*

(d) *Distance from the floor = 4m.*

(e) *Distance from the floor = 5m.*

(f) *Distance from the floor = 6m.*
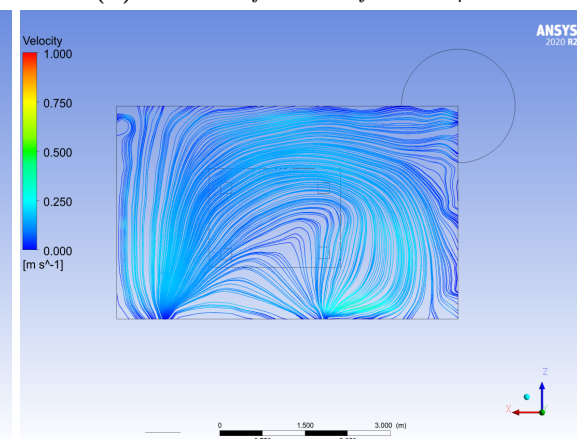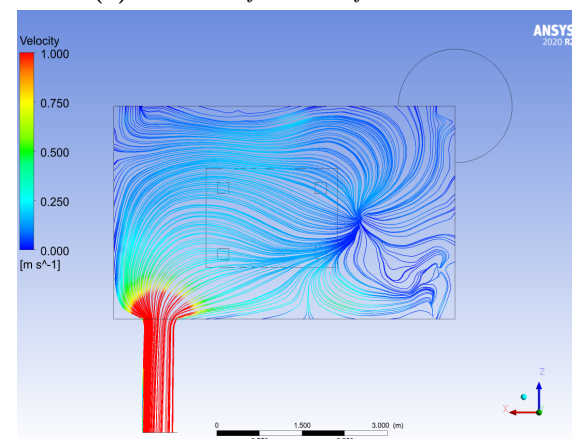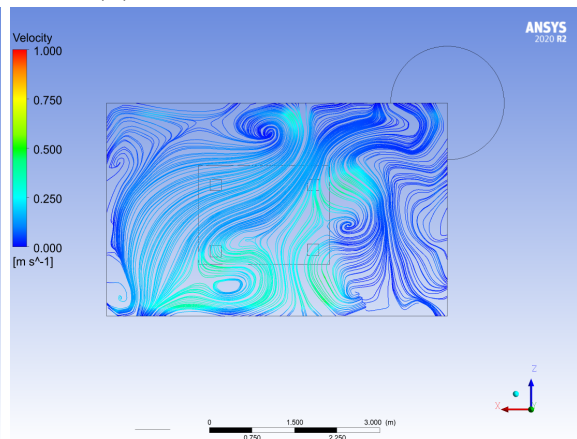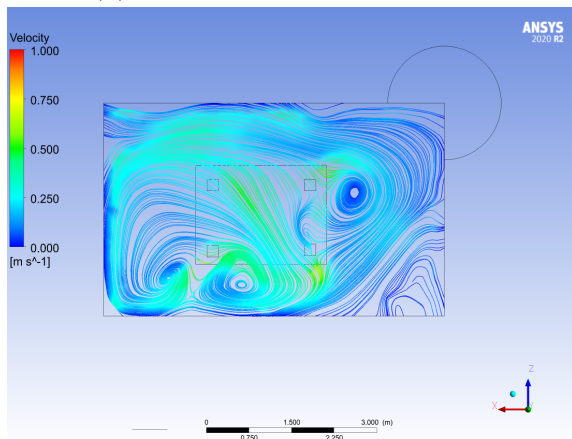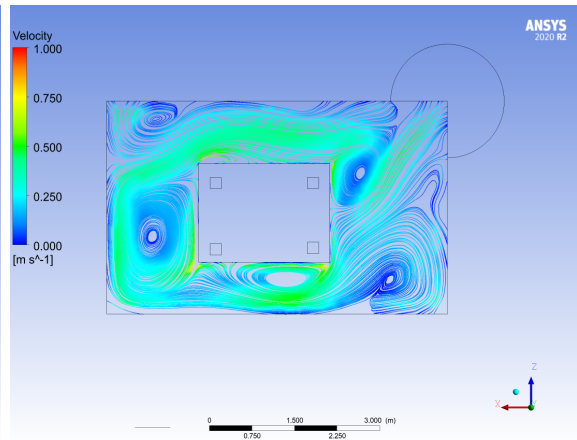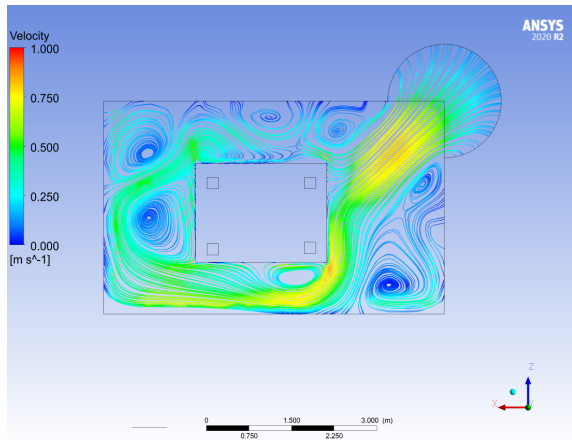
Figure C.1: *Horizontal streamline profiles in the interval $1-6\,m$.*

C.2 Vertical streamline profiles
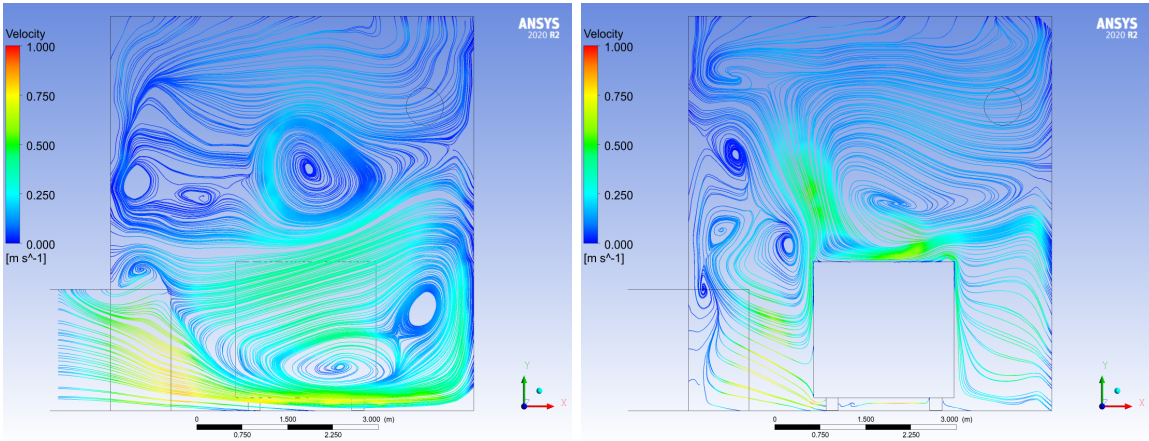
(a) *Distance from the east wall = 0,5m.*

(b) *Distance from the east wall = 1,5m.*
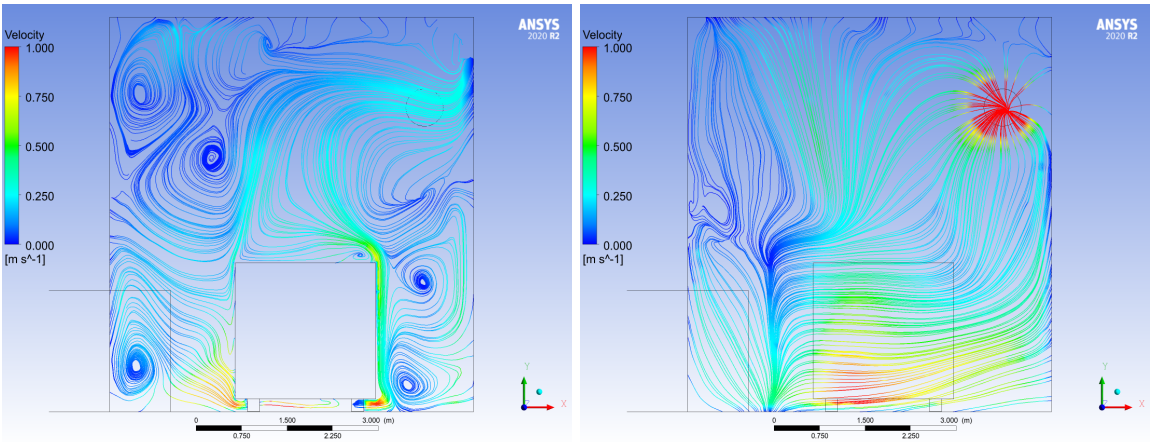
(c) *Distance from the east wall = 2,5m.*

(d) *Distance from the east wall = 3,5m.*

Figure C.2: *Vertical streamline profiles in the interval* $0,5 - 3,5\,m$.

D   Appendix D: Streamline profiles for the valve hall

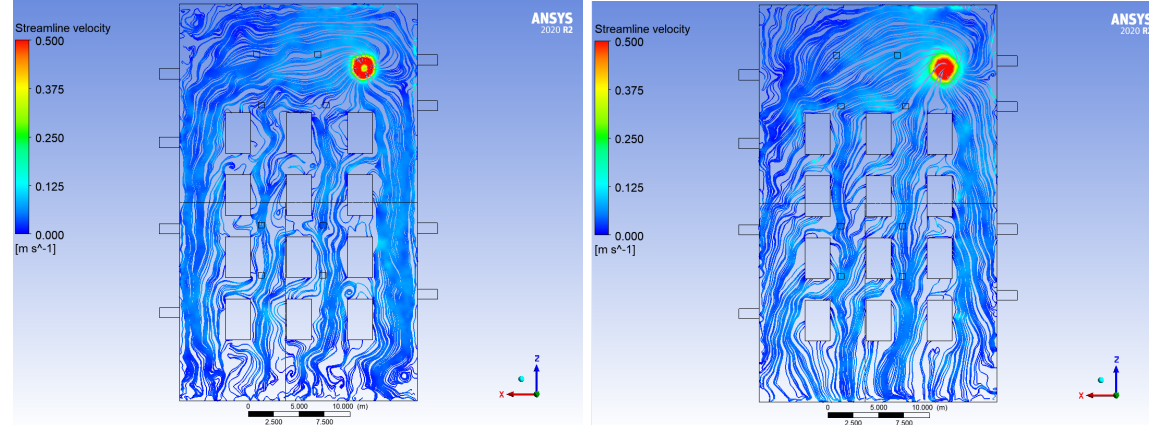## D.1   Horizontal streamline profiles
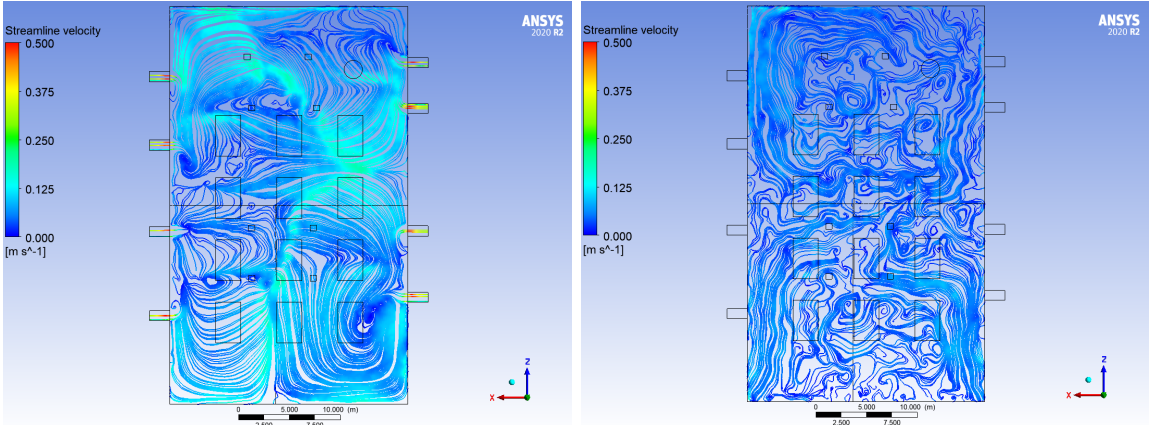
(a) *Distance from the floor = 1m.*

(b) *Distance from the floor = 3m.*
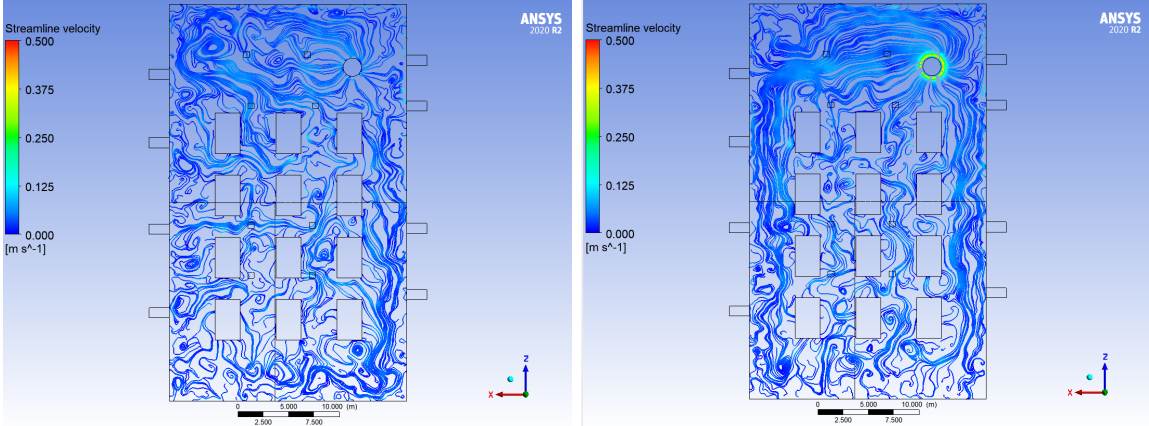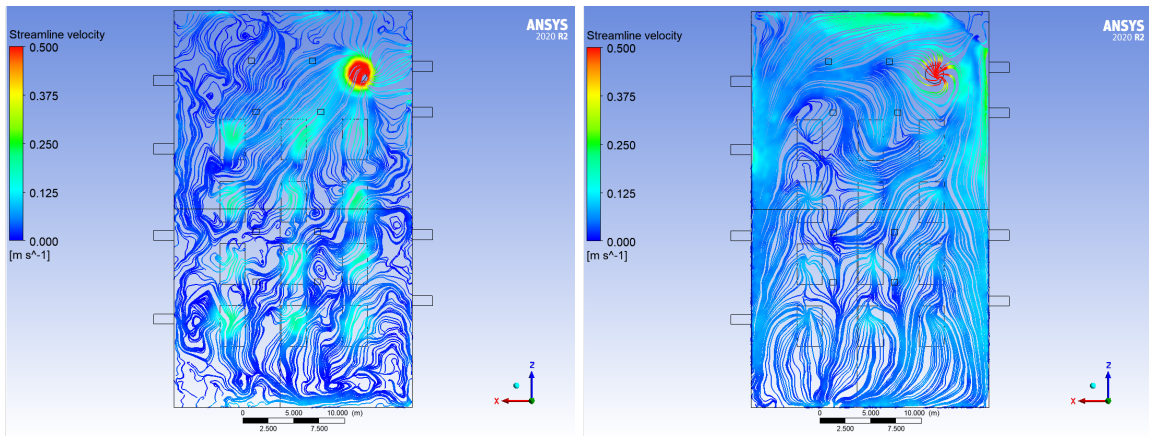
(c) *Distance from the floor = 5m.*

(d) *Distance from the floor = 7m.*

(e) *Distance from the floor = 9m.*

(f) *Distance from the floor = 11m.*

Figure D.1: *Horizontal streamline profiles in the interval $1 - 11\,m$.*

(a) *Distance from the floor = 13m.*

(b) *Distance from the floor = 15m.*

Figure D.2: *Horizontal streamline profiles in the interval $13 - 15\,m$.*
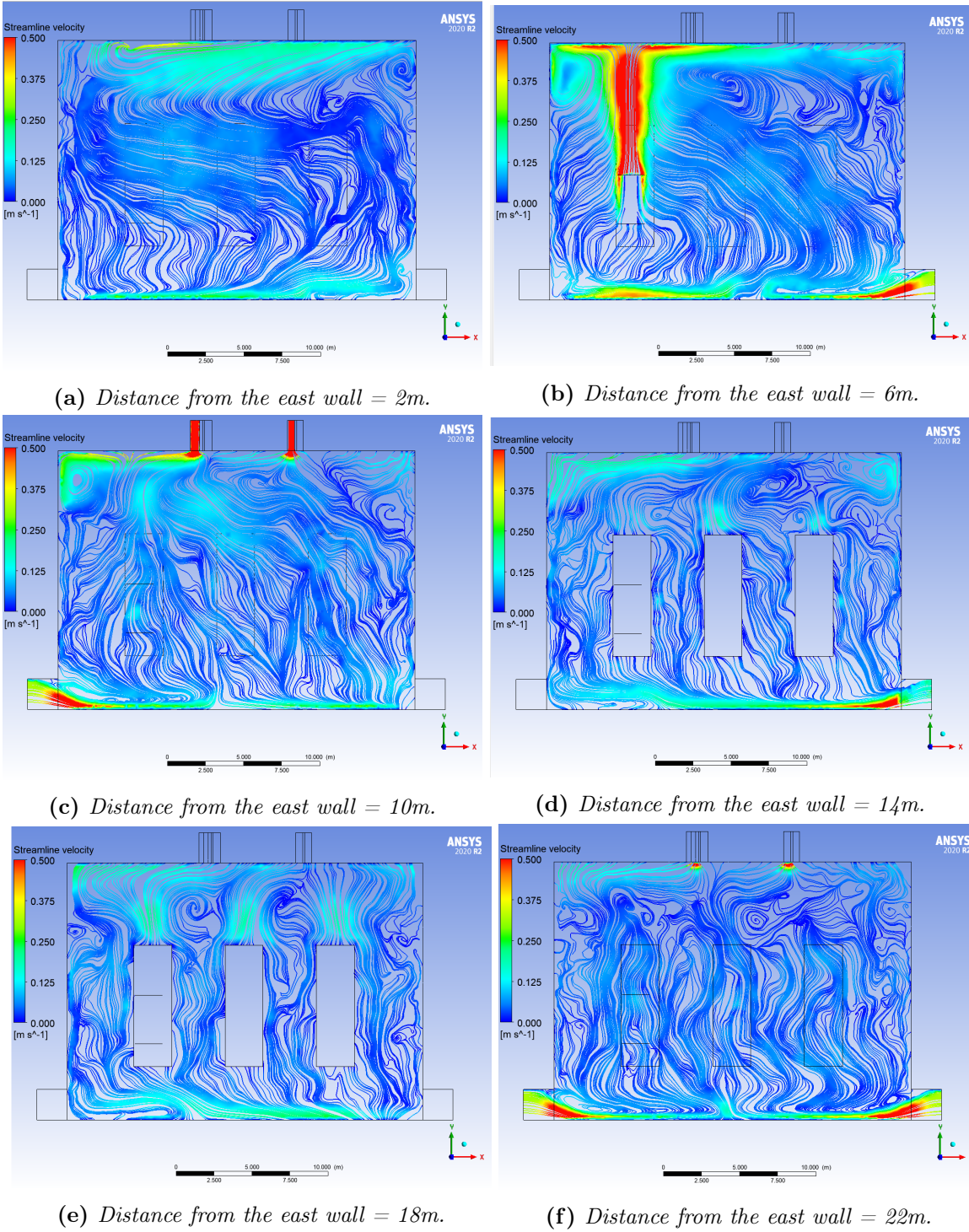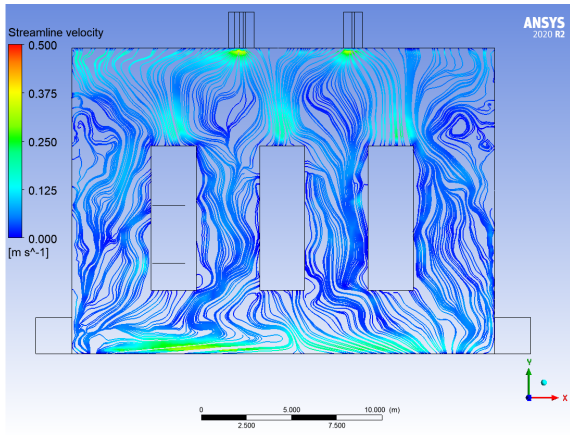
X

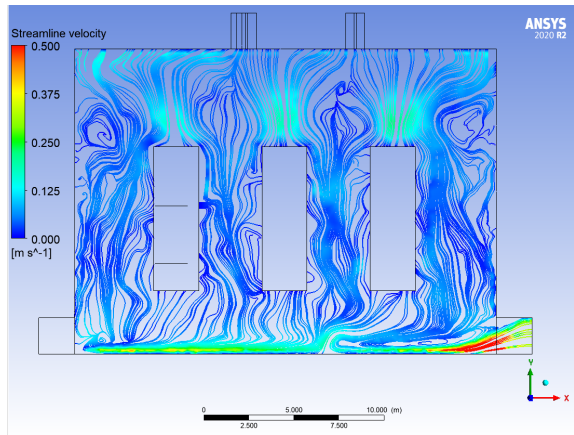## D.2   Vertical streamline profiles

(a) *Distance from the east wall = 2m.*

(b) *Distance from the east wall = 6m.*

(c) *Distance from the east wall = 10m.*

(d) *Distance from the east wall = 14m.*

(e) *Distance from the east wall = 18m.*

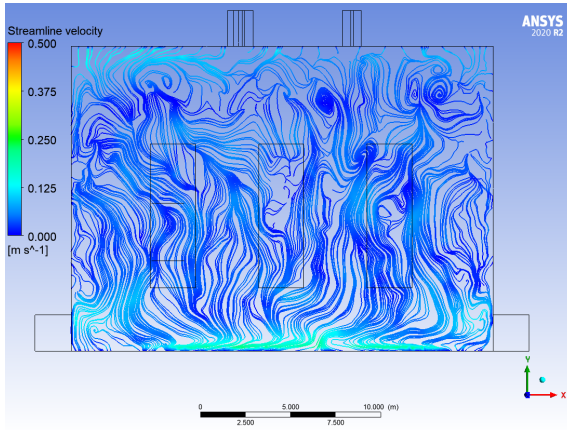**(f)** *Distance from the east wall = 22m.*

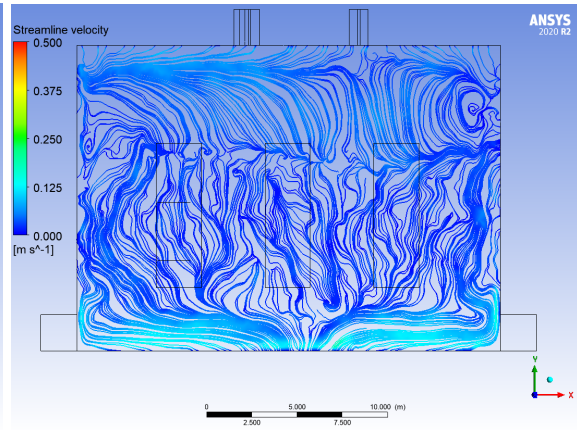**Figure D.3:** *Vertical streamline profiles in the interval $2 - 22\,m$.*

(a) *Distance from the east wall = 26m.*

(b) *Distance from the east wall = 30m.*

(c) *Distance from the east wall = 34m.*

(d) *Distance from the east wall = 38m.*

Figure D.4: *Vertical streamline profiles in the interval* $26 - 34\,m$.